LIQUEFIED NATURAL GAS HAZARDS MITIGATION

WITH HIGH EXPANSION FOAM

A Dissertation

by

BIN ZHANG

Submitted to the Office of Graduate and Professional Studies of
Texas A&M University
in partial fulfillment of the requirements for the degree of

DOCTOR OF PHILOSOPHY

Chair of Committee,	M. Sam Mannan
Committee Members,	Charles Glover
	Mahmoud El-Halwagi
	Debjyoti Banerjee
Head of Department,	M. Nazmul Karim

December 2015

Major Subject: Chemical Engineering

ABSTRACT

The gas industry boom driven by the advancement of horizontal drilling and hydraulic fracturing technologies provides a solution to a growing demand on energy, especially clean energy. The liquefaction process reduces the volume by 600 times through converting natural gas into Liquefied Natural Gas (LNG) that promotes inter-regional trade using LNG transportation carriers and trucks. LNG vapor cloud and pool fire are two major hazards in the LNG facilities, where LNG is processed and stored in a large volume. NFPA 59A requires mitigation measures to reduce risks to a tolerable level in the LNG facilities. High expansion foam has been proved to be effective for mitigating the vapor hazard and controlling LNG pool fire, and is recommended by NFPA 11 and NFPA 471.

This work aims to experimentally study the mitigation effect of high expansion foam on LNG vapor and fire hazards. The blanketing effect on vapor hazard was conducted in a wind tunnel using liquid nitrogen, where heat radiation and convection were provided by a bulb panel and a fan. The results concluded that the blanketing effect could reduce 70% of the heat flux from radiation and convection for vaporization. The warming effect on vapor hazard was studied using liquid nitrogen with a self-constructed foam generator and a foam test apparatus. The vapor temperature was increased after the foam application. The temperature difference of vapor and foam was measured with a special design of thermocouple installation. The formation of vapor channel was studied in terms of the size and location. The foam breaking rate was investigated for tests with

different release scenarios. The LNG fire control effect was studied through a large scale LNG pool fire field test conducted at Brayton Fire Training Field, College Station, TX. High expansion foam was applied to mitigate the fire after the fire was fully developed. The initial negative effect of foam application was minimized by using a new foam generator with a feature to prevent water discharge into the LNG pool. The mitigation effect was studied in terms of the mass burning rate, flame geometry, thermal radiation, burning velocity field, fire control time, and flame temperature. The foam application could reduce 75% of mass burning rate, 79% of flame length, and 97% of thermal radiation.

DEDICATION

The work is dedicated to my family for the endless support on everything in my life, and my beloved friends.

ACKNOWLEDGEMENTS

I would like to thank my advisor and committee chair, Dr. M. Sam Mannan for his guidance and support throughout the course of this research. I would like to extend my gratitude to my committee members, Dr. Charles Glover, Dr. Mahmoud El-Halwagi, and Dr. Debjyoti Banerjee for their suggestions and support on this research

I would like to thank my team leader, Dr. Yi Liu for this guidance and support. I also want to thank Dr. Delphine Laboureur for helping me with visualization techniques, Brian Harding for his effort working with me to build the foam generator and run numerous liquid nitrogen tests in the lab, Nirupama Gopalaswami for working with me in the LNG fire field test. Thanks also go to other members of Mary Kay O'Connor Process Safety Center (MKOPSC), especially those who were involved in the LNG pool fire field test.

Finally, I want to thank Dr. William S. Saric from the Department of Aerospace Engineering, Texas A&M University, for lending the IR cameras, and Dr. Jerrod W. Hofferth for filming the LNG pool fire test. Thanks also goes to Dr. Luc Vechot and Dr. Tomasz Olewski for providing the equipment and support in the tests conducted in Ras Laffan Industrial City, Qatar.

NOMENCLATURE

A	Area of heat transfer [m^2]
D	Characteristic length D (diameter of the pool) [m]
E	Effectiveness coefficient of foam in reducing heat transfer
g	Gravity [m/s^2]
h_{FC}	Heat transfer coefficient [$W/m^2 \cdot K$]
k	Thermal conductivity [$W/m \cdot K$]
L	Latent heat of liquid nitrogen at boiling temperature [kJ/kg]
L_{flame}	Flame length [m]
$\dot{m}$	Vaporization or burning rate [kg/s]
Nu	Nusselt number
Pr	Prandtl number
q_{Cond}	Heat flux of conduction [W/m^2]
q_{Conv}	Heat flux of convection [W/m^2]
q_{Rad}	Heat flux of radiation [W/m^2]
q_{NConv_N}	Heat flux of natural convection without foam [W/m^2]
q_{NConv_F}	Heat flux of natural convection with foam [W/m^2]
q_{FConv_N}	Heat flux of forced convection without foam [W/m^2]
q_{FConv_F}	Heat flux of forced convection with foam [W/m^2]
q_{Rad_N}	Heat flux of radiation without foam [W/m^2]
q_{Rad_F}	Heat flux of radiation with foam [W/m^2]

q^*_{IFoam}	Heat flux from foam at the initial application [W/m^2]
q_N	Heat flux into liquid nitrogen without foam [W/m^2]
q_F	Heat flux into liquid nitrogen with foam [W/m^2]
Q_N	Actual heat flux from convection and radiation [W/m^2]
Q_F	Apparent heat flux with foam [W/m^2]
R	Reduction factor
Re	Reynolds number
t	Time [s]
T	Temperature [K]
T_{air}	Air temperature [K]
T_b	Boiling temperature of liquid nitrogen [K]
T_{liquid}	Liquid temperature [K]
T_i	Initial temperature [K]
u	Wind velocity [m/s]
z	Depth of pit substrate [m]
α	Thermal diffusivity [m^2/s]
ρ_a	Air density [kg/m^3]

TABLE OF CONTENTS

Page

LIST OF FIGURES

Page

LIST OF TABLES

Page

1. INTRODUCTION

1.1 Introduction

The global demand on energy keeps increasing with a growing world population and economic development. World Energy Outlook predicts a 37% growth on energy demand by 2040 [1]. Natural gas will continue to be one of the major energy sources together with oil and coal. The natural gas demand increases by more than 50 %, which is the fasted growing rate among all the fossil fuels [1]. With the goal of limiting emissions as required by the regulations, the power stations in the United States are shifting to natural gas for the electricity generation, since it is believed as the cleanest fuel. The production of natural gas grows in most regions of the world to meet the demand. The development and application of new technologies, *e.g.*, horizontal drilling and hydraulic fracturing, allows to produce the shale gas, which is conventionally impossible. The Liquefied Natural Gas (LNG) promotes the inter-regional trade with a concentrated energy density. The use of LNG enhances the availability, but also rises a concern on the safety of the handling.

The LNG accident in Cleveland in 1944 brought the attention on LNG hazards, which killed 130 people due to fire and explosion after a vapor release from a LNG storage tank [2]. Since then, the gas industry has evolved in terms of the safety, but also the complexity of the LNG supply chain. For the onshore gas industry, the production of shale gas requires more liquefaction facilities and LNG storage tanks, and put more LNG transportation trucks on the road. The LNG import terminals have been turning

into the export terminals, since the gas production is surpassing the gas consumption in the United States. For the offshore gas industry, LNG carriers have been popular for the inter-regional transportation. The recent development of the Floating Liquefied Natural Gas (FLNG) introduces a new opportunity for LNG production as well as a challenge for safe operation. The response to these challenges tends to produce more regulations, standards and guidelines, which demand a better understanding of the LNG hazards and the safety measures for the hazards mitigation. A review of current understanding serves as a basis for a furfure study on the LNG hazards mitigation.

1.2 LNG

1.2.1 Natural gas

Natural gas is a major fossil fuel, which consists mainly methane and other components as described in Table 1. It can be used directly as an energy source for the daily use; it can be used to generate electricity in the power station; and it can be used as a feedstock in the chemical industry.

There is an abundance of natural gas reserves from three major sources, associated gas in the oil field, non-associated gas in the natural gas field, and coalbed methane. The proven natural gas reserves for each country vary from sources. Table 2 shows the top five countries in terms of proven natural gas reserves based on The World Factbook.

Table 1 Typical composition of natural gas [3]

Methane	CH_4	70-90%
Ethane	C_2H_6	20%
Propane	C_3H_8	
Butane	C_4H_{10}	
Carbon Dioxide	CO_2	0-8%
Oxygen	O_2	0-0.2%
Nitrogen	N_2	0-5%
Hydrogen sulphide	H_2S	0-5%
Rare gases	A,He,Ne,Xe	trace

Table 2 Natural gas proven reserves [4]

Rank	Country	Volume (billion cubic meter)	Date of information
1	Russia	47,800	1 January 2013 est.
2	Iran	33,610	1 January 2013 est.
3	Qatar	25,200	1 January 2013 est.
4	Turkmenistan	17,500	1 January 2013 est.
5	United States	9,459	1 January 2012 est.

Natural gas costs little compared with other fuels. Figure 1 shows the comparison of the spot price for crude oil and natural gas normalized by the energy generated. The crude oil price was seven times of the natural gas price in 2012. The natural gas price will remain lower than that of crude oil as the natural gas prices increases in the next 25 years.

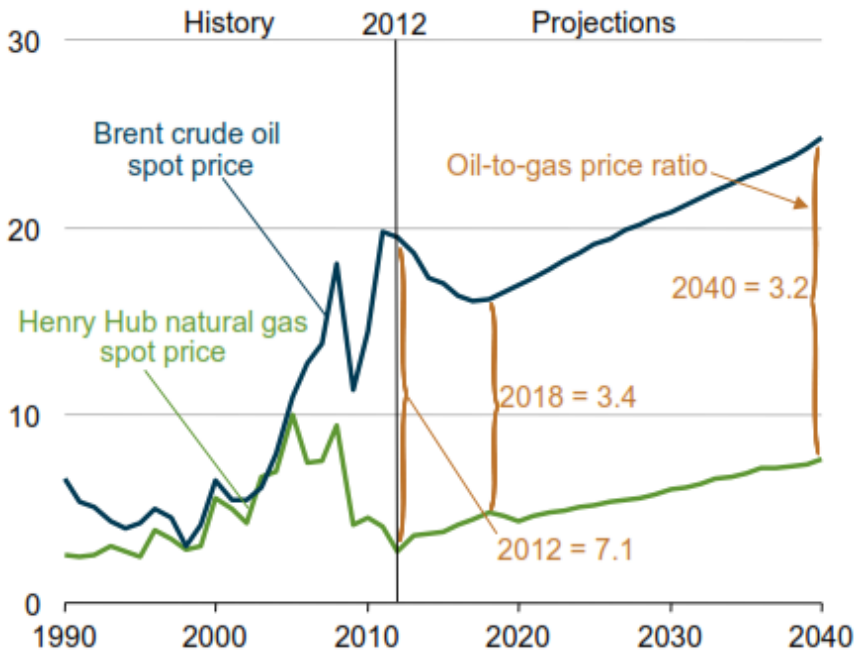

Figure 1 Comparison of spot prices for crude oil and natural gas. (2012 dollars per million Btu) [5]

Natural gas use is expected to rise due to the abundance of the natural gas reserves and low price. Figure 2 shows the example of the energy use in the US. Natural gas is one of the major fuels in U.S. The share of natural gas use was 27% in 2012, and will jump to 30% in 2040. The use of petroleum and other liquids will drop down to 31% in 2040. By then, natural gas together with petroleum and other liquids will account for 61% of the energy use. With respect to power generation sector, the use of the natural gas for electricity generation will significantly increase, while the use of the coal and nuclear will remain relatively stable as shown in Figure 3.

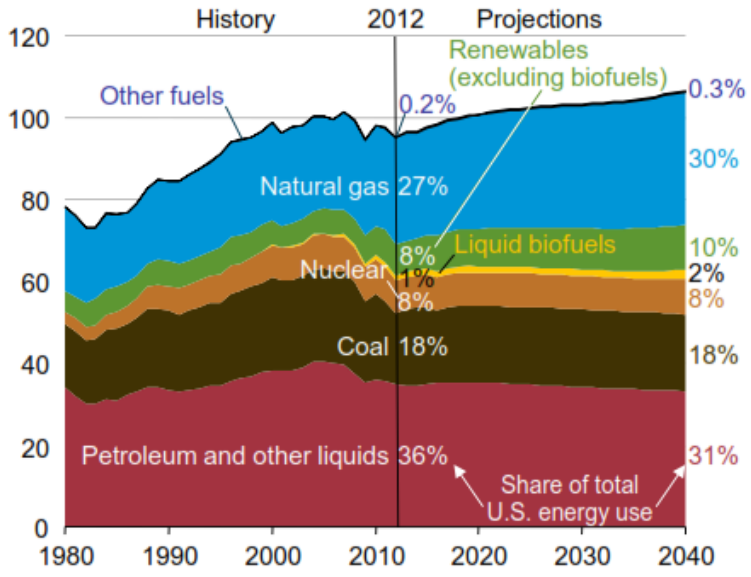

Figure 2 Primary energy use by fuel in the U.S. (quadrillion Btu) [5]

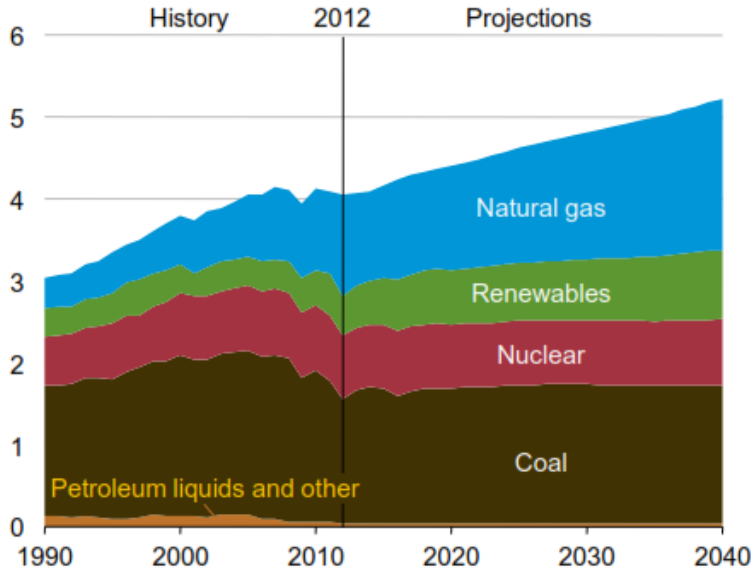

Figure 3 Electricity generation by fuel in U.S. (trillion kilowatthours) [5]

With the growing use of the natural gas, the production of natural gas is increasing to maintain the supply and demand balance. The production of natural gas will increase significantly, among which much of the production is from the unconventional sources, tight gas and shale gas as shown in Figure 4. The latest progress of technologies, *i.e.*, horizontal drilling and hydraulic fracturing, booms the production of shale gas, which was not possible due to the poor permeability of the shale formation.

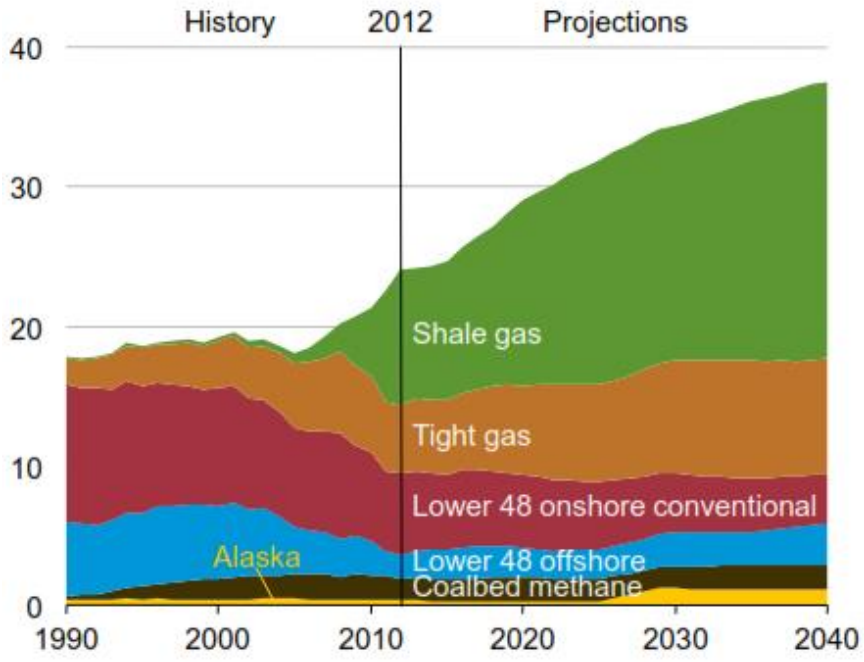

Figure 4 U.S. natural gas production by source (trillion cubic feet) [5]

The production of natural gas is expected to surpass the consumption in near future in the U.S. Therefore, some of the existing LNG import terminals have been authorized to re-export delivered LNG, including Freeport, TX, Sabine, LA, Hackberry, LA [6]. Additional import and export terminals have been approved by Federal Energy

Regulatory Commission (FERC), The United States Maritime Administration (MARAD) and United States Coast Guard (USCG) as shown in Figure 5.

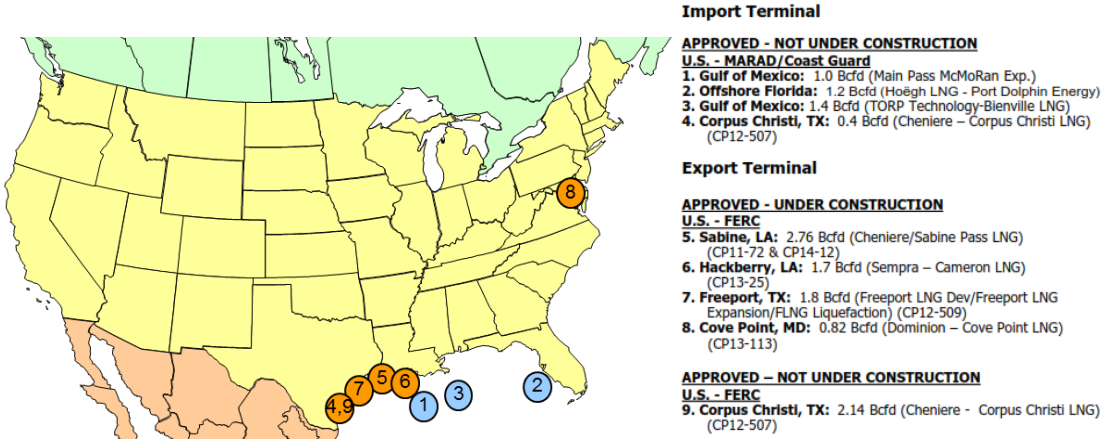

Figure 5 LNG import and export terminal in the U.S. [6]

1.2.2 Liquefied natural gas (LNG)

Liquefied natural gas (LNG) is a liquid form of natural gas. The liquefaction process involves cooling natural gas to approximately -162 ˚C at the atmospheric pressure. LNG forms at a result of the condensation of natural gas. The volume reduces approximately 600 time in this process; therefore, the energy density of LNG is increased, which makes it economically feasible to store LNG in the tank and transport LNG to locations where pipelines are not available.

The liquefaction process requires a purification process to remove certain components before the liquefaction process to produce LNG, which makes LNG has a higher methane concentration. The typical LNG produced at a peak shaving plant

contains about 95% of methane, while Refrigerated Liquid Methane (RLM), a kind of highly purified LNG, can contain up to 99% of methane.

Several processes are available for the liquefaction of natural gas, including Nitrogen expander cycles, Cascade process, Single mixed refrigerant process (SMR), Precooled MR processes, which were compared by Bronfenbrenner et al [7]. The propane precooled MR process (C3MR) stands out among the other processes because of its versatility to meet various existing and new challenges, *e.g.*, demand for large train capacity, monetization of natural gas resource in cold climate and higher demand for LNG with a lower heating value and Wobbe Index [8].

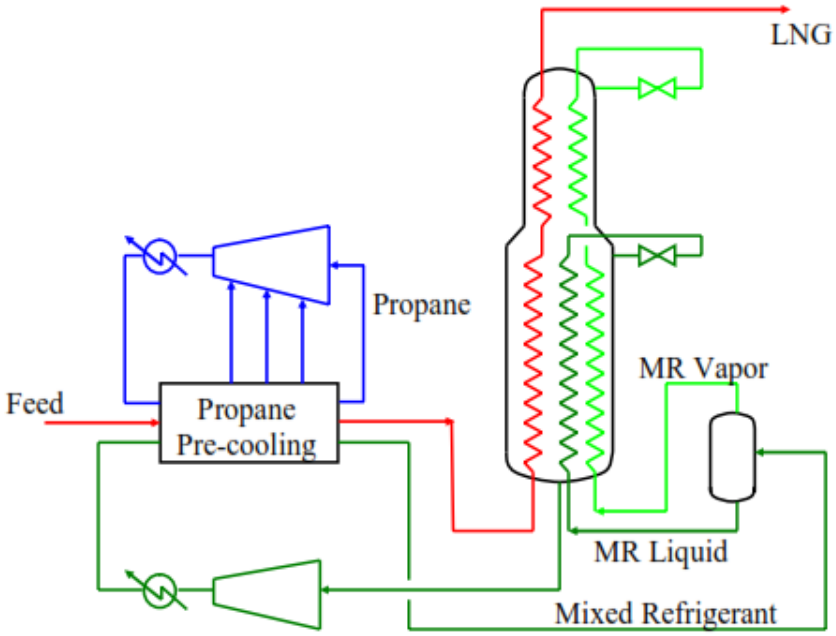

Figure 6 Propane pre-cooled mixed refrigerant (C3MR) process [8]

A schematic diagram of the C3MR process is shown in Figure 6. The C3MR train capacity is more than 5 million tons per annum (MTA) with a single main cryogenic heat exchanger (MCHE); The C3MR process together with alternative pre-cooling fluids accommodates the need to produce LNG in cold climates; Low heating LNG can be achieved in C3MR process with the integration of NGL/LPG recovery with various feed conditions.

LNG is stored in the storage tank before it is loaded in carriers for shipment at the liquefaction facilities or distributed through pipelines to end users at the import terminals. There are floating storage tanks at the offshore receiving terminals; however, LNG is mainly stored in the onshore storage tanks. The existing onshore storage tanks include single containment tank, double containment tank, full containment tank, membrane tank and in-ground tank [9]. Membrane tanks are mainly built in France and South Korea. In-ground tanks are popular in Japan and other Asian countries, where land is very limited and expensive. Single containment tank and full containment tank are introduced below, since they are widely used worldwide.

Single containment tank, as shown in Figure 7, is most used currently because of its proven reliability in the past. Single containment tank has one inner tank and one outer tank, but only the inner cylindrical tank is able to contain the LNG, which is made of 9% nickel steel to withstand the low temperature of cryogenic liquid. The outer tank, which is made of carbon steel, aims to hold the insulating material in the annular space between tow tanks. Single containment tank requires a surrounding dike as the secondary containment, which can contain a least 100% of the tank storage capacity in

case of a complete failure of the tank. Because of the requirement of constructing the dike, single containment tank need a larger area of land.

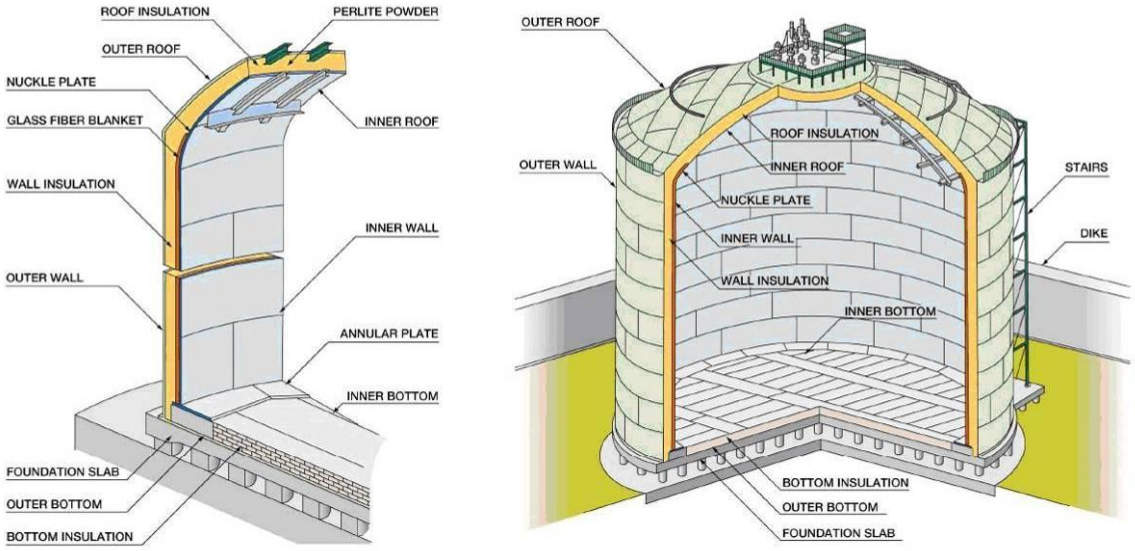

Figure 7 LNG single containment tank. (Source: Kawasaki Heavy Industries, Ltd.) [9]

Full containment tank is one kind of double containment tank. They both have the second containment when the inner tank fails. The difference is that the double containment tank has the wall made of post-stressed concrete for the outer tank, which can contain the liquid in case of the loss of primary containment, but leave the vapor to escape. The full containment tank has the wall made of pre-stressed concrete for the outer tank. The annular space between two tanks is sealed as shown in Figure 8; therefore, the second containment can keep both vapor and liquid in a normal condition.

The full containment tank accounts for most LNG storage tanks built in the past ten years worldwide [9].

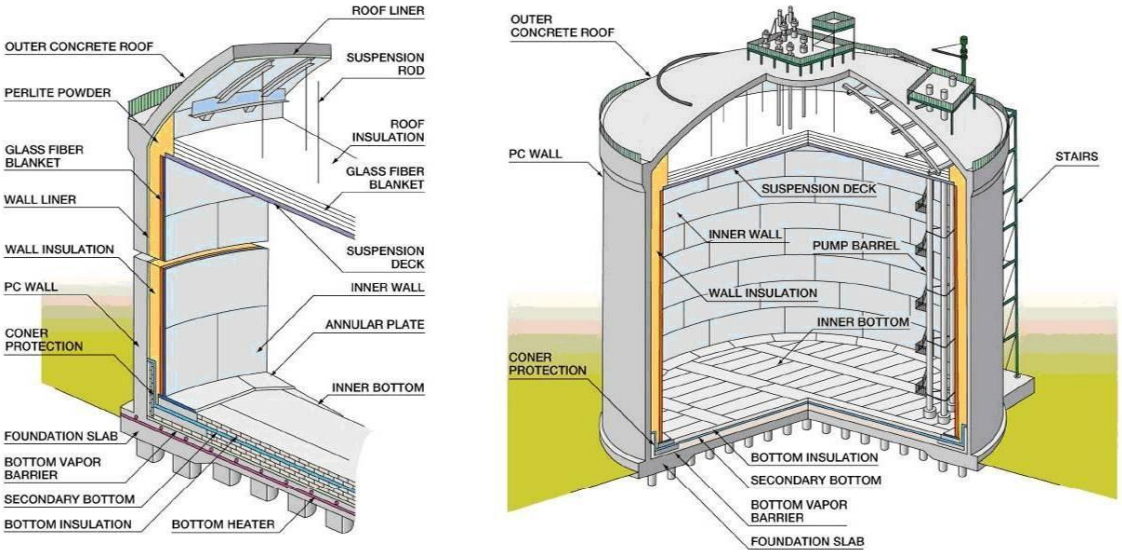

Figure 8 LNG full containment tank. (Source: Kawasaki Heavy Industries, Ltd.) [9]

1.2.3 LNG hazards

The spill of LNG can result in several hazardous scenarios, mainly because LNG has a low boiling temperature; and it is flammable when mixing with air by a certain ratio after the vaporization. The cryogenic hazards, vapor hazards and fire hazards are discussed below.

The cryogenic hazard of LNG is the cryogenic burns. LNG is a cryogenic liquid with a boiling temperature of -162 ˚C. The spilled LNG liquid will remain at the boiling temperature before it vaporizes. The direct exposure to LNG can result in cryogenic burns to skins and bodies contacting the cryogenic liquid. The cryogenic burns can be

caused by the exposure to the cold vapor, but with a much slower rate. Also, it is possible for personnel to escape from the cold vapor before any injuries. Proper personal protective equipment can be used to reduce the risk caused by an accidental exposure to LNG.

LNG will vaporize to cause vapor hazards after it is spilled. The huge temperature difference between the ambient and the LNG results in a vigorous vaporization. The LNG vapor volume is 600 times of that in a liquid form. The LNG vapor has a higher density than ambient air (at 15 ˚C) when the vapor temperature is below -114 ˚C. Therefore, the vaporization of LNG will result in a much larger vapor cloud than the liquid LNG pool. The vapor cloud will stay at the ground level and travel to a long distance in the downwind direction before it is heated enough to have a higher buoyance than the ambient air. The vapor cloud can cause cryogenic burns and asphyxiation. The risk is much higher once the vapor cloud is ignited at a concentration approximately from 5% to 15% in the air. In an open filed, the ignition will cause a flash fire. The fire will flash back the liquid pool and end up with a pool fire. In a confined space, the ignition may cause a vapor cloud explosion (VCE). The early detection of a release is important; however, the low temperature of LNG makes it difficult to add an odorant.

The thermal hazard is the primary concern of LNG fire hazards. A pool fire is more severe than a flash fire, because it emits more heat and lasts a longer period of time. The pool formation is an important factor to demine the pool fire hazard. The pool spreading determines the size of the liquid pool, which has a significant impact on the

mass burning rate, therefore, the total combustion heat of the fire. A portion of the total heat emits through radiation to cause a thermal hazard.

1.2.4 Hazards mitigation techniques

A number of the techniques have been tested regarding to the mitigation effects on LNG vapor hazards and fire hazards, including high expansion foam, dry chemicals, Foamglas® and water curtain [10–17].

High expansion foam has been proven to be effective to control both vapor hazards and fire hazards experimentally [12, 14–17]. The mitigation mechanisms are mainly based theoretical understanding. High expansion foam is an aqueous foam with expansion ratio ranging from 200 to up to 1000. When it is applied into the dike containing LNG, a foam blanket will be formed on top of the LNG pool. In the vapor dispersion scenario, the foam blanket helps to reduce the vaporization rate by blocking the heat from convection and radiation, and increase the LNG vapor buoyance by heating the vapor passing through the foam zone. In the pool fire scenario, the foam blanket contribute to reducing the mass burning rate by blocking the flame back radiation to the LNG pool. Therefore, the total heat of the fire is reduced, so is the thermal hazard. The cooling effect and oxygen dilution effect provided the vaporization of water in the foam also contribute to reducing thermal radiation of the reduced flame.

Dry chemicals for LNG application is a Potassium Bicarbonate based fine powder. It can be used to extinguish the LNG pool fire in combination with high expansion foam application. The high expansion foam application can significantly reduce the heat for an LNG fire, so that the fire fighter can approach the fire to use dry

chemicals. The dry chemicals functions to extinguish the fire by interfering the chemical chain reaction in the combustion zone of a liquid fire.

Foamglas® is a specially formulated cellular glass, which has a number of features suitable for an LNG pool fire suppression [18]. The glass cube is not flammable and has a very low density. Therefore, it can float in the LNG pool to behave as a blanket. Also, Foamglas® is very stable so that it can be put into the LNG dike as a passive safety measure before there is an LNG release. Previous work by Suardin et.al, has proved that Foamglas® system is an effective measure for LNG fire suppression, but not ideal for the LNG vapor control [13].

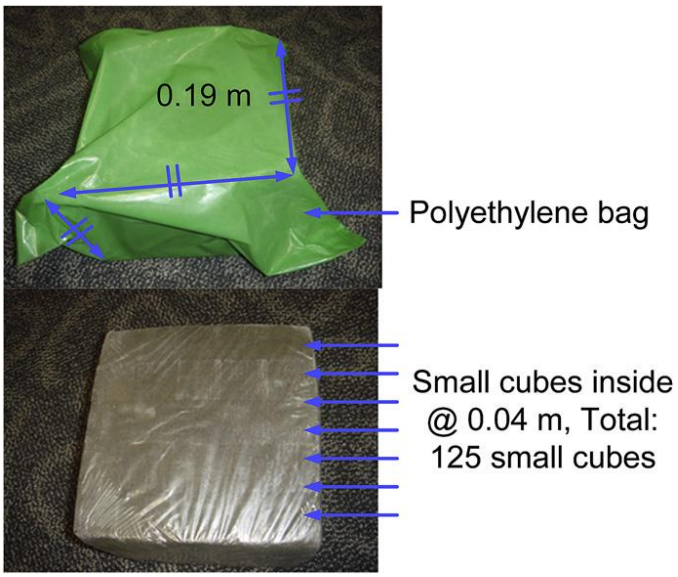

Figure 9 Foamglas® block [13]

Water curtain is a safety measure to control LNG vapor. The water curtain is generated by spraying water through various nozzles, which can enhance the LNG vapor

dispersion through three mechanisms, vapor dilution with entrained air, heat transfer to increase vapor buoyancy, momentum transfer to push vapor upward [10, 11].

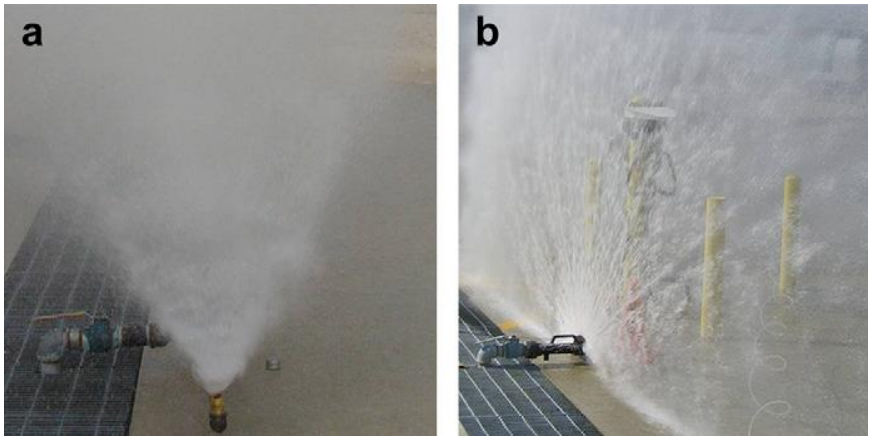

Figure 10 Water curtain by various nozzles. (a) full cone spray nozzle, (b) flat fan spray nozzle [10]

1.3 Expansion foam

1.3.1 Introduction

Expansion foam is one of the firefighting foams, which is an unstable medium consisting of air bubbles, foam concentrate and water. Expansion foam was invented in early 1950s. Herbert Eisner at the Safety in Mines Research Establishment (now Health& Safety Laboratory) in England proposed the idea of high expansion foam for coal mine firefighting. Later, Will B. Jamison together with US bureau of Mines continued to conduct this work. At least 400 formulas were tested before it was patented with a suitable chemical. In 1964, the patents of high expansion foam were bought by Walter Kidde & Company (now Kidde) [19].

Expansion foam is classified by the expansion ratio, which is the volumetric ratio between foam and the foam solution required to produce the same amount of foam. NPFA 11 defines high expansion foam as the foam with 200 or up expansion ratio as shown in Table 3.

Table 3 Expansion foam classification [20]

Expansion foam type	Expansion ratio
Low expansion foam	0-20
Medium expansion foam	20-200
High expansion foam	200-1000 or more

1.3.2 Expansion foam application

High expansion foam has some special features which shape the applicable areas of high expansion foam. With the same amount of foam solution, the volume of produced high expansion foam is much larger than that of low and medium expansion foam as shown in Figure 11, which makes it perfect to fight fires in an enclosed space, such as, warehouse, aircraft hangars, mines, and shipboard. The high expansion foam will rapidly takes up the space and displace the air and fuel vapor. In addition, high expansion foam is applied for the liquid fires, including LNG. Since the expansion ratio is very high, the water content per volume of foam is quite low. High expansion is referred as “dry foam” in some cases. There is minimized concern on the introduction of water into the liquid fuel pool, which may cause boilover for petroleum pool fires, or escalate the LNG fires. High expansion foam can be used as a vapor barrier for spilled

hazardous chemicals. It becomes more popular for mitigating vapor of LNG spills. Since high expansion foam can quickly form a foam blanket on top of the pool with little concern of water introduction, since it is very “dry”.

Figure 11 High and medium expansion foam

1.3.3 Foam generation

The foam generation process involves properly mixing foam concentrate, water and air with a certain proportion of each component. First step is to mix foam concentrate with water with a specified ratio to obtain the foam solution. Then, the air is introduced into the foam solution through proper agitation to generate foam with various expansion ratio, which is determined by the air volume per volume of foam solution. In order to achieve the foam generation process, different approaches are taken for a small scale academic purpose and a big scale industrial purpose.

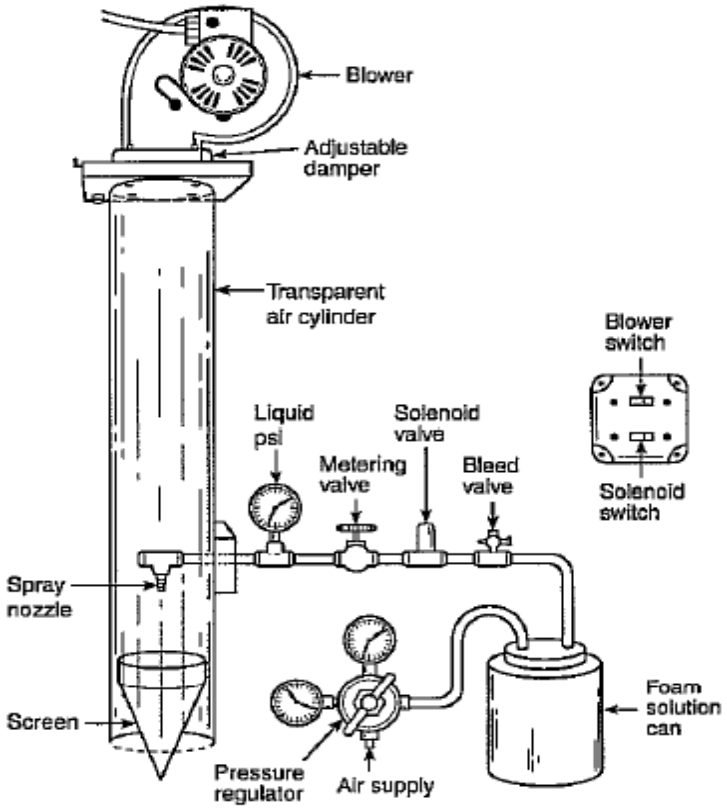

Figure 12 Schematic diagram of a foam generator from NFPA 11 [20]

NFPA 11 provides a schematic design of a foam generator for academic purpose as shown in Figure 12. In this design, the foam solution is premixed by diluting foam concentrate with water. The foam solution is stored in a tank with a tube connecting pressurized air and another tube to direct the solution to the spray nozzle. Since the system relies on the pressure from the air to push the foam solution during the operation process, the foam solution tank must be air tight and strong enough to withstand the maximum pressure that the system requires. Along the pipe from the tank to the spray nozzle, there are a number valves and one pressure gauge. The metering valve is used to

control the flow rate of the foam solution. The solenoid valve is a safety measure to remotely control the flow. The bleed valve is used to vent the pressure in the system when it is needed. The pressure gauge is an indicator of the pressure before the foam solution is sprayed through the nozzle. After leaving the nozzle, the foam solution will end up with wetting the screen at the bottom end of a vertical cylinder. At the top end the cylinder, a blower is installed with a damper in front of the air outlet. The air flow provided by the blower will be controlled by the damper in terms of the flow rate. The air flows along the cylinder, which will be entrained in the foam solution at the screen, which is the "agitation". The foam is produced when the foam solution leaves the screen with entrained air.

Industrial foam generators usually take advantage of flowing water to power the foam generator, including driving the blower fan and mixing foam concentrate with water as shown in Figure 13. Before the foam solution arrives at the inlet of the foam generator, a proportioning system is used to mix the foam concentrate and water. For instance, the recommended proportioning system for JET-X high-expansion foam generators is the balanced type consisting of a bladder tank and proportioner, which can accurately prepare the foam solution with minimal loss of water pressure [21]. Once the foam solution reach the foam generator, it drives the blower fan to provide air flow and spray the foam solution onto the foam screen. Similarly, the agitation is finished when the air flows through the screen entrained in the foam. A JET-X-15A (LNG) foam generator is shown Figure 14 with the foam produced.

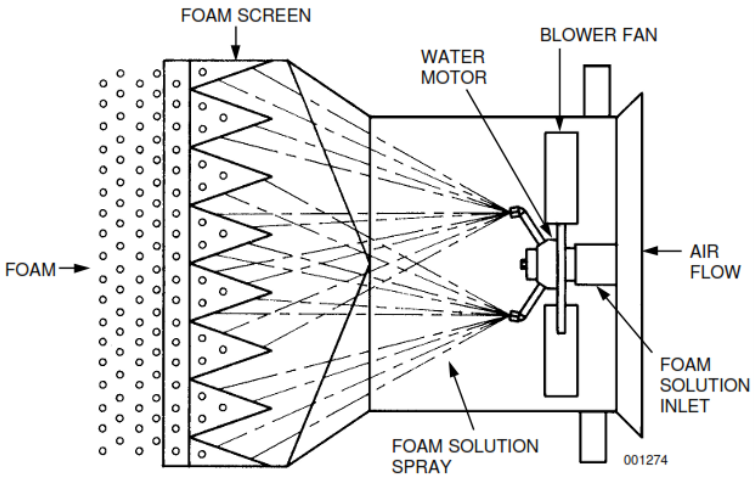

Figure 13 JET-X high-expansion foam generators schematic diagram [21]

Figure 14 High expansion foam generation with JET-X-15A (LNG)

2. PROPOSED PROBLEMS

2.1 Introduction

The hazards of an LNG spill have been studied experimentally and theoretically [22–30], as well as the mitigation effects of the high expansion foam [12, 14–17]. This section will identify the vapor hazards and fire hazards of an LNG spill on land, summarize the previous work regarding to the mitigation effects of the high expansion foam application and propose the problems that this work will address.

2.2 Vapor hazard mitigation

2.2.1 American Gas Association

American Gas Association sponsored University Engineers Inc. on a number of LNG tests in 1970s [15]. One scope of the project was to study the mitigation effect of high expansion foam on vapor dispersion control at high vaporization rate. LNG vapor dispersion tests were conducted for spills into pans of 5 ft. and 10 ft. in diameters. After high expansion foam application, the LNG vapor concentration was reduced by 80% at a distance of one pool diameter. It was found that expansion ratio is the only factor to affect the methane concentration in the downwind direction. Expansion foam with 1000 expansion ratio had a better performance than that with 500 expansion ratio in terms of vapor concentration reduction. The vaporization rate of LNG was increased by the high expansion foam application, that is the boil-off effect, but it was small in absolute terms. The unwanted boil-off effect was less significant for foam with 750 expansion ratio than

those with 1000 and 500. The warming effect of the foam provided by the water content helped to increase the vapor buoyance and reduce the vapor concentration at the ground level, even though the vaporization was increased by the boil-off effect.

2.2.2 Takeno's work

Takeno and the collaborators conducted experimental work to study the effect of high expansion foam on vaporized cryogenic gas dispersion [14]. The tests were conducted in the two experimental setups with liquid nitrogen.

The setup shown in Figure 15 was used to study the effect of high expansion foam on warming the cryogenic vapor evolving from the liquid pool. The bottom was the container for liquid nitrogen with a shield curtain above to held high expansion foam. The setup was large enough to install thermocouples in the foam zone above the liquid pool. The high expansion foam was applied in batch mode and semi-batch mode that means foam was replied when the height of foam blanket was reduced to half of the curtain height. The flow paths of vaporized vapor were observed during the tests. The temperature measurement proved that the vapor temperature was increased by warming effect of high expansion foam through heat transfer between foam and vapor.

The setup shown in Figure 16 was used to study the boil-off effect of high expansion foam. This setup consisted of a load cell to measure the mass of liquid nitrogen. Since the water content in the foam was a heat source due to its huge temperature difference from that of the liquid nitrogen, the foam application increased the vaporization rate of the liquid nitrogen, which is the boil-off effect. In this work, a

heat transfer model was developed to predict the boil-off effect, which was compared with the experimental measurement.

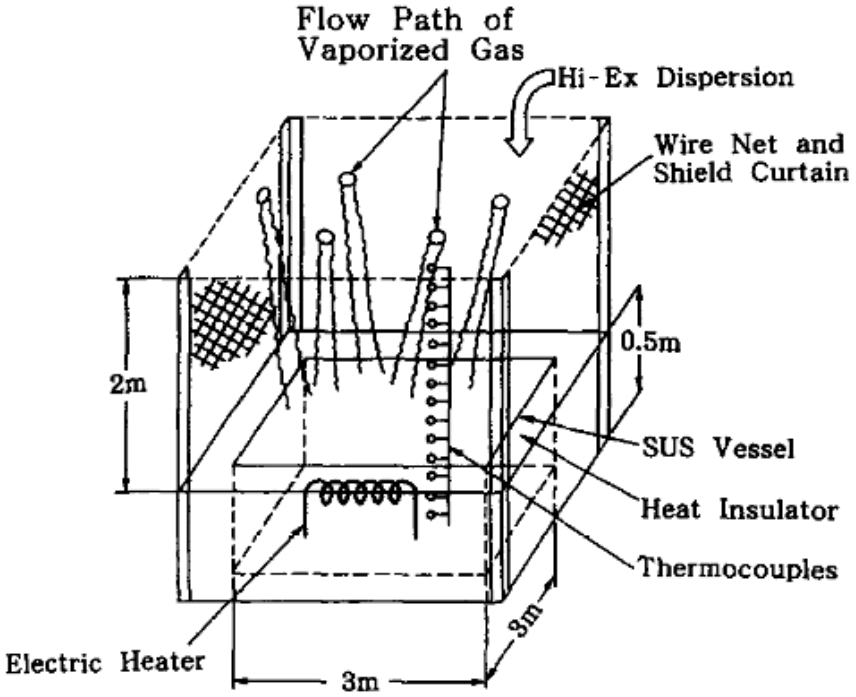

Figure 15 Experimental setup to study the warming effect of high expansion foam on cryogenic vapor [14]

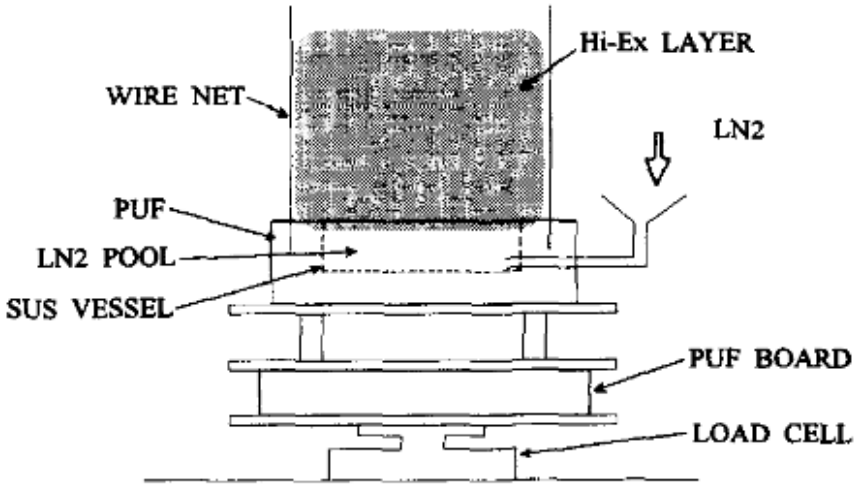

Figure 16 Experimental setup to study the boil-off effect of high expansion foam on cryogenic liquid pool [14]

2.2.3 Mary Kay O'Connor Process Safety Center

Mary Kay O'Connor Process Safety Center (MKOPSC) has conducted several series of field tests at Brayton Fire Training Filed (BFTF) at College Station, TX, USA. One series of tests were conducted to study the high expansion foam application for vapor hazards mitigation [16].

Yun studied the mitigation effect of high expansion foam on LNG vapor dispersion through a small scale field test and a large scale field test [16]. The small scale setup consisted an LNG container with a dimension of 0.91m x 0.91m x 0.61m. The transparent box above the container could hold the foam up to 1.83m. During the test, the transparent box allowed the observation of foam collapse and the physical interaction between foam and LNG as shown in Figure 17. The high expansion foam begun to collapse once it was applied on top the LNG pool. The collapse rate was

determined by the foam height with time. The rate was 0.17 m^3/min at the beginning and was reduced to 0.05 m^3/min after 11 min. When the LNG vapor evolved from the bottom, there was an interaction with foam before it escaped from the top of foam blanket. The vapor flow pushed the foam to form a channel. The heat transfer between cryogenic vapor and water in the foam froze the wall along the channels as the ice passages.

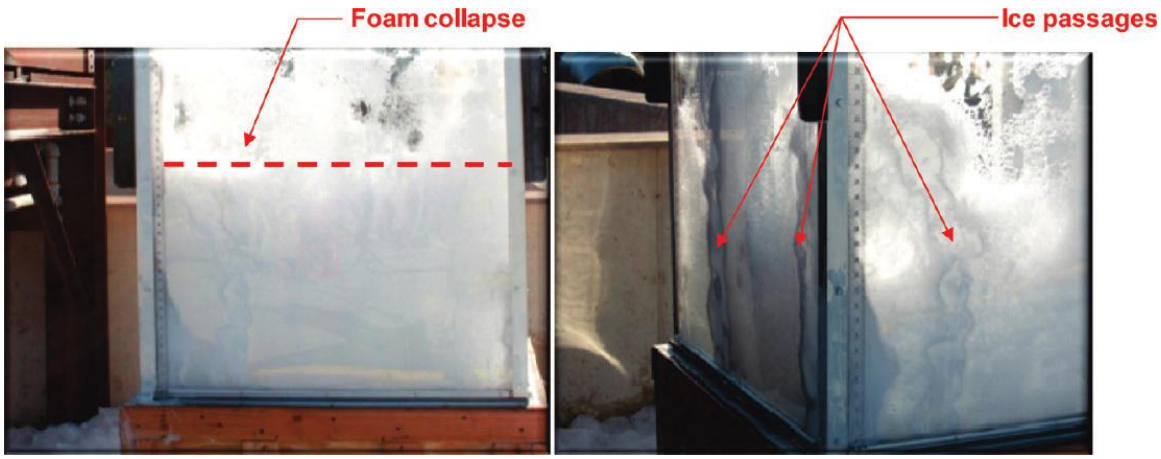

Figure 17 Foam collapse and the formation of ice passages [16]

The large scale test were conducted in the big pit with a dimension of 10.1m x 6.7m x 1.2m. Since an additional 1.2 m wooden fence was installed above the pit, foam was applied up to 2.4 m. The temperature profile was measured above the LNG pool. The measurement in the foam blanket and above the foam blanket were showing different trends. However, both measurement indicated that foam application increased the vaporization rate at the beginning due to the direct water discharge into the pool, but contributed to increasing vapor temperature to enhance the vapor dispersion upwards to

the air. As a result, the LFL and ½ LFL distance were significantly reduced at the ground level as shown in Figure 18, which were 89% reduction for LFL and 80% reduction for ½ LFL.

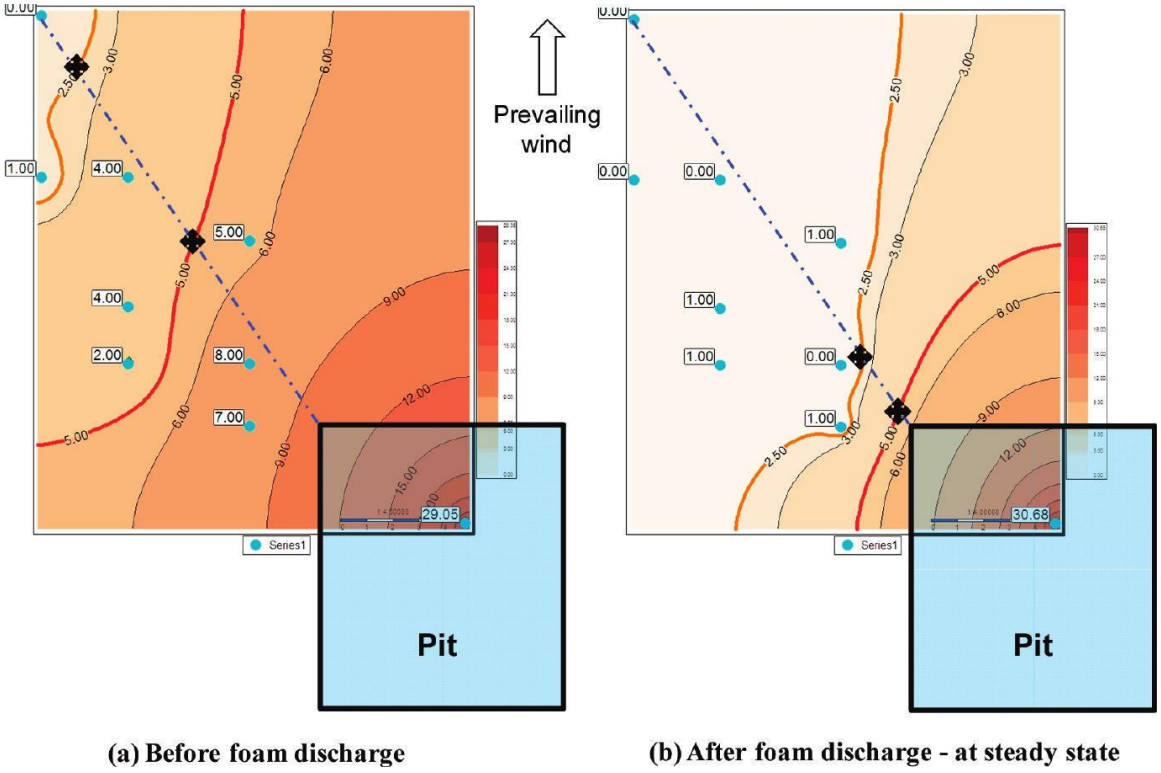

Figure 18 Methane vapor concentration contour in vapor dispersion test [16]

2.3 Pool fire control

2.3.1 American Gas Association

University Engineers Inc. also conducted LNG fire tests with high expansion foam application at high burning rates in 1970s. The burning rates of LNG pool fires were up to 1.5 in/min. The expansion foam with 500 expansion ratio was identified to

provide the best performance for fire control in both crosswind and downwind direction as shown in Figure 19 and Figure 20. With high quality and small bubble foam application, the thermal radiation of the LNG pool fire was reduced by more than 95% at a distance of one pool diameter. The foam had a burn back resistance, which means once the fire is controlled, it can be maintained by a lower foam application rate, especially for the small bubble foam.

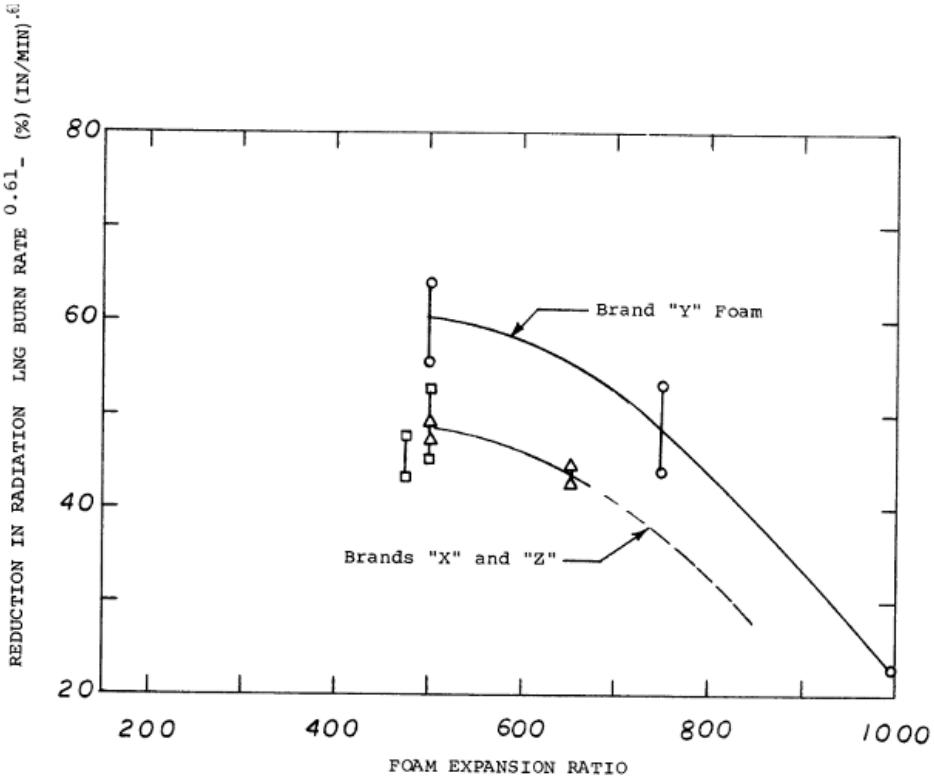

Figure 19 Effect of foam expansion ratio on radiation reduction in crosswind direction [15]

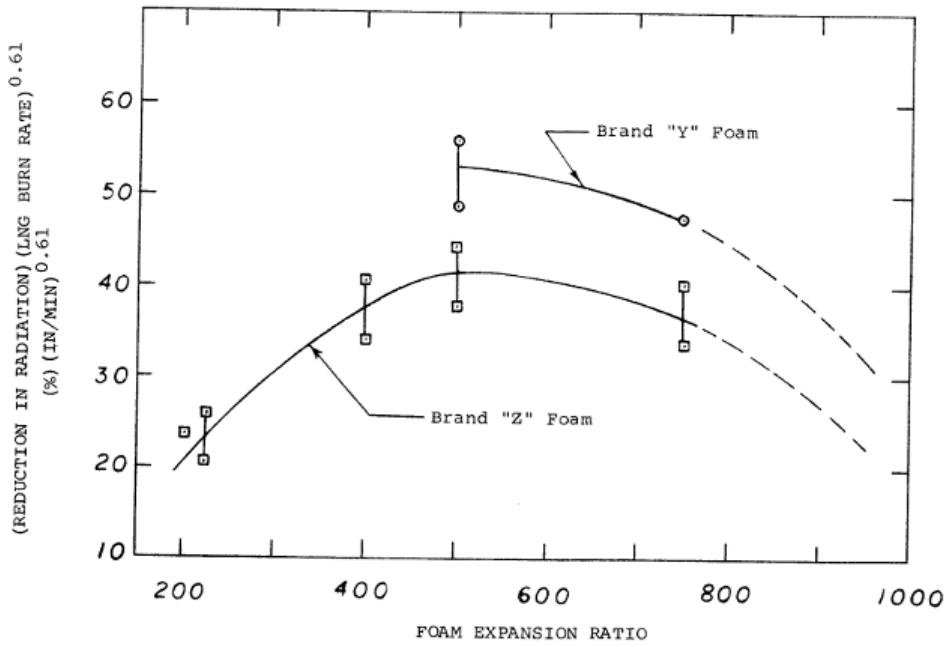

Figure 20 Effect of foam expansion ratio on radiation reduction in downwind direction [15]

2.3.2 Mary Kay O'Connor Process Safety Center

Mary Kay O'Connor Process Safety Center (MKOPSC) has conducted several series of field tests at Brayton Fire Training Filed (BFTF) at College Station, TX, USA. Some tests studied the use of high expansion foam to control LNG pool fire, as well as other fire suppression system, such as Foamglas® [12, 13, 17].

Suardin primarily studied the control time of LNG pool fires after high expansion foam application [12]. The tests were conducted in two pits. The large pit was 10.1m long, 6.7 m wide, and 1.2 m high with no lip above the ground. The marine pit was 6.7m long, 6.7 m wide and 2.4 m high with 1.2 lip above the ground. The effect of foam application rate was investigated in the large LNG pit. The tests in the large pit were conducted with three different foam application rates. The LNG pool fire test with

higher foam application rate required less time to control the thermal hazard as shown in Figure 21. The marine pit need much longer time to control the fire, since it had a lip above the ground, which made it vulnerable to the burn back of the fire.

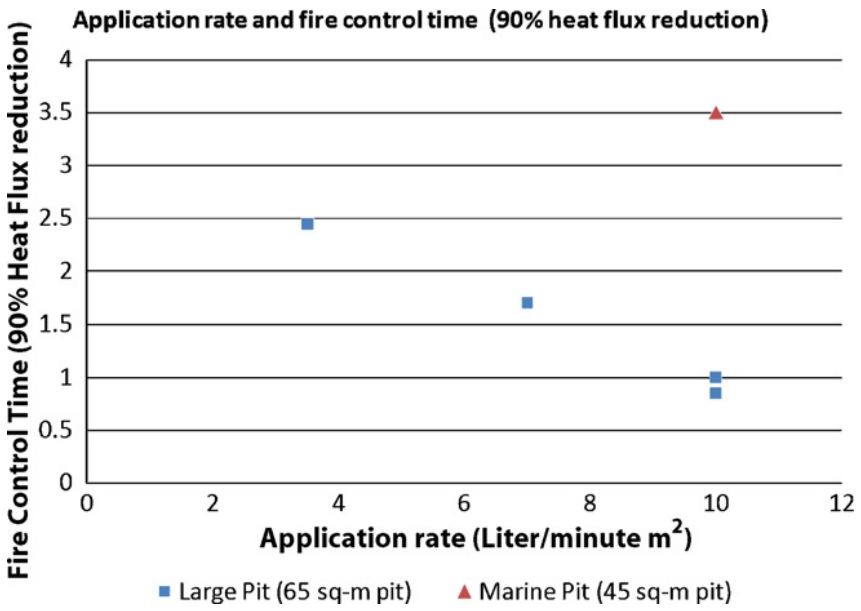

Figure 21 LNG pool fire control time with various foam application rates and pit configurations [12]

Yun also conducted two LNG pool fire tests in the large pit (65 m^2) with high expansion foam application [17]. A total of 166 thermocouples were used in these tests to provide three dimensional temperature profile in the foam blanket and above the foam blanket. More than 10 radiometers were installed at four directions surrounding the pit, which provided the contour the thermal exclusion zone in the test. As shown in the Figure 22, with 1.2 m foam application, the thermal hazard distances were reduced by 50% on average for four directions. However, the thermal hazard distances were slightly

increased right after the foam application for a few seconds, which was caused by the direct water discharge into the pool before the good quality foam was produced. In addition, the regular video camera was used to capture the flame geometry information in the tests. It was found that the radiation measurements were proportional with the flame length.

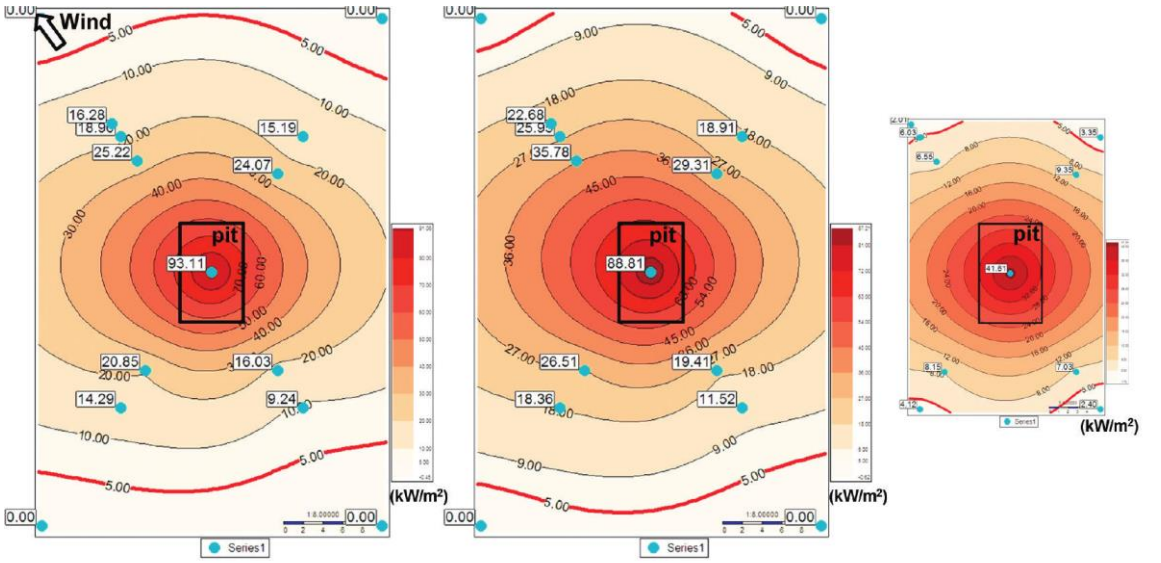

Figure 22 Reduction of LNG fire thermal exclusion zone with high expansion foam [17]

2.4 Proposed problems

2.4.1 Research gaps

There have been a number of experimental work since 1960s to study the vapor dispersion and pool fire hazards after an LNG spill, which were summarized by The Fire

Protection Research Foundation [31] and Raj [32]. These tests provided the information to enhance the understanding on these phenomena, and obtained data to develop and validate theoretical models. However, LNG spill tests with mitigation measures were very limited, which are essential to understand the mechanisms and physical interaction of the mitigation systems. With respect to high expansion foam application on LNG spills, previous work provided some findings, but also revealed some gaps for future study.

There was a misunderstanding on the mitigation mechanisms of high expansion foam on LNG vapor hazard. Previously, it was believed that high expansion foam could mitigate LNG vapor hazard by raising vapor temperature through warming effect; the boil-off effect of foam increased LNG vaporization rate, which was offset by the warming effect [33]. Takeno studied the boil-off effect of foam using liquid nitrogen. The experimental results were compared with the proposed model as shown in Figure 23. Since foam application will provide a foam blanket above the LNG pool, the foam blanket may have a blocking effect to block heat radiation and convection, which surpasses the boil-off effect. The blanketing effect of high expansion foam is the combination of blocking effect and boil-off effect, which has not been known to be existed, therefore not studied.

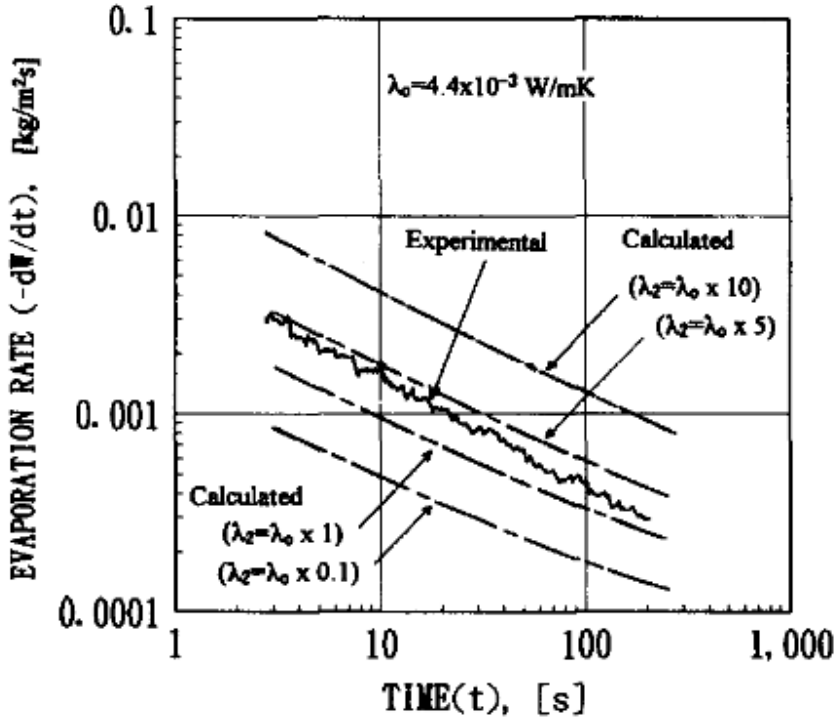

Figure 23 Boil-off effect of high expansion foam on liquid nitrogen pool [14]

There is a lack of understanding on the physical interaction between LNG and foam in the vapor hazard mitigation scenario. In large scale field tests, it is not possible to observe the physical interaction, since the potential LNG fire hazard prohibits people or device from being too close to the release location. Also, the concrete pit wall does not allow the observation on phenomena inside the pit. The physical interaction between LNG and foam includes the formation of vapor channel, foam breaking rate, warming effect of foam on LNG vapor.

The study of large scale LNG pool fires was limited in previous study, especially for LNG fire tests with high expansion foam application. Previous work on LNG fire mitigation using high expansion foam focused on the thermal radiation and mass burning

rate; while other aspects were rarely studied, *e.g.* flame geometry, flame velocity field and temperature distribution in the flame. In addition, it was found that high expansion foam application caused an initial negative effect in the old setup, which means the flame size was increased due to the initial water discharge before good foam was produced from the hydraulic foam generator. The initial negative effect requires a caution to use high expansion foam for LNG hazards control, since it may escalate the hazard if not used properly.

2.4.2 Research objectives

This work aims to experimentally study the mitigation effects of high expansion foam on LNG vapor hazard and pool fire hazard.

The mitigation effect of high expansion foam on LNG vapor hazard is shown schematically in Figure 24. The foam blanket on top of an LNG pool has several effects. There is a boil-off effect between the LNG pool and foam at the LNG-foam interface. The heat transfer between LNG and foam freezes the foam and boils LNG. The boil-off effect is not desirable, since it is a tradeoff of the mitigation effect by increasing the vaporization rate of LNG. The foam blanket can block the heat radiation and convection to reduce the vaporization rate, which is called as blocking effect. The combination of the boil-off effect and blocking effect is defined as the blanketing effect. The vapor evolving from the LNG pool passes through the foam blanket. There is heat transfer between the LNG vapor and the foam, which warms the vapor and freezes the foam along the vapor channel. The warming effect increases the vapor temperature, therefore, the vapor buoyancy, which enhances the vapor dispersion upward into atmosphere. With

all these effects of foam, the LNG vapor concentration will be reduced at the ground level for an LNG spill pool.

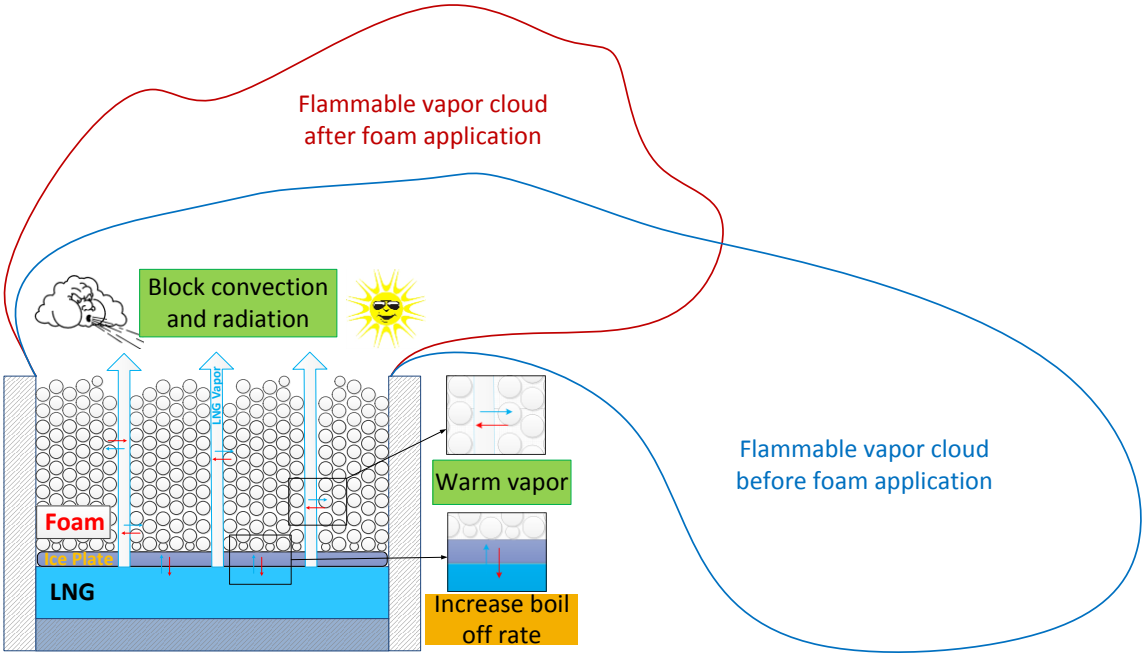

Figure 24 Mitigation effect of foam on LNG vapor hazard

The methodology of this study is shown in Figure 25. The vapor hazard mitigation tests will be conducted using liquid nitrogen, since liquid nitrogen is a safe analogue of LNG in terms of physical properties. The first part aims to study the blanketing effect on LNG vapor hazard, which is the effect on vaporization rate. This work will be conducted in a wind tunnel, where the radiation and convection can be provided by a bulb panel and a fan. The second part aims to study the warming effect of high expansion foam and the physical interaction of LNG and foam system. A new lab scale foam generator will be built based on the schematic design of NFPA 11. Some

improvements will be made to better meet the need for lab scale foam application tests. The warming effect will be studied through measurement of temperature profile in the foam blanket. A special design of thermocouple installation will be used to investigate the temperature difference between vapor and foam. The physical interaction of LNG and foam system will be studied by the observation of vapor channel formation and foam breaking rate.

The fire hazard control study will be conducted through an LNG pool fire test with high expansion foam application. A new type of industrial foam generator will be used for foam application, which has a large foam generation capacity and has a tray to collect the discharged foam solution before good foam is generated. The study will focus on the thermal radiation, mass burning rate and flame temperature. In addition, visualization techniques, *i.e.* video camera, IR camera, and high speed camera, will be used to study the flame size and flame velocity field.

At last, the findings in this work will be summarized, which can be used to provide recommendations for the industrial application of high expansion foam for LNG spill hazard mitigation during emergency response.

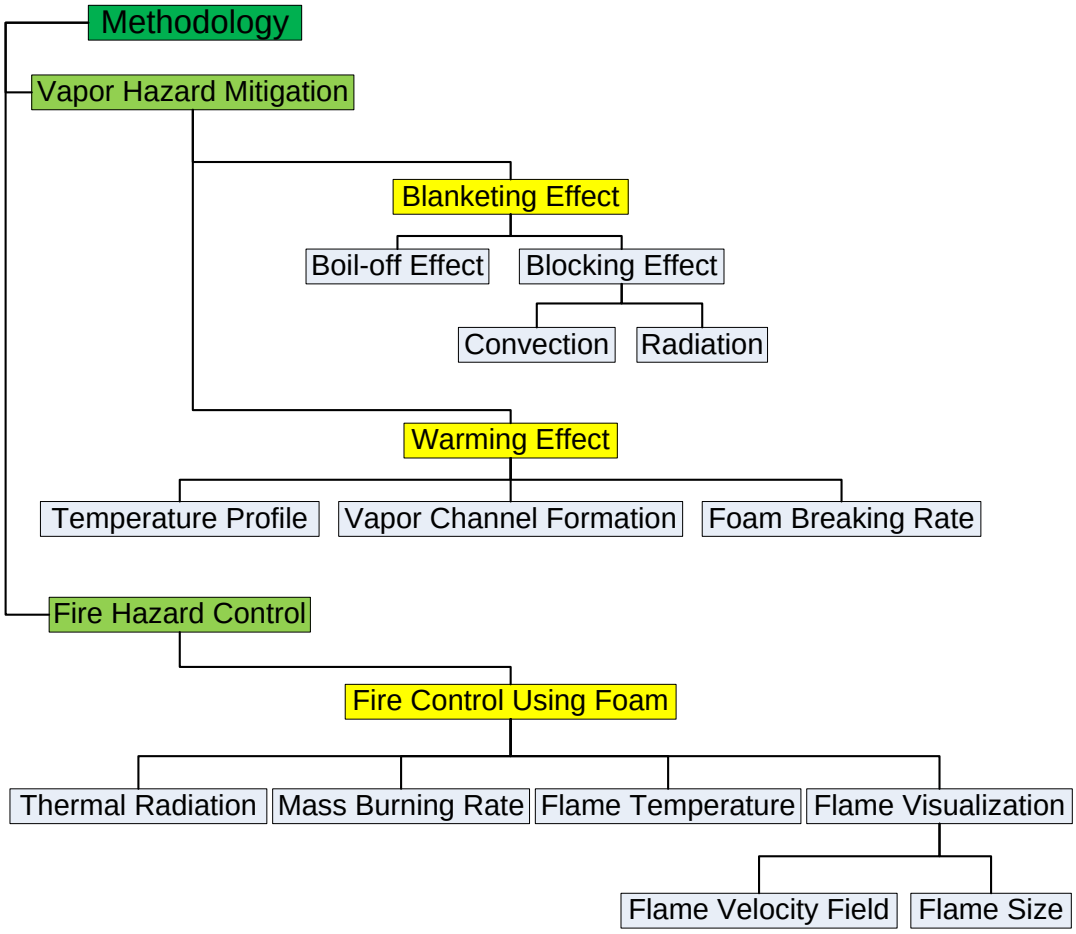

Figure 25 The methodology of high expansion foam research

3. BLANKETING EFFECT ON VAPOR HAZARD*

3.1 Introduction

Natural gas is a clean energy, because its combustion emits little sulfur dioxide, small amounts of nitrogen oxides, no ash, and much less carbon dioxide per unit of energy produced when compared with oil and coal [34]. Now, natural gas is the world's fastest-growing fossil fuel with a consumption growth projection of 5239 billion cubic meter in 2040 from 3200 billion cubic meter in 2010 [35].

Liquefied Natural Gas (LNG) facilitates the storage and transportation, but raises safety concerns in terms of vapor hazard and pool fire. Because of the cryogenic nature of LNG, an accidental release of LNG in massive volume can result in an LNG pool with continuous vaporization followed by the formation of an LNG vapor cloud. The high density of LNG vapor associated with low temperature makes it more likely to migrate in a downwind direction at the ground level, which causes a flammable vapor cloud as the vapor hazard. NFPA 59 A requires a thorough evaluation of potential consequences and the definition of an "exclusion zone" at LNG facilities to guide facility siting, and requires mitigation measures to reduce the risk to a tolerable level [36].

* Reprinted from Journal of Hazardous Materials, Volume 280, Bin Zhang, Yi Liu, Tomasz Olewski, Luc Vechot, M. Sam Mannan, Blanketing effect of expansion foam on liquefied natural gas (LNG) spillage pool, Pages 380–388, Copyright (2014), with permission from Elsevier.

High expansion foam has been recommended in NFPA 11 and NFPA 471 for LNG hazard mitigation [20, 37]. The vapor hazard of an LNG spill was believed to be mitigated by high expansion foam through warming effect [33], which is the heat transfer between foam and LNG vapor, to raise the vapor buoyancy and enhance vapor dispersion. The boil-off effect, defined as the heat transfer between foam and LNG liquid, offsets the mitigation effect by increasing the vaporization rate [33]. Since high expansion foam can generate a layer of foam blanket on the top of a liquid pool, the blocking effect is expected to reduce heat input to the pool for vaporization by blocking radiation and convection. The blanketing effect of foam on LNG vaporization is a combination of boil-off and blocking effect discussed above, and remains unclear.

In 1974, University Engineers Inc. conducted a series of vapor dispersion tests with an LNG spill on land. The effect of expansion foam on vapor dispersion was examined, and the vapor concentration can be reduced up to 80% during an LNG high boil-off period at a distance of one pool diameter of the spill [15]. In 1996, Takeno studied the ability of high expansion foam to raise the temperature of vaporized cryogenic gas; it was concluded that approximately 92% of the heat held in the applied foam was transferred into vapor to increase the buoyancy in this specific test [14]. Since 2005, Mary Kay O'Connor Process Safety Center has performed a series of LNG spill tests with high expansion foam at the Brayton Fire Training Field (BFTF) in College Station, TX, USA [12, 16, 17, 38]. Suardin confirmed the reduction of LNG vapor concentration at the ground level after high expansion foam application using a hydrocarbon camera [38]; Yun determined that foam application is effective for reducing

LFL distance by 89% [16]. The effectiveness of high expansion foam has been proven by these studies in terms of reducing downwind LNG vapor concentration or LFL distance. However, more work is required to study the mitigation mechanisms of high expansion foam and LNG system. With respect to the effect on vaporization rate, Takeno concluded that foam application acted as a heat source for vaporization, but the blocking effect of foam on convection and radiation was not studied [14].

Table 4 Properties of LNG and liquid nitrogen

Properties	LNG (methane)	Liquid nitrogen
Molar mass, g/mol	16.04	28.01
Boiling temperature, K	112	77
Liquid density at the boiling temperature, kg/m^3	423	808
Vapor density at the boiling temperature, kg/m^3	1.78 (at 113 K)	3.38 (at 78 K)
Latent heat of vaporization, kJ/kg	510	199
Heat capacity of gas at 0 ℃, kJ/kg ∙K	2.14	1.07

This work aims to experimentally study the blanketing effect of high expansion foam on an LNG spill on land. Seven tests were conducted in a wind tunnel with approximate dimensions of 10m x 2.5m x 2.5m, in which natural interference was prevented, and additional props were installed to apply stable forced convection and radiation. Liquid nitrogen (LN_2) was used due to its similar thermal properties with LNG as shown in Table 4, so that the results are valid to explain LNG behavior. The boil-off effect and the blocking effect were studied through seven well-designed tests, in which

various heat transfer mechanisms, *i.e.*, natural convection, forced convection, and radiation, were applied manually. Then, the blanketing effect was characterized quantitatively by comparing boil-off and blocking effects.

3.2 Experimental setup and methodology

3.2.1 Test apparatus and materials

To study the vaporization process, a container with a capacity of 0.023 m^3 (0.48 m x 0.48 m x 0.10 m) was used to contain LN_2. It was made by combining several pieces of polystyrene foam board using anti-cryogen paste. The container has five heat flux sensors embedded at one depth and eight thermocouples at two different depths within the bottom wall of the container to monitor the temperature profile and heat flux through the bottom wall. Two additional heat flux sensors were attached to the outside surface of the side walls with thermally conductive paste to measure the heat flux through the side walls and the temperature of outside surfaces. An additional 30 centimeters of transparent fence was installed above the polystyrene container in Test 2-Test 7 to be described in detail in section 3.2.2, in which foam of 30 centimeters high was applied in Test 5-Test 7 ("foam" refers to high expansion foam hereafter unless otherwise specified). The sketch of the test apparatus and detailed positions of sensors are shown in Figure 26.

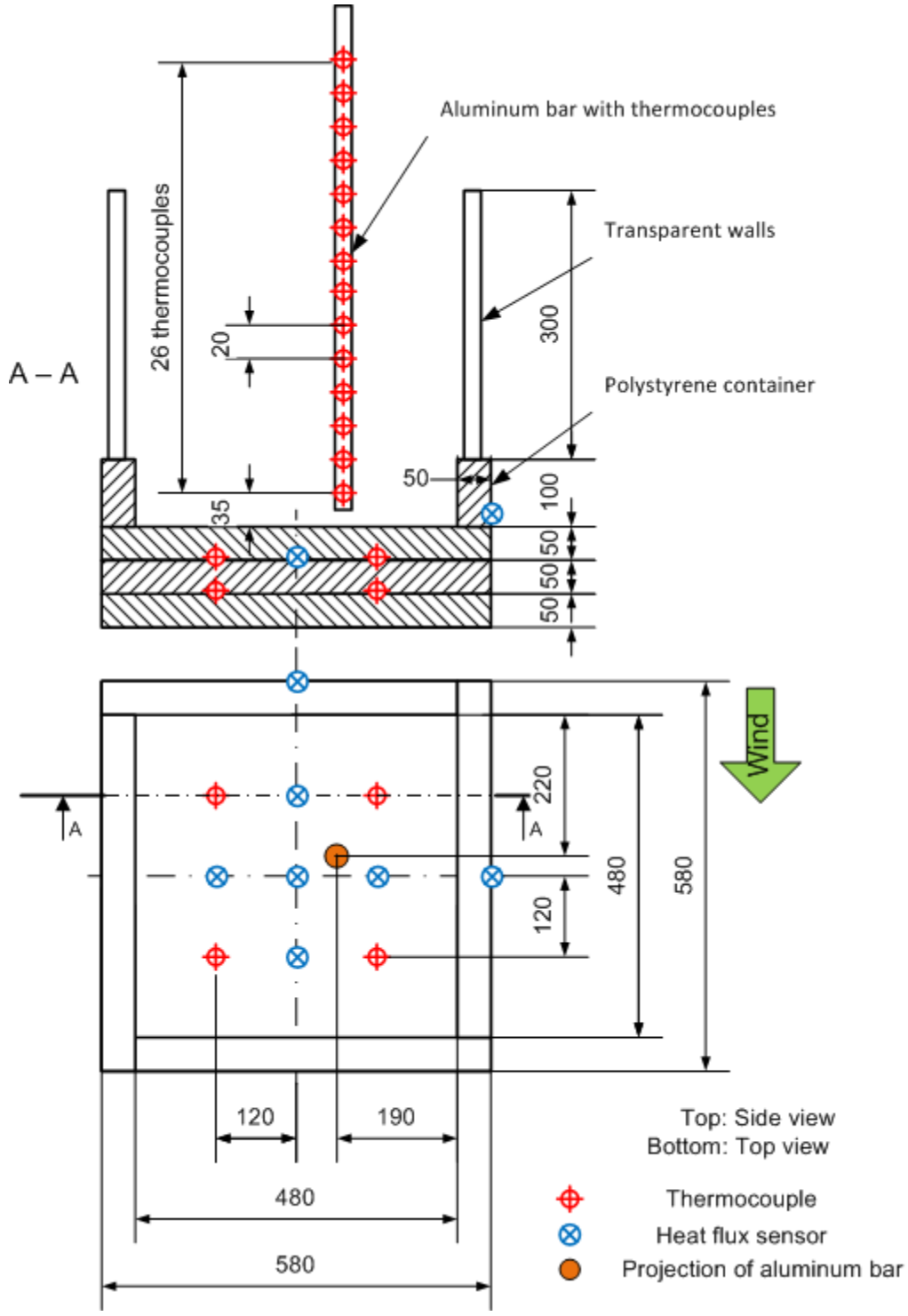

Figure 26 The polystyrene container with thermocouples and heat flux sensors (unit: mm)

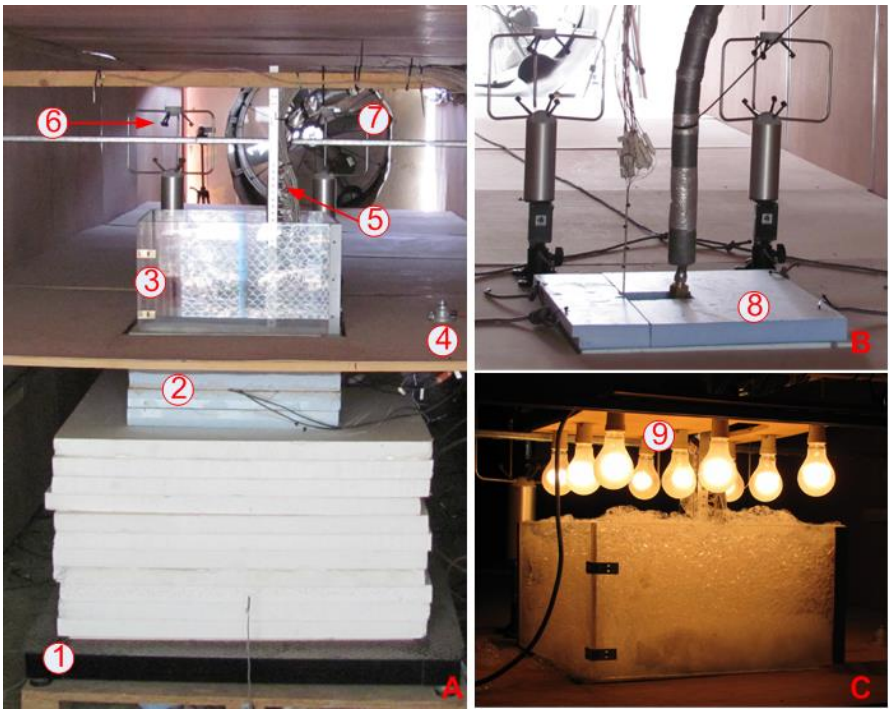

Figure 27 The experimental setup for LN_2 vaporization tests. A: the setup for Test 2-7; B: the setup for Test 1; C: the setup with bulbs panel (1, balance; 2, polystyrene container; 3, fence for foam containment; 4, radiation sensor; 5, aluminum bar with 26 thermocouples; 6, ultrasonic anemometer; 7, fan; 8, polystyrene lid; 9, bulbs panel)

This experiment was conducted in 2012 in a wind tunnel located at Ras Laffan Industrial City (RLIC) in Qatar as shown in Figure 27. The inner surface of the wind tunnel was decorated with wood boards to ensure a good wind tunnel effect, and the ground wood boards were fixed at approximately 1m high, the same elevation as the upper edge of the polystyrene container. The test container was placed on a scale (4 load cell mild steel scale, RadWag, Poland) with readability of 10 g to monitor the mass loss rate of LN_2. The scale was placed in the center line of the wind tunnel, approximately 6 m away from the head end of the wind tunnel, where a fan was placed to supply the

forced convection with a maximum wind speed of 2.2 m/s. The wind speed was measured using an ultrasonic anemometer (Model 81000, R.M. Young Company, USA), which was about 10 cm closer to the fan than the foam fence, and about 45 cm high. A panel with 9 bulbs was employed to provide radiation, which was measured using a radiation sensor (LP02, CAMPBELL SCIENTIFIC, INC., USA). All the measuring equipment was connected to a data acquisition system to record the experimental data for a systematic analysis. A summary of experimental facts is illustrated in Table 5.

Table 5 Summary of experimental facts

Air temperature, ℃	39.1 ± 1.5
Relative humidity	20.7 ± 9.8
Foam concentrate	Expandol
Foam concentrate specific gravity (20 ℃)	1.00 - 1.02
Foam concentrate viscosity (20 ℃), mm^2/sec	7.0
Foam generator	Fomax 7
Estimated foam expansion ratio	800 : 1
Estimated foam density, kg/m^3	2.47

3.2.2 Experimental procedure

One blank radiation test and one blank foam test were conducted separately to study the radiation intensity from the bulbs panel and the mass loss rate of foam without LN_2 present. Seven tests with LN_2 were designed and conducted with various conditions through a combination of foam application, convection, and radiation. Table 6 shows detailed experimental conditions for all seven tests.

Table 6 Experimental condition for each test

Test		Foam	Fan	Bulb	Wind speed (m/s)	Radiation[a] (W/m^2)	Setup	Scope
1		NO	OFF	OFF	0.16 ± 0.17	1.03 ± 0.66	Figure 27B (lid on)	Conduction
2		NO	OFF	OFF	0.39 ± 0.17	11.43 ± 2.17	Figure 27A	Natural convection
3		NO	ON	OFF	1.73 ± 0.25	9.78 ± 0.81	Figure 27A	Forced convection
4		NO	OFF	ON	0.32 ± 0.14	166.99 ± 3.94	Figure 27C	Radiation
5	a	YES	OFF	OFF	0.14 ± 0.13	0.99 ± 0.56	Figure 27A	Foam effect on natural convection
	b	YES	OFF	OFF	0.06 ± 0.08	1.05 ± 0.26	Figure 27A	
	c	YES	OFF	OFF	0.10 ± 0.13	0.98 ± 0.33	Figure 27A	
6	a	YES	ON	OFF	1.82 ± 0.24	3.16 ± 0.82	Figure 27A	Foam effect on forced convection
	b	YES	ON	OFF	1.78 ± 0.24	1.84 ± 0.65	Figure 27A	
	c	YES	ON	OFF	1.81 ± 0.25	1.39 ± 0.66	Figure 27A	
7	a	YES	OFF	ON	0.05 ± 0.08	180.48 ± 5.19	Figure 27C	Foam effect on radiation
	b	YES	OFF	ON	0.04 ± 0.05	174.10 ± 2.87	Figure 27C	
	c	YES	OFF	ON	0.08 ± 0.12	175.36 ± 4.22	Figure 27C	

[a] Radiation only indicates the use of bulbs panel, but not the actual radiation on the pool, because the sensor was put outside the container as shown in Figure 2A. The radiation intensity is given in terms of an average and standard deviation, which is the same as the wind speed.

3.2.2.1 Blank radiation test

The radiant intensity was measured at 6 different vertical distances away from the bulb panel. At each elevation, the heat flux was recorded at 9 different horizontal positions as indicated in Figure 28, in which the average values as well as the standard deviations are given. Different from the solar radiation, the radiation of the bulb panel had a significant gradient at various elevations. The radiation and the associated

deviation became smaller at a larger distance away from the panel. A relatively stable radiation intensity of 500 W/m^2 was achieved at positions further than 350 mm, which is in the range of a typical solar radiation, which ranges from 0 W/m^2 at night to approximately 1000 W/m^2 [39].The space between the two dash lines is where the LN_2 pool surface may locate during the experiment. In this space, a distance independent radiation with a small deviation from center to corner was applied; therefore, the radiation to the LN_2 pool can be considered a constant during the experiment, even though the liquid level changed due to vaporization.

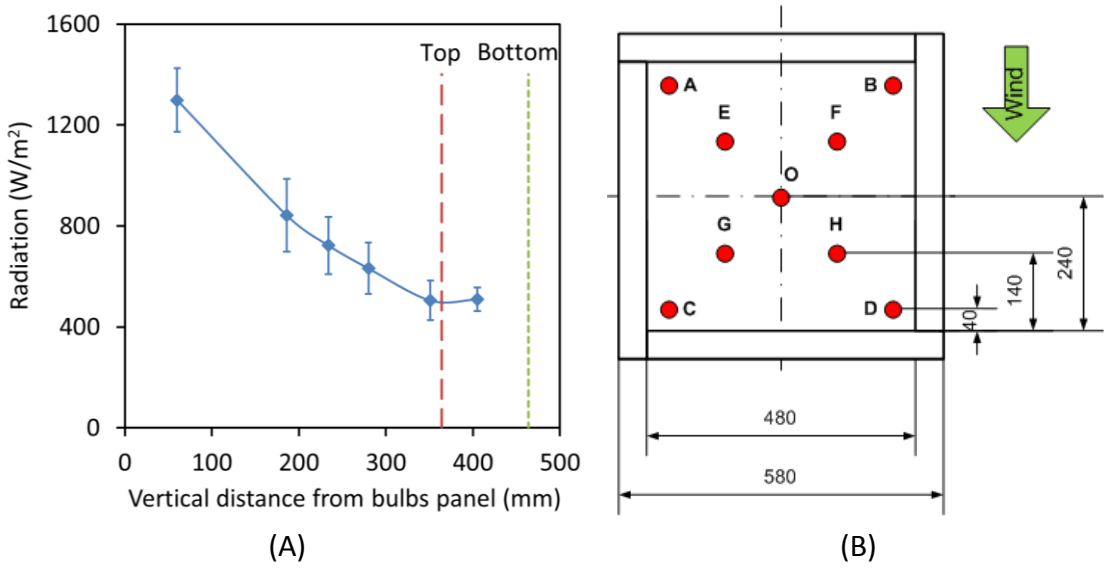

Figure 28 The blank radiation test. (A) indicates the radiation intensity at six different distances from the bulbs panel, top is the liquid nitrogen container's top and bottom is the container's bottom in this figure; (B) indicates the nine locations to measure radiation at each distance. (unit: mm)

3.2.2.2 Blank foam test

To determine the mass loss rate caused by the evaporation of the water contained in the foam, foam of 30 centimeters high was applied in the fence at atmospheric condition without LN_2 present. The measured mass loss rate is only 0.011 g/s as shown in Figure 29A, which is ignorable when compared to the mass loss rates during Tests 5-7. The mass loss rates are 0.38, 0.60 and 0.49 g/s for Test 5, 6 and 7. The test durations are 1143 s, 522 s and 963 s, respectively.

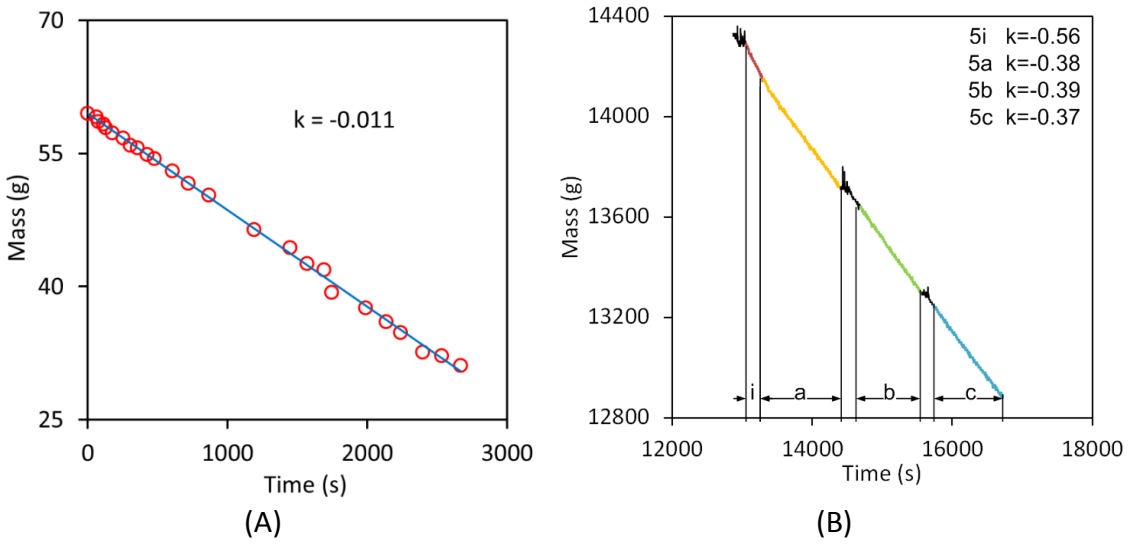

Figure 29 Mass loss rates. (A) Blank foam test; (B) Test 5. (*k* is the slope for each test and indicates the vaporization rate, g/s; symbol i represents the initial stage of first foam application; symbols a, b, and c represent three repeated tests with foam application)

3.2.2.3 Conduction study

An advantage of using polystyrene to build the container is that conduction from the container can reach a steady state in a limited time, and Reid's work has obtained

similar results using other insulating materials [40]. In order to characterize the blanketing effect of foam, the constant conduction was determined in Test 1. The head end was covered by two wood boards to prevent air circulation in the wind tunnel. LN_2 was spilled into the container up to 18kg; then, the container was covered by a polystyrene lid to eliminate convection and radiation as shown in Figure 27B. The test continued for approximately one hour to cool down the container, and a constant conduction was achieved at approximately 22 minutes. The constant conduction was determined by the mass measurement using the balance, while a theoretical calculation was employed to validate the result based on temperature and heat flux measurements at the bottom of the container.

3.2.2.4 Convection and radiation study without foam

The contribution of various heat sources, including natural convection, forced convection, and radiation, was studied without foam application in Test 2, Test 3, and Test 4, respectively. After Test 1, the lid was removed and the transparent fence was installed to start Test 2 as shown in Figure 27A. In this test, the vaporization rate of LN_2 was determined by conduction and natural convection. After about 30 minutes, the wood boards at the head end were removed, and the fan was turned on to start Test 3. In this test, the vaporization rate of LN_2 was determined by conduction and forced convection. After another 20 minutes, the fan was stopped, and the head end of wind tunnel was covered with wood boards again. The bulbs panel was installed above the container as shown in Figure 27C. Test 4 began by turning on the bulbs. In this test, the vaporization rate of LN_2 was determined by conduction, natural convection, and radiation.

3.2.2.5 Convection and radiation study with foam

The blanketing effect of foam on the vaporization rate under various conditions was studied through Test 5, Test 6, and Test 7, which were analogous tests of Test 2, Test 3, and Test 4, but with foam present in the transparent fence. Since foam is not a stable medium, it disappears between 10 and 20 minutes depending on the test conditions. In order to obtain reliable data, foam application was repeated for three times in each test.

3.2.3 Data analysis method

A typical mass curve of LN_2 obtained from Test 5, is shown in Figure 29B. The vaporization rate of LN_2 is determined by linear regression of the mass curve for each test; therefore, the slope is vaporization rate, and the high coefficient of determination confirms a constant vaporization rate of LN_2 in each test. During each foam application, the vaporization rate is also examined at 100-second intervals, which further confirms a steady control of foam on the vaporization rate. Once the vaporization rate is determined, it will be converted to heat flux into an LN_2 pool.

3.3 Results and discussion

Foam affects the vaporization rate of LN_2 by altering the mechanisms of heat transfer to the liquid pool. The possible heat transfer mechanisms at three stages of the experiment are shown in Figure 30, which are pre-foam stage, initial foam stage, and ice plate stage.

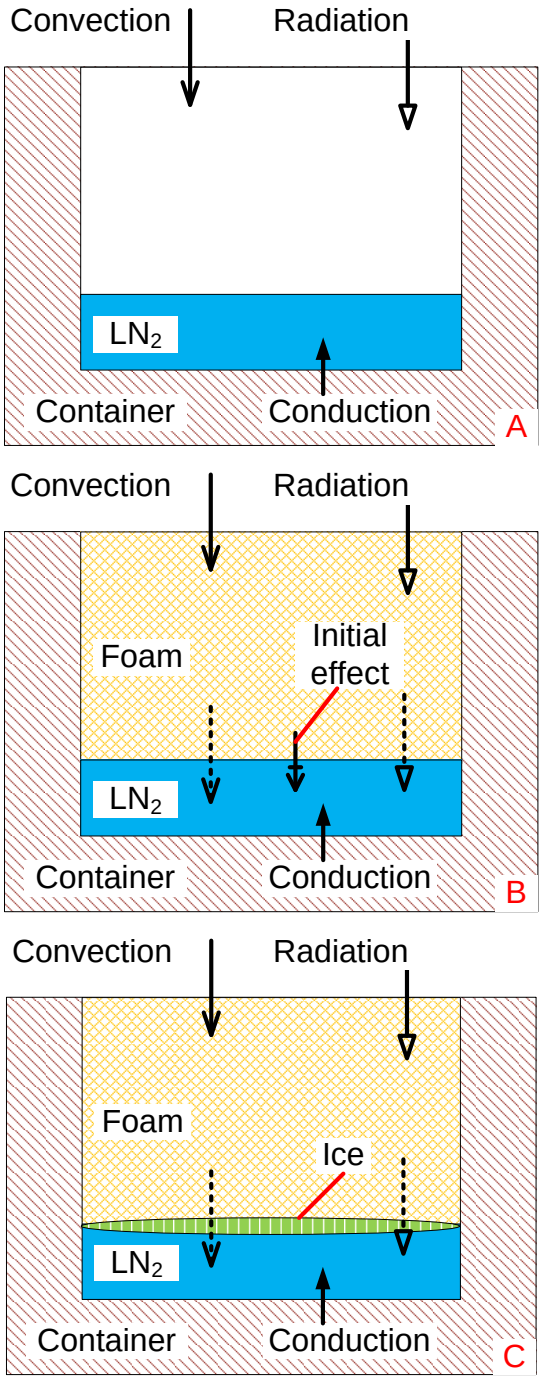

Figure 30 Heat transfer mechanisms for the liquid nitorgen vaporization at three stages of foam application. A: pre-foam stage; B: initial foam stage, and C: ice plate stage

When LN_2 is released into the container, the vaporization rate is determined by conductive, convective, and radiant heat at the pre-foam stage. When foam is applied to provide a foam blanket above the LN_2 pool, the conductive heat remains the same, whereas convective and radiant heat was blocked, and water drainage of foam acts as an extra heat source, since it has a much higher temperature than LN_2. Water drainage of foam can be induced by different mechanisms, *e.g.*, radiation, convection, and LN_2 (cooling effect). With a foam application, the heat is from conduction and water drainage of foam. Because foam contacts with LN_2 directly at the initial stage, it contributes to inducing water drainage. In approximately 300 seconds, an ice plate can be generated gradually at the LN_2 surface by freezing the drainage water, which leads to the ice plate stage. The ice plate acts as a physical barrier to prevent foam from contacting with LN_2, but has pores allowing vapor to penetrate through it, which was discussed previously by Takeno [14]. Therefore, water drainage is assumed to be caused mainly by radiation or convection at the ice plate stage, but not the cooling effect of LN_2.

3.3.1 Conduction

Besides mass measurement, conductive heat flux was also obtained through heat flux sensors and thermocouples installed in the bottom of the LN_2 container as shown in Figure 26. A model developed by Briscoe and Shaw [41] was employed to estimate the thermal properties of the polystyrene container, which considers the container's bottom as semi-infinite solid. This one-dimensional conduction can be described by equation (1). Temperature and heat flux profile at various depths are given in equations (2) and (3). A non-linear least squares method was employed to regress thermal diffusivity and

thermal conductivity associated with polystyrene using equations (2) and (3), which gave α= 4.69E-07 m^2/s and k = 0.0276 W/(m·K). A thermal conductivity of 0.033 W/(m·K) was reported in the *CRC Handbook of Chemistry and Physics* [42]. With the determination of these two parameters, heat flux from side walls and the bottom were calculated and converted into vaporization rates of LN_2, and summed up as the total vaporization rate due to conduction. The air temperature was used as the boundary condition of exterior surface for the calculation of heat flux from the side walls. The comparison of vaporization rate of mass measurement is shown in Figure 31. The vaporization rate of mass measurement was higher than that of theoretical calculation at the beginning, which may be due to the generation of LN_2 aerosol caused by the violent boiling process; however, once the test vessel was cooled down after around 10 min, the experimental results were well predicted by the calculation. Reid found that conduction can reach a steady state at a certain time in a Styrofoam test with LNG [40]; a steady state was also observed after 1350s based mass measurement in this study, which agreed with the theoretical calculation very well as shown in Figure 31. Therefore, the mass measurement is validated in the conduction study, and adopted for data analysis of other tests.

$$\frac{\partial T}{\partial t} = \alpha \frac{\partial^2 T}{\partial^2 z} \tag{1}$$

$$T = T_i - (T_i - T_b) \cdot \mathrm{erfc}\left(z / 2\sqrt{\alpha \cdot t}\right) \tag{2}$$

$$q = -k\frac{\partial T}{\partial z} = \frac{k(T_i - T_b)}{(\pi\alpha t)^{1/2}}\exp(-z^2/4\alpha t) \tag{3}$$

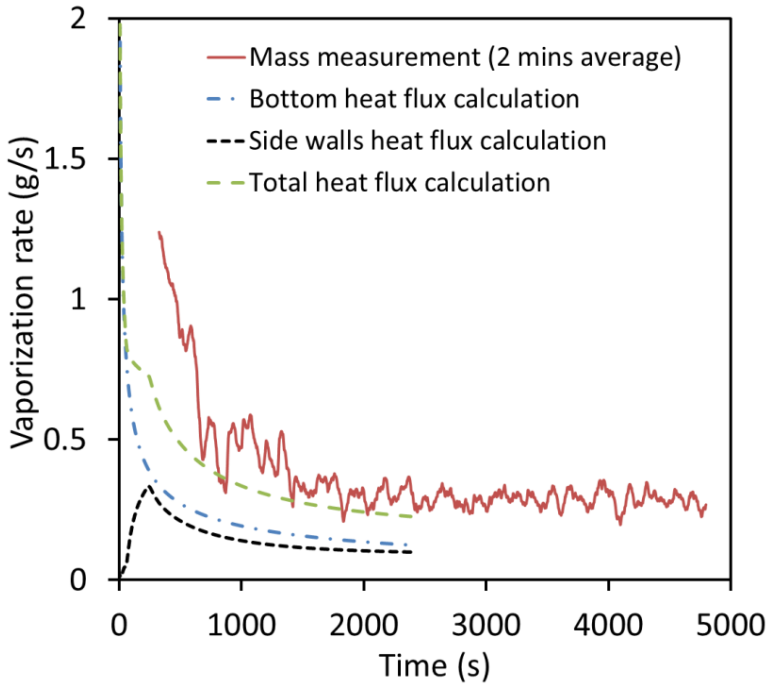

Figure 31 Experimental and theoretical vaporization rate of liquid nitrogen due to conduction

3.3.2 Convection and radiation

To determine the contribution of each heat source and the effects of foam on them, a general heat balance is given as equation (4). Generally, the total heat transfer includes conduction, convection, radiation, and heat input from the water drainage induced by LN_2 once foam is applied. The convection and radiation can be either the actual values without foam, or the apparent values with foam present. With foam present, the actual convection and radiation can induce water drainage, and the water

drainage provides the heat input to the LN_2. The heat input is here called "apparent convection" or "apparent radiation" regardless of the real mechanism. They are named as convection and radiation in this work on behalf of the discussion on foam effects by comparing actual values and apparent values. For each specific test condition, the convective and radiant heat fluxes are given in equations (5) and (6), respectively. The governing equation of heat balance is listed in Table 7 for each test. The heat flux contributed by each heat transfer mechanism is calculated from vaporization rates and summarized in Table 8.

Table 7 The governing equations of heat balance

Test No.	Governing equation[a]
1	$q_1 = \dot{m}_1 L / A = q_{\text{Cond}}$
2	$q_2 = \dot{m}_2 L / A = q_{\text{Cond}} + q_{\text{NConv\_N}}$
3	$q_3 = \dot{m}_3 L / A = q_{\text{Cond}} + q_{\text{FConv\_N}}$
4	$q_4 = \dot{m}_4 L / A = q_{\text{Cond}} + q_{\text{NConv\_N}} + q_{\text{Rad\_N}}$
5[b]	$q_5^* = \dot{m}_5^* L / A = q_{\text{Cond}} + q_{\text{NConv\_F}} + q_{\text{IFoam}}^*$
5	$q_5 = \dot{m}_5 L / A = q_{\text{Cond}} + q_{\text{NConv\_F}}$
6	$q_6 = \dot{m}_6 L / A = q_{\text{Cond}} + q_{\text{FConv\_F}}$
7	$q_7 = \dot{m}_7 L / A = q_{\text{Cond}} + q_{\text{NConv\_F}} + q_{\text{Rad\_F}}$

[a] L is the latent heat of nitrogen vaporization, and A is the bottom area of the LN_2 container.

[b] Test 5 before the formation of ice plate, and q_{IFoam}^* is the initial effect of foam application.

$$q = q_{\mathrm{Cond}} + q_{\mathrm{Conv}} + q_{\mathrm{Rad}} + q^{*}_{\mathrm{IFoam}} \tag{4}$$

$$q_{\mathrm{Conv}} = \begin{cases} q_{\mathrm{NConv\_N}} & \text{(Natural convection without Foam)} \\ q_{\mathrm{FConv\_N}} & \text{(Forced convection without Foam)} \\ q_{\mathrm{NConv\_F}} & \text{(Apparent natural convection with Foam)} \\ q_{\mathrm{FConv\_F}} & \text{(Apparent forced convection with Foam)} \end{cases} \tag{5}$$

$$q_{\mathrm{Rad}} = \begin{cases} q_{\mathrm{Rad\_N}} & \text{(Radiation without Foam)} \\ q_{\mathrm{Rad\_F}} & \text{(Apparent radiation with Foam)} \end{cases} \tag{6}$$

The heat flux to the LN2 pool is 295 W/m^2 contributed by natural convection (Test 2) and 885 W/m^2 contributed by forced convection (Test 3). Forced convection was dominant as a heat source to vaporize LN2 even at a low wind speed of 1.73 m/s. The LN2 level was approximately between 7.68 and 8.07 cm in the container in Test 3. A general method to calculate the heat transfer rate of convection is described in equation (7). Heat transfer coefficient hFC can be obtained through equation (8) with the Nusselt number (Nu). The wind velocity in the work was relatively low, and a simple calculation of the Reynolds number (Re) indicated a laminar flow according to a critical Reynolds number (Rec) of 320,000 assumed in a similar work [43]. The methods of calculating the Nusselt number are available in the literature [44, 45]. The method for laminar flow is given in equation (9). Using this approach, the estimated convective heat transfer rates are 783 W/m^2 for natural convection and 1650 W/m^2 for forced convection. This approach overestimates convection at low wind speeds, which is supported by previous results in lab-scale tests [43].

Table 8 Vaporization rate and heat flux of various mechanisms

Test No.	1	2	3	4	5[a]	5[b]	6[b]	7[b]
Vaporization rate (g/s)	0.29	0.63	1.31	0.92	0.56	0.38	0.60	0.49
Linear regression R^2	0.9996	0.9981	0.9983	0.9988	0.9876	0.9982	0.9769	0.9977
Heat flux (W/m^2)								
Total	252	547	1137	799	486	330	518	425
q_{Cond}	252	252	252	252	252	252	252	252
q_{NConv_N}	-	295	-	295	-	-	-	-
q_{FConv_N}	-	-	885	-	-	-	-	-
q_{Rad_N}	-	-	-	252	-	-	-	-
q^*_{IFoam}	-	-	-	-	156	-	-	-
q_{NConv_F}	-	-	-	-	78	78	-	78
q_{FConv_F}	-	-	-	-	-	-	266	-
q_{Rad_F}	-	-	-	-	-	-	-	95

[a] Test 5 before the formation of ice plate

[b] Vaporization rates and R^2 of Test 5-7 are an average of three repeated tests

$$q_{convection} = h_{FC}\left(T_{air} - T_{liquid}\right) \tag{7}$$

$$h_{FC} = \frac{Nu \cdot K}{D} \tag{8}$$

$$Nu_{\text{Laminar}} = 0.664\ \text{Re}^{1/2}\ \text{Pr}^{1/3} \tag{9}$$

In Test 4, radiation that was actually absorbed by LN_2 was approximately 252 W/m^2. It represents approximately 50% of the radiation at the same elevation in the blank radiation test (Figure 28). It is consistent with previous results in lab-scale tests [43], where the ratio of the radiative heat absorbed to the incident radiation was between 50% and 65%.The unabsorbed portion of the radiation may be reflected by the liquid surface, or absorbed by the vapor above the liquid.

3.3.3 The blanketing effect of foam

3.3.3.1 Blanketing effect on each heat transfer mechanism

The blanketing effect was examined by the effectiveness of foam on reducing the heat flux from convection and radiation to the LN_2 pool, which is defined as

$$E = \frac{q_{\text{N}} - q_{\text{F}}}{q_{\text{N}}} \tag{10}$$

By comparing the individual apparent heat flux of each heat transfer mechanism in Tests 5-7 with actual heat flux in Tests 2-4, the apparent heat fluxes contributed by natural convection, forced convection, and radiation after foam application are reduced to 78 W/m^2, 266 W/m^2, and 95 W/m^2 from actual values of 295 W/m^2, 885 W/m^2, 252 W/m^2 respectively (Table 8). With the foam application of 30 centimeters, the effect of convection and radiation on the vaporization rate of LN_2 was greatly reduced. The effectiveness of foam on reducing the heat flux from natural convection, forced convection and radiation are 74%, 70%, and 62%, respectively (Figure 32).

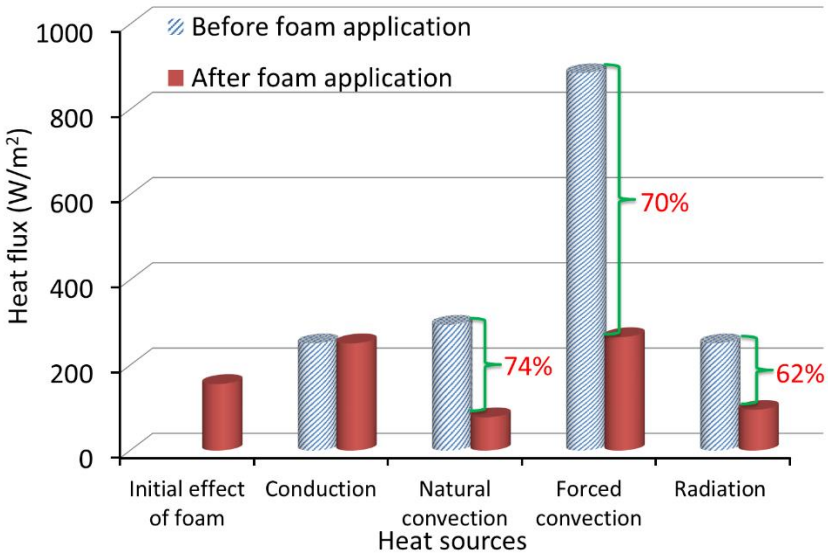

Figure 32 Blanketing effect of foam on each heat transfer mechanism based on heat flux for liquid nitrogen vaporization

3.3.3.2 Blanketing effect on overall heat transfer mechanism

The overall heat fluxes excluding conduction are compared between Tests 5-7 and Tests 2-4, and a linear correlation is proposed for this work as indicated in equation (11).

$$Q_F = (1 - R) \times Q_N \tag{11}$$

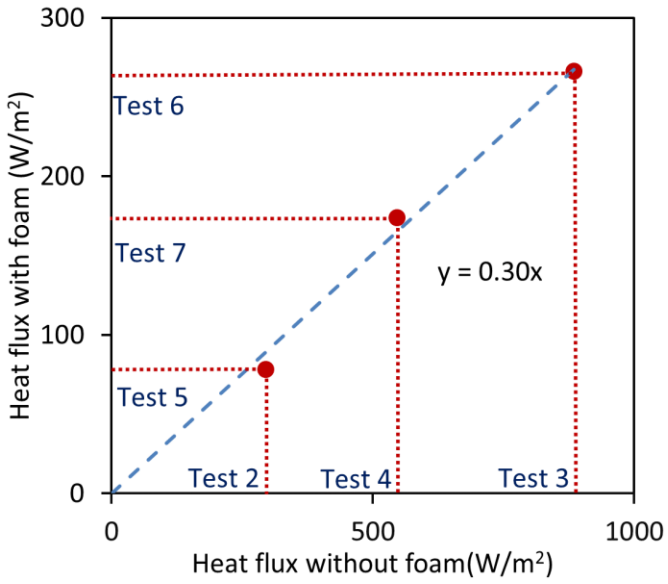

Figure 33 The blanketing effect on the overall heat transfer mechanism. (the heat flux for each test excluding conduction, since foam does not have effect on conduction)

The correlation is validated by the linear regression as shown in Figure 33. The reduction factor R is 0.7 in this case, which indicates 70% of convective and radiant heat overall was eliminated by the foam. The heat flux reduction are 217, 619 and 374W/m^2, respectively, which are 40%, 54% and 47% of total heat flux when the constant conduction is considered.

3.3.3.3 Initial negative effect

The use of foam for LNG hazard mitigation requires a precaution, since a negative effect was observed to escalate the hazard due to direct water discharge to the LNG pool during the initial foam application [17]. In this work, foam was delicately applied to avoid direct water discharge, therefore the initial negative effect is small as shown in Figure 32. At the initial stage of the first foam application in Test 5, the

vaporization rate of LN_2 was higher than that in the ice plate stage with steady control. The initial negative effect (q^*_{IFoam}) of foam is considered the heat transfer from the warm foam to the cold liquid pool, caused by direct contact of foam with LN_2. A similar phenomenon was described by Takeno's work [14].

The initial effect was further compared with the reduction of convection and radiation by foam application, and the holistic blanketing effect was studied. The initial effect was determined as 156 W/m^2 during approximately the first 300 seconds. The water of foam freezes to generate an ice plate with pores at the interface of LN_2 and foam. The ice plate continues to grow with more water coming down from foam, until one entire ice plate is formed as a physical barrier to eliminate the initial effect. The initial effect was obtained in Test 5, and the heat flux may vary with other conditions; however, the total heat input of this effect should be similar, and can be estimated by the product of the heat flux of initial effect and its duration, *i.e.,* 156 W/m^2 x 300 s = 47 kJ/m^2. Compared with the effect of foam on reducing the convection, the heat flux rate of initial effect (q^*_{IFoam}=156 W/m^2) of the foam is less than the reduction of convection by foam ($q_{FConv\_N} - q_{FConv\_F}$ = 619 W/m^2 for forced convection, and $q_{NConv\_N} - q_{NConv\_F}$ = 217 W/m^2 for natural convection); while the duration of the initial effect (300 s) is also shorter than the duration of each foam application, *e.g.,* 522 seconds on average with forced convection in Test 6. The initial effect (47 kJ/m^2) accounts for 14% of total reduction for forced convection for each foam application (619 W/m^2 x 522 s = 323 kJ/m^2) in this work. This percentage is expected to be less if a thicker layer of foam is

applied, or foam is applied repeatedly, because the initial effect will remain the same, but the duration of foam will be larger. Note that foam also can reduce radiation. Therefore, the initial negative effect is ignorable compared to the blanketing effect if foam is properly applied.

3.3.4 Mechanism of foam blanketing effect

With foam application, water drainage is considered the direct heat source for the vaporization of LN_2, while air convection or solar radiation acts as a factor to affect the foam drainage rate, which can be proved by the breaking of the foam and the accumulation of the ice plate. Clearly, heat flux from foam to LN_2 pool increases with the water drainage rate.

Many factors can affect the water drainage rate, including both environmental conditions and the physical properties of foam. The external heat transfer mechanisms can affect the water drainage rate, *e.g.*, forced convection in Test 6 resulted in a higher water drainage rate than other tests with radiation and natural convection. Also, the water drainage rate is also an intrinsic property of foam, determining the effectiveness of foam. Therefore, heat absorbed by LN_2 from foam for vaporization varies with different external heat transfer mechanisms, while the effectiveness of foam remains the same for all the tests.

3.4 Conclusion

This work quantitatively studied the effect of foam on different heat transfer mechanisms for a cryogenic liquid pool, including natural convection, forced

convection, and radiation. Experimental conditions were well controlled in a wind tunnel specially built for this experiment. The main findings are summarized below.

The blanketing effect has been studied quantitatively, which does not affect conduction, but helps reduce 70% of the heat input from convection and radiation to the liquid nitrogen pool in this work. Water drainage of foam before the formation of the ice plate adds extra heat to vaporize liquid nitrogen, but it is small and negligible compared to its role in reducing the convective or radiative heat transfer.

The water drainage rate of foam is essential to determine the blanketing effect on the vaporization rate of cryogenic liquid. External factors, *e.g.*, wind speed and radiation intensity, play important extrinsic roles in determining the drainage rate foam. However, the physical properties of foam, *e.g.*, stability of foam, also play an important intrinsic role to determine the effectiveness of foam. A study on the relationship between the drainage rate and the external factors as well as the physical properties of foam will be a meaningful topic in the future. Future work on the experiment with other conditions, *e.g.*, various wind speeds and radiation levels, will be beneficial on the study of blanketing effect.

4. WARMING EFFECT AND OTHER PHYSICAL INTERACTIONS

4.1 Introduction

Natural gas has become more popular as a fuel and a feedstock for the chemical industry, because it has an abundance of reserve; it emits much less carbon dioxide, nitrogen oxides, sulfur dioxide and particulates compared with other foil fuels [34]. In the USA, natural gas was previously imported, but in the future it will be exported due to the production of shale gas. Many export terminals have been approved or proposed [46].

The liquefaction of natural gas provides benefits for the storage and transportation, because liquefied natural gas (LNG) has a higher energy density and a reduced volume. However, an LNG spill may cause a catastrophic incident as demonstrated by Cleveland East Ohio Gas explosion, which killed 130 people [2]. One of main hazards is the LNG vapor hazard after a spill, which is the vapor cloud evolving from the LNG pool and remaining at the ground level due to dense gas behavior. The vapor cloud is flammable at a volumetric concentration approximately between 5 % and 15 %. Therefore, a fire or an explosion may occur if the vapor hazard is not properly mitigated.

Previous work has proved that high expansion foam is effective for mitigating LNG vapor hazard [15, 16]. These works focused on determining the vapor concentration reduction with high expansion foam application. However, the mitigation mechanism has barely been studied. It was commonly believed that the mitigation effect

only relied on the warming effect of foam on raising LNG vapor buoyance. Zhang's work concluded that foam could also reduce the vaporization rate of LNG with blanketing effect to control the hazard [47]. The lack of understanding on the physical interaction of foam and LNG system demands additional experimental work.

In this work, a foam generator was built based on the schematic design from NFPA 11. Improvements were made to better meet the need of lab tests. A foam test apparatus was designed and constructed. Tests using liquid nitrogen (LN_2) were conducted with high expansion foam application. The findings regarding to the physical interaction of foam and LNG system were presented.

4.2 Experiment and methodology

4.2.1 Experimental setup

The experimental setup consisted a foam generator and a foam test apparatus as shown in Figure 34. With the foam generator, the foam solution from the tank was pumped to the spray nozzle through the stainless steel hose. The main body of the foam generator is shown in Figure 35. Prior to reaching the nozzle, the foam solution went through a pressure gauge, which can indicate the flow pressure. The spray nozzle was inside of a transparent air cylinder. The foam solution was sprayed onto a conical screen in front of the nozzle. At the other end of the air cylinder, the air was dragged and pushed in the direction of the screen by the fan. The damper was used to control air flow rate. The foam was generated when air passed through screen and was entrained in the foam solution. The finished foam was discharged at the end the air cylinder with a deflector to control the angle of release.

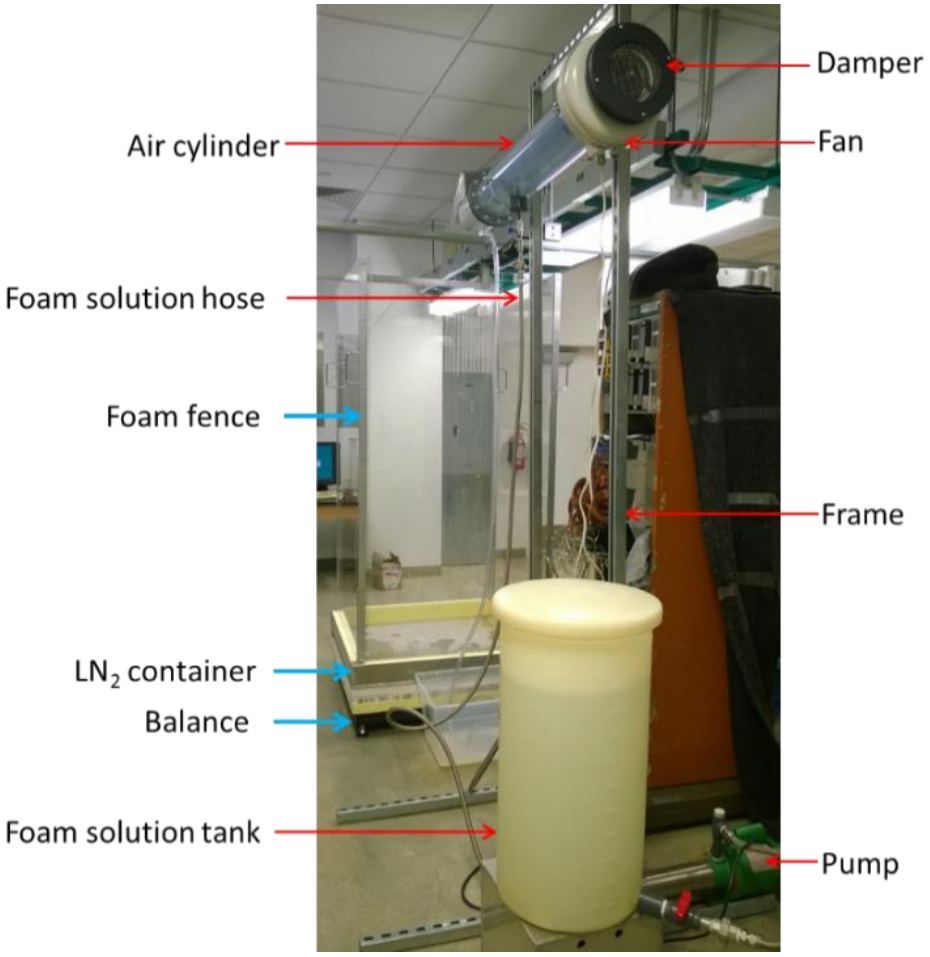

Figure 34 Experimental setup in the lab

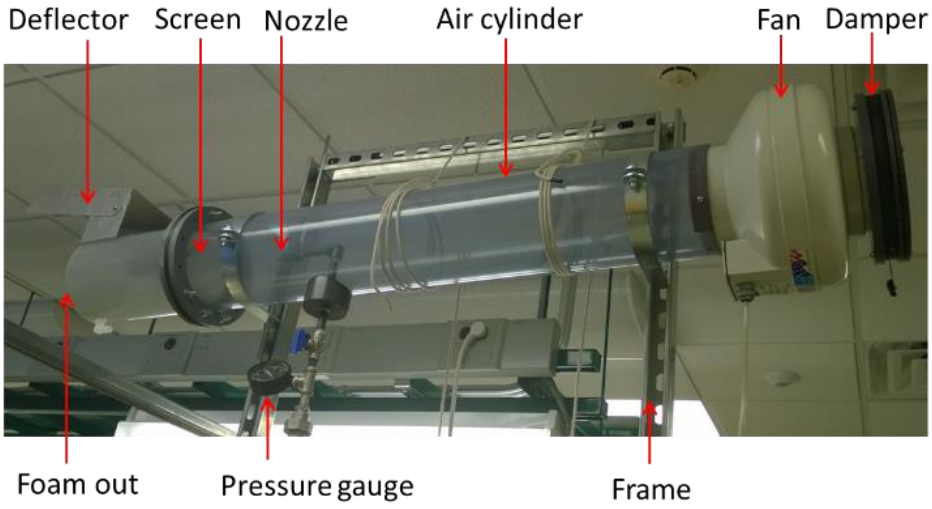

Figure 35 Main body of foam generator

The foam test apparatus consisted of three main parts, balance, liquid nitrogen container, and foam fence as shown in Figure 34. The detailed information is shown in Figure 36. The balance (Scale WPT/4 300 C7, RadWag, Poland)) was at the bottom to measure the mass. A chamber was built above the balance using insulation material, which contained a heating sheet to control the heat input for vaporization. On top of the heat chamber, there was a double-containers system to contain liquid nitrogen. The inner container (0.84 m × 0.84 m × 0.1 m) was used to contain liquid nitrogen; the outer container had a trench rim to support the foam fence. Salt water was poured into the trench to seal the small gap between foam fence and outer container. The sponge between the two containers helped to prevent salt water from freezing after liquid nitrogen was released into the inter container. The foam fence was made of polycarbonate. Ten pairs of thermocouples (T type TJC300 series, Omega Engineering, USA) were installed inside of the foam fence to measure the vapor and foam

temperature. An oxygen sensor (MF010-1-LC3, Honeywell, USA) was used on the top of foam fence to monitor the oxygen level. The foam height in the foam fence was recorded using a video camera during the tests.

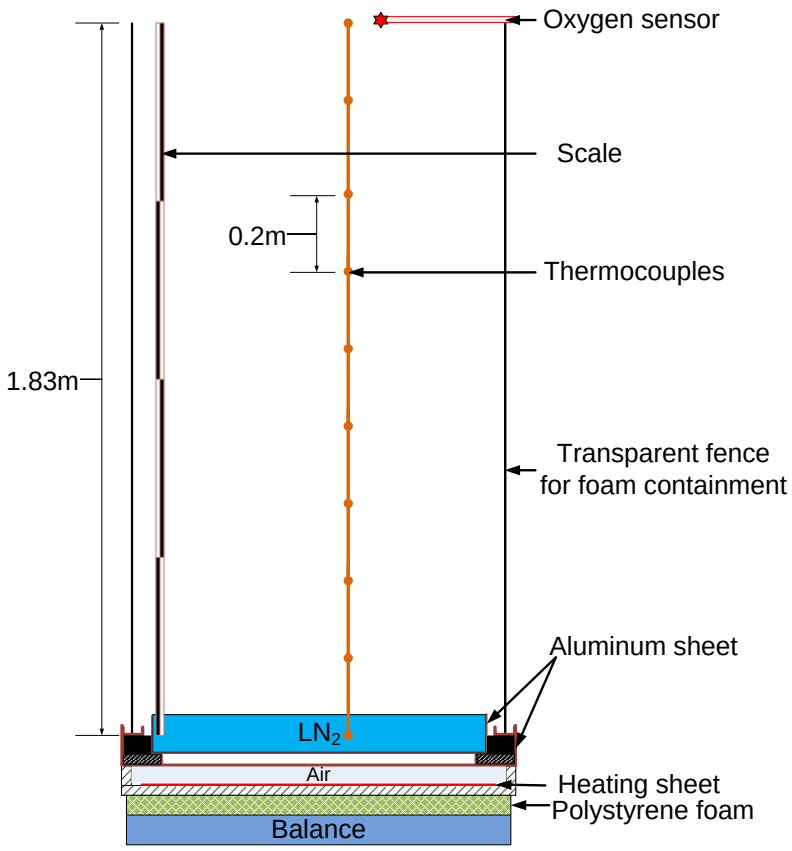

Figure 36 Schematic diagram of foam test apparatus

4.2.2 Summary of tests

There were seventeen liquid nitrogen tests with high expansion foam application. The expansion foam ratio, which is defined as the volumetric ratio between foam and foam solution supplied, ranged from 330 to 680. The tests were conducted in two

methods. Method A was to release liquid nitrogen into the inner container without foam fence. Once the inner container was filled, the foam fence was put on followed by foam application. Method B was to have the foam fence installed. The cryogenic hose was inserted through a hole on the foam fence to release liquid nitrogen. Once the inner container bottom was fully covered by liquid nitrogen (approximately 4 kg of liquid nitrogen), high expansion foam was application. More vapor was released and interacting with foam using the method B, because the inner container was not fully cooled down, and there was flash of liquid nitrogen during the release.

4.3 Results and discussions

4.3.1 Performance of foam generator

The quality of foam can be characterized by two parameters, expansion ratio and foam generation rate. The expansion ratio is shown in Figure 37. The data points on the left of the dashed line were obtained using a small nozzle (BETE WL 1), but the equivalent pressure for a large nozzle (BETE WL 1 ½) was used in order to plot the data together. The expansion ratio is basically the volumetric ratio of entrained air and foam solution. Generally, expansion ratio reduced with increasing pump pressure, because high pressure caused high flow rate of foam solution. The effect of damper was also studied. The damper was set as 12.5 %, 25 %, 50% and 100% open. If all the air was entrained in the foam, 100% open damper should have produced the highest expansion ratio foam at a given pressure, because it can provide the maximum air flow rate. However, the results indicated that 50 % open damper generated foam with highest expansion ratio in most cases. The maximum air flow rate provided by the fan was too

large for foam solution to entrain all the air in the foam. Some of the air escaped into the atmosphere without generating foam. The range of expansion ratio using current setup was from 300 to 850, which can be extended in either direction by switching the spray nozzle.

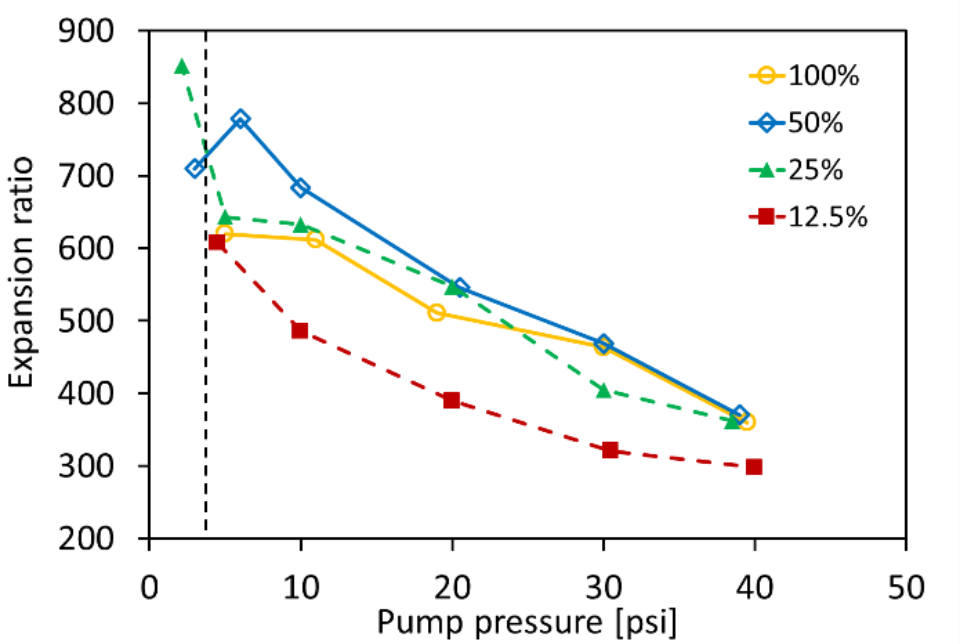

Figure 37 Foam expansion ratio and pump pressure

The volumetric foam generation rate is mainly determined by the air entrainment rate. Similarly, 50% open damper had the highest foam generation rate as shown in Figure 38. Due to the increase of foam solution on the screen, increasing pump pressure led to an increase of foam generation rate. The foam generation rate using current setup ranged from 1.26 to 2.17 m^3/min.

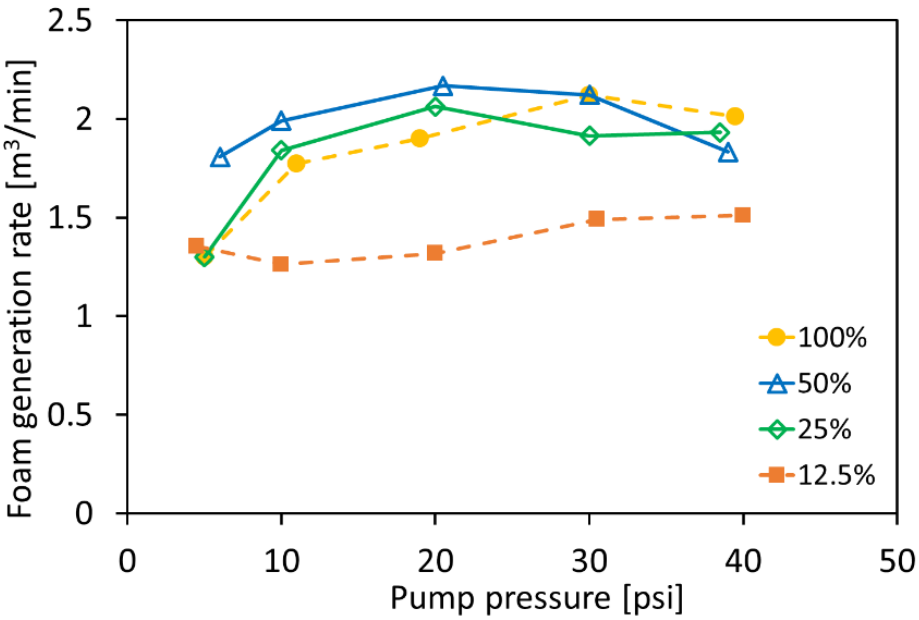

Figure 38 Foam generation rate and pump pressure

4.3.2 Temperature profile of vapor and foam

The temperature profiles were measured in the foam fence as shown in Figure 39. The measurement from several elevations were selected and shown, which were 0.18m (2d and 2u), 0.38m (3d and 3u), 0.58m (4d and 4u), 1.60m (9d and 9u) and 1.83m (10d and 10u) above the bottom of liquid nitrogen container. At each elevation, a pair of thermocouples were used and the installation method is shown in Figure 40. The upward thermocouple can be easily assessed from the top, which aims to measure the foam temperature. The downward thermocouple can be easily assessed from the bottom, which aims to the measure the vapor temperature evolving from the pool. Figure 39 shows the temperature profile for the first foam application. This test was conducted using method A. After the foam fence was put on top of the liquid nitrogen container,

the temperature in the foam fence reduced slowly, since the vaporization rate was relatively small after the container has been cooled down. The foam application temporarily increased the vaporization rate due to the initial boil-off effect, which decreased the temperature at all elevations. After the thermocouples were fully covered by high expansion foam, the old vapor were replaced by foam and the new vapor raised from the bottom. The heat transfer between foam and the remaining vapor increased the temperature, which was later decreased due to the continuous supply of vapor from the pool. The downward thermocouples indicated a lower temperature, since rising vapor had a larger effect on downward thermocouples and foam had a larger effect on upward thermocouples. Previous work has used thermocouples to measure the temperature profile in the foam zone [14, 16]; However, the foam zone is a multi-phase medium; one thermocouple at one location could not measure the temperature of both foam and vapor. This work proposed a method to measure the temperature of both foam and vapor.

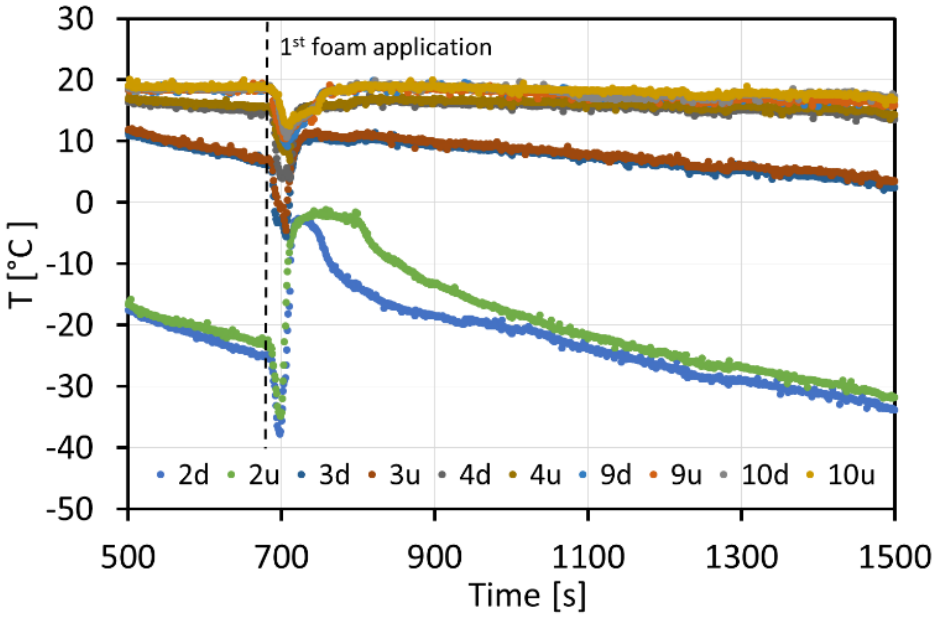

Figure 39 Temperature profile in a test conducted using method A. From the bottom to the top, the curves are 2d, 2u, 3d, 3u, 4d, 4u, 9d, 9u, 10d, 10u

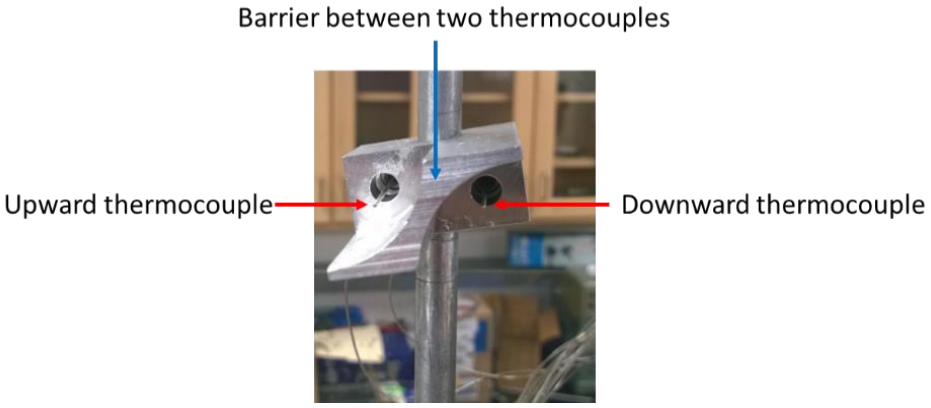

Figure 40 Installation of thermocouples

4.3.3 Vapor channel and foam breaking rate

The formation of vapor channels in the foam is an important physical interaction in the system. After the foam application, the liquid nitrogen pool was smothered for a very short period of time. The vapor accumulated due to continuous vaporization, and found a way out later. Figure 41 (a) shows the opening at the top of foam zone. Figure 41 (b) and (c) show the vapor channels formed in the middle and at the corner of the foam fence. The vapor was always trying to escape from the weakest location, such as the corner, since the corner usually was filled with foam last. Even though foam was reapplied in many tests to cover the existing channels, vapor channels would often form at the same location. The diameter of the vapor channel varied between tests, which could be as large as approximate 0.08m as shown in Figure 41 (b) (the distance between two adjacent blue lines was 0.15m).

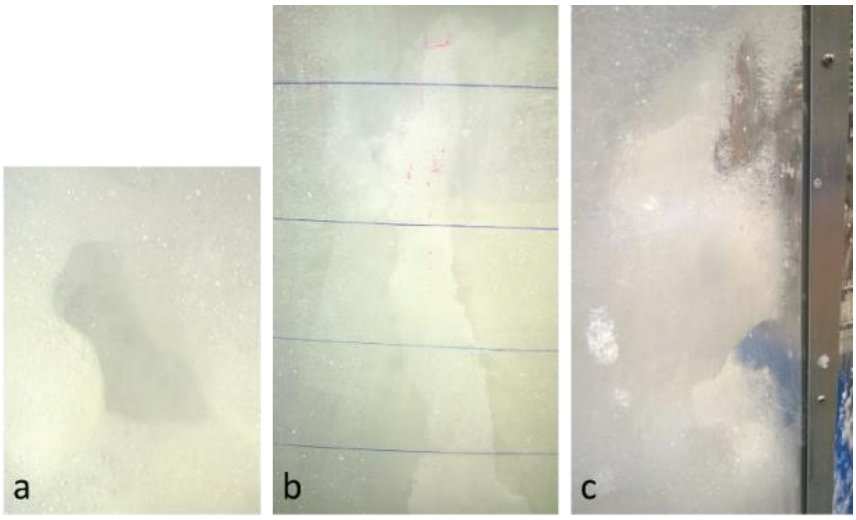

Figure 41 Formation of vapor channel

The foam breaking process was recorded using a video camera for all the tests. The foam height information was obtained by analyzing the video with MATLAB code. The foam height for two selected tests are shown in Figure 42 and Figure 43. These two tests were conducted using different methods as described previously. They both showed similar trend in terms of foam breaking rate. The breaking rate was largest right after the first foam application, which was followed by a transition regime before foam break rate reached a steady state. At the steady state, foam breaking rate was smaller. The foam was reapplied; however, the reapplication did not interfere with the steady state to cause a large foam breaking rate. The initial high foam breaking rate was probably caused by the vigorous interaction of foam with liquid nitrogen and nitrogen vapor at the beginning. Since the test conducted using method B produced more vapor, the foam breaking rate was a little larger in initial regime; however, the difference of vaporization rate did affect the foam breaking rate at steady state as shown in Table 9.

Table 9 Foam breaking rate

Test	Test method	Initial rate (mm/min)	Steady state 1 (mm/min)	Steady state 2 (mm/min)	Steady state 3 (mm/min)
1	A	28	4.2	2.9	3.7
2	B	31.8	-	4	3.7

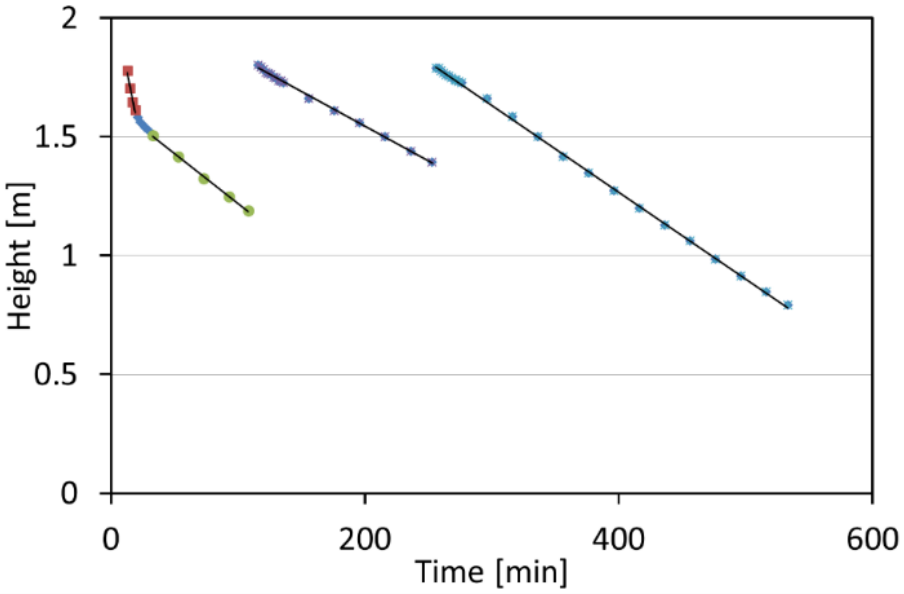

Figure 42 Foam breaking rate in a test conducted using method A

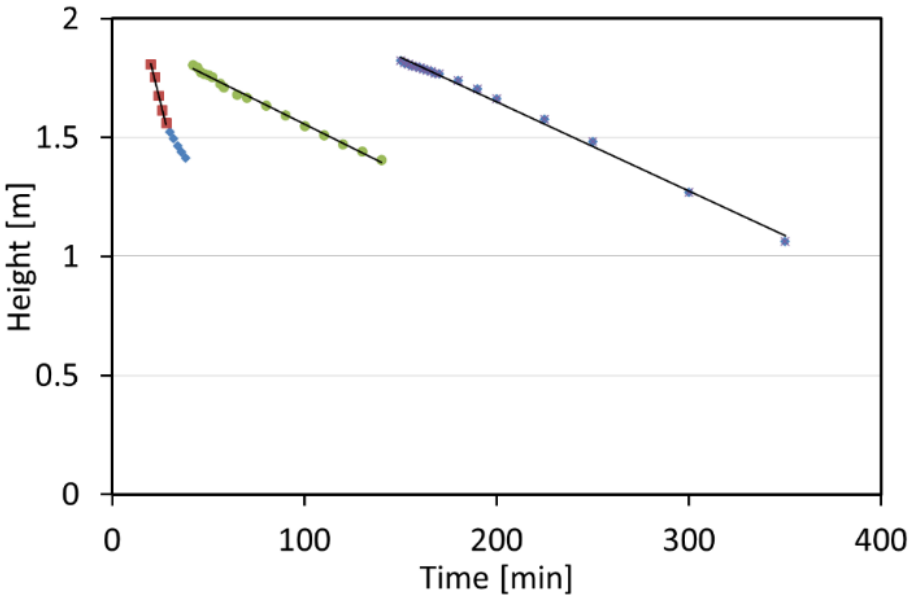

Figure 43 Foam breaking rate in a test conducted using method B

4.3.4 Boil-off effect

The boil-off effect has been discussed in some of the previous work [14, 47]. This work continues to investigate the boil-off effect with a larger scale test. The mass curve and corresponding vaporization rate are shown in Figure 44. The blue curve is a typical mass curve of tests using method A. After the foam fence was put on, liquid nitrogen was vaporizing prior to foam application. The vaporization rate was labeled as "a". High expansion foam was applied, the peak vaporization rate was labeled as "b". When the vaporization rate started to stabilize, the vaporization was labeled "c". Similar information was gathered for three foam applications in 17 tests. The difference between "a" and "b" is the initial boil-off effect "d". The difference between "a" and "c" is the boil-off effect at the steady state "e". The boil-off effect is shown in Figure 45, as well as standard deviation. The initial boil-off effect decreased with multiple foam applications. The duration of each initial boil-off decreased as well, which were 92 s, 63 s, 52 s on average. The boil-off effect at the steady state was much smaller than initial boil-off effect. The steady state boil-off effect can only be observed during the first foam application.

The study conducted in the wind tunnel could only observe the initial boil-off effect during first foam application and there was no steady state boil-off effect [47]. Regarding the initial boil-off effect, the new foam generator could direct foam application into the test apparatus, which was not possible in the previous work [47]. The directed foam application allowed better observation of initial boil-off effect. Therefore, the initial boil-off effect was observed for second and third foam application.

Regarding the steady state boil-off effect, it was not observed in the previous work [47]. Because the foam fence was only 0.3 m high, there was natural convection without foam application. Compared with natural convection, the steady state boil-off effect was too small to be observed. In this work, the height of foam fence was 1.83 m. Therefore, there was almost no natural convection effect on the liquid pool and the steady state boil-off effect was observed. With the use of the new foam generator, the boil-off effect was studied in much more detail. The results indicated that the boil-off effect was small. It attenuated with multiple foam applications in terms of magnitude and time duration.

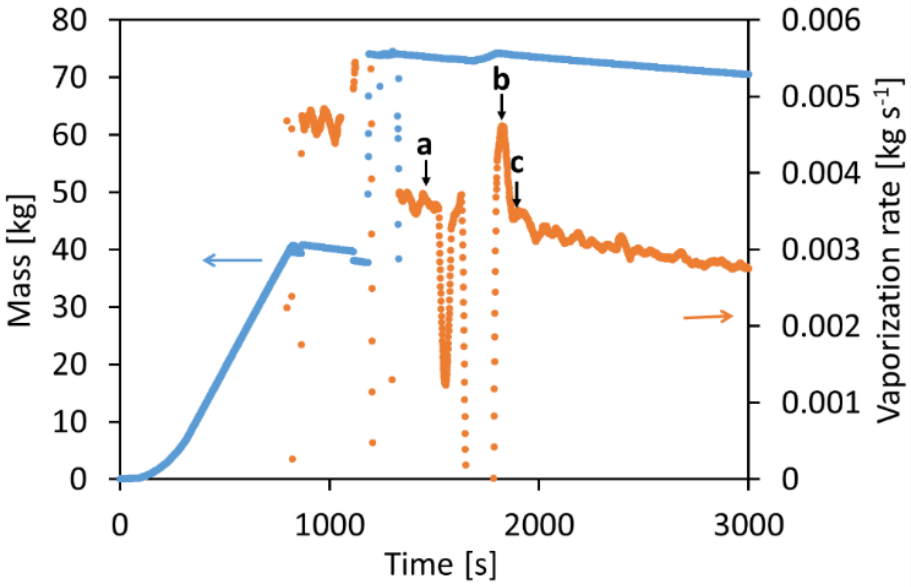

Figure 44 Mass curve and vaporization rate

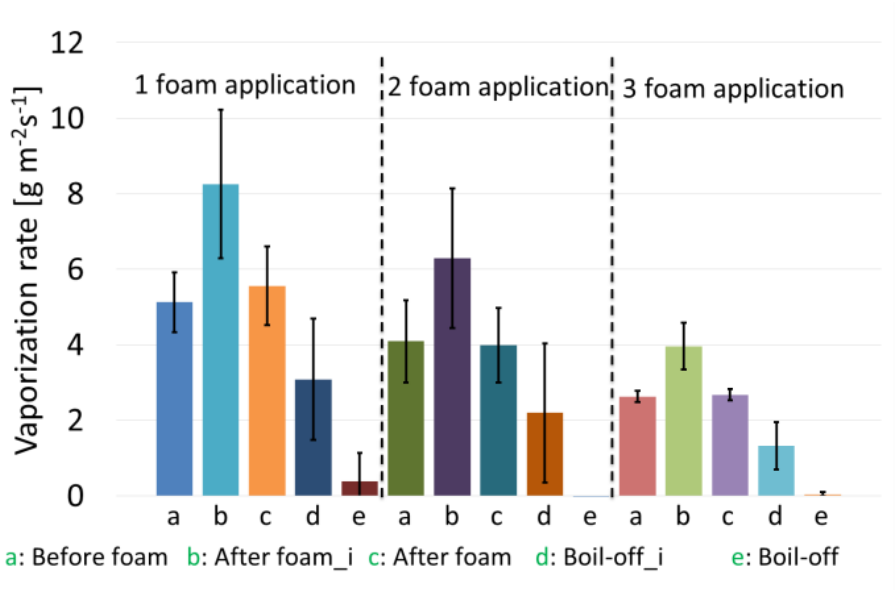

Figure 45 Boil-off effect of foam application

4.3.5 Oxygen measurement

Oxygen concentration on top of the foam fence is a key parameter to study, since it indirectly indicates the concentration of nitrogen in the air during the test. The oxygen concentration in air is 20.9%. When nitrogen evolved from the liquid nitrogen container and raised to the top of the foam fence, nitrogen replaced oxygen to reduce oxygen concentration. One oxygen sensor was fixed at the top of the foam fence as shown in Figure 36, which has a measurement range between 0.1 and 25 % oxygen. The installation of oxygen sensor is shown in Figure 46. An additional protection screen was used to protect the oxygen sensor from contacting the foam, because the water of the foam may damage the sensor. But the holes on the screen still allowed a good vapor circulation around the sensor.

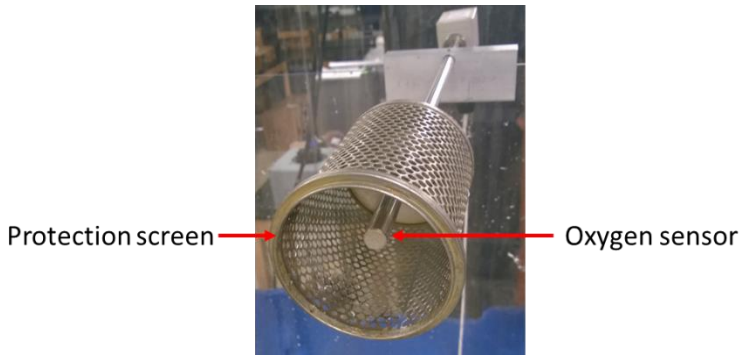

Figure 46 The installation of oxygen sensor

The oxygen concentration from two selected tests are shown in Figure 47 and Figure 48. The test in Figure 47 was conducted using method A. The oxygen concentration was reduced slowly after the foam fence was put on top of the container for liquid nitrogen, since the vaporization rate of liquid nitrogen was slow after the container was cooled down. During the first foam application, the oxygen concentration quickly dropped to approximately 13%, because the initial boil-off effect increased the vaporization rate of liquid nitrogen. When the first foam application was finished, the oxygen concentration returned to the normal level in the air. Because the foam blanket blocked the vapor pathway. After approximate one minute, nitrogen vapor pushed the foam and found a way out at the top. The location of the vapor exit was random, but often at the location that foam could not easily reach, such as the corner of the foam fence and the area below the oxygen sensor. When the vapor exit was not below the oxygen sensor, the change of oxygen concentration could not be measured as shown in Figure 47 after the first foam application. The oxygen centration returned to the normal level in the air after the initial boil-off effect. For the second and third foam application,

there was a reduced initial drop of oxygen concentration due to the boil-off effect, which was consistent with results in the section 4.3.4, *i.e.* the initial boil-off effect attenuated with foam application number. The oxygen centration returned to the normal level in the air until a vapor exit was formed below the oxygen sensor, *e.g.* the oxygen level dropped to approximate 16% at around 9000 second in Figure 47.

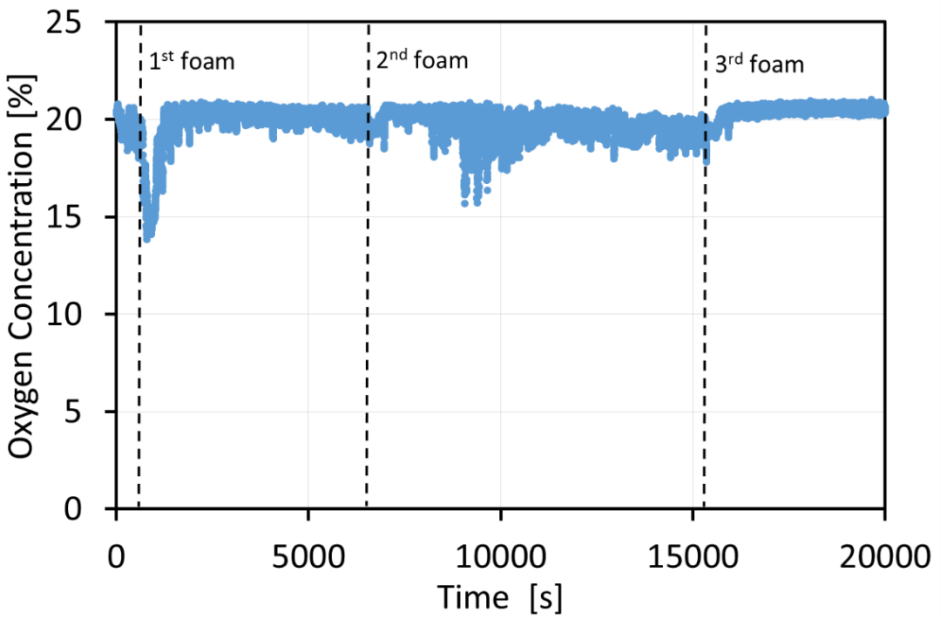

Figure 47 Oxygen measurement in a test conducted using method A

Figure 48 shows an oxygen measurement in a test conducted using method B. Because there was a continuous release of liquid nitrogen, the more vapor was evolving from the bottom. The oxygen concentration wad rapidly reduced to 3 % after the release of liquid nitrogen. Similarly, the oxygen concentration was increased to approximate 20 % with a full foam application to block vapor pathway. The oxygen concentration begun

to drop right after the vapor channel was formed, since much more vapor was raising from the bottom than the test conducted using method A. The oxygen concentration was as low as 6% before the second foam application. After the second foam application, the release of liquid nitrogen was stopped; therefore, the oxygen concentration begun to increase and approached to approximate 20 %.

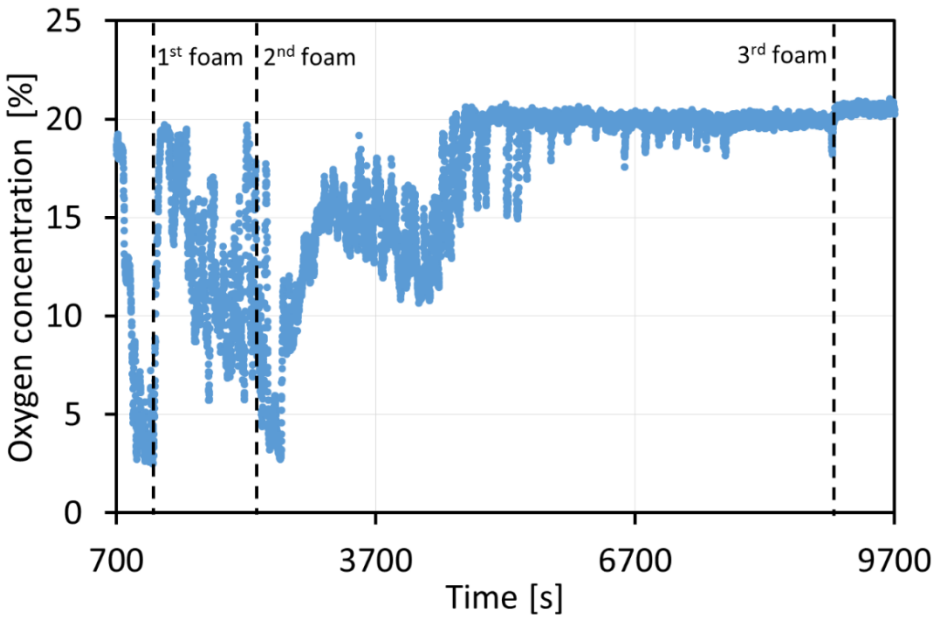

Figure 48 Oxygen measurement in a test conducted using method B

4.4 Conclusion

This work used a new self-constructed foam generator. The performance of the foam generator was characterized in terms of foam expansion ratio and generation rate. With the current setup, the range of foam expansion ratio was from 300 to 850, and the foam generation rate ranged from 1.26 to 2.17 m^3/min. The temperature profile above

the liquid pool indicated a temperature increase right after foam application. A temperature difference between foam and vapor was measured by a pair of thermocouples with special design. The formation of the vapor channel was discussed in terms of vapor channel location and size. The foam breaking rate was obtained through video analysis for tests conducted using two different methods. The boil-off effect was studied with more details, which confirmed that the boil-off effect was small and did not last long. The oxygen concentration on top of the foam fence was studied, which depends on the scenario of liquid nitrogen release and vapor channel location.

5. LNG POOL FIRE WITH FOAM APPLICATION

5.1 Introduction

One major hazard of the LNG spillage pool is the thermal radiation of a pool fire [48]. The spilled LNG forms a pool in the impoundment, and the vaporized LNG vapor will migrate long enough to find an ignition source if it is not properly controlled by safety measures, such as a dike, water curtain and high expansion foam. Once the vapor is ignited, the fire will flash back to the pool and cause a pool fire.

NFPA 59 A defines the "thermal exclusion zone" for an LNG fire using the criteria of 5 kW/m^2, and other organizations in the US and other countries adopt a similar radiation intensity [49]. In order to mitigate the risk of an LNG fire to a tolerable level in the facility, mitigation measures are required by NFPA 59 A [36]. High expansion foam was recommended by NFPA 11 and NFPA 471 [20, 37]. The expansion foam application helps to reduce the thermal hazard, but usually does not extinguish the fire. The mitigation effect of foam can reduce the mass burning rate, flame size, and radiation as discussed in previous work [12, 15, 17].

University Engineers Inc. conducted a number of tests for LNG spills on land in a project sponsored by the American Gas Association. The work regarding to expansion foam application found that high quality, small bubble foam reduces the LNG mass burning rate; foam with 500 expansion ratio provides the best fire control; and it can reduce up to 95% of fire radiation [15]. MKOPSC has been involved in the LNG safety research with expansion foam since 2004 [12, 17]. Suardin's work validated the

effective foam application rate (10 L/min m^2) for pool fire control [12]. Yun studied the effect of foam on the reduction of thermal exclusion zone and determined the minimum effective foam depth, 0.61 m, for LNG pool fire control [17].

Previous work found that the water discharge to the pool from the hydraulic foam generator at the beginning of foam generation could escalate the hazard rather than mitigate the hazard [17]. The hydraulic foam generator is not able to make good expansion foam immediately after it is started. Water will come out of the foam generator for a few seconds before good quality foam is produced. The added water is a heat source to vaporize LNG in the pool. The additional vapor will feed the fire to cause a larger flame and emit more heat, which is the initial negative effect. This initial water input requires a precaution when high expansion foam is used for LNG hazard mitigation. This work will use a new version of foam generator from ANSUL, USA, which has a new design to catch the water discharge and eliminate the initial negative effect. Also, this foam generator has a larger foam generation capacity. This work aims to study the mitigation effect of this new foam application setup, including mass burning rate, thermal radiation at downwind and crosswind direction, fire control time, maximum radiation reduction, temperature profile in the flame and foam blanket. In addition, visualization technique is used to study the fire and mitigation effect of foam, such as regular video camera, high speed camera and Infrared camera.

5.2 Material and methodology

5.2.1 Experimental setup

The LNG fire test was conducted at Brayton Fire Training Field (BFTF) in College Station, TX, USA. The setup is demonstrated in Figure 49. The big concrete pit was used in this work in order to obtain results that are more applicable to a real scale fire. The pit is 1.22 m deep below the ground with no lip above the ground. There were nine radiometers (Medtherm Corporation, USA) installed at the downwind and crosswind directions. One of the closest radiometers to the fire (R9) has a range of 120 kW/m^2 (Gardon gage type), the others have a range of 30 kW/m^2 (Schmidt-Boelter type). A thermocouple tower and a thermocouple block were installed in the pit. The thermocouple tower has six thermocouples (type K, shielded, 6.4 mm in diameter, Omega Engineering Inc., USA) installed between 0.5 m and 2.5 m high from the pit bottom surface, aiming to measure the temperature profile in the flame and the foam blanket. The thermocouple block has 24 thermocouples installed, and each thermocouple is 1 cm away from the next one at an elevation ranging from 0.64 cm to 24.64 cm from the pit bottom, aiming to determine the mass burning rate. The foam generator was placed at the upwind direction. The weather station and cameras were located at the crosswind direction. Radiometers and thermocouples were connected to the Data Acquisition System (DaqBoard 2005, Omega Engineering Inc., USA), which recorded the experimental data at 1Hz. Other information, such as weather, videos and foam generation operation condition, was recorded for further analysis. The fire was visualized by several CCD cameras, and a high-speed camera (Phantom v4.2, Vision

Research, Inc., USA) recording series of 4000 images at 1000Hz, as well as a FLIR SC3000 infrared camera with a temperature range of [253- 2273] K.

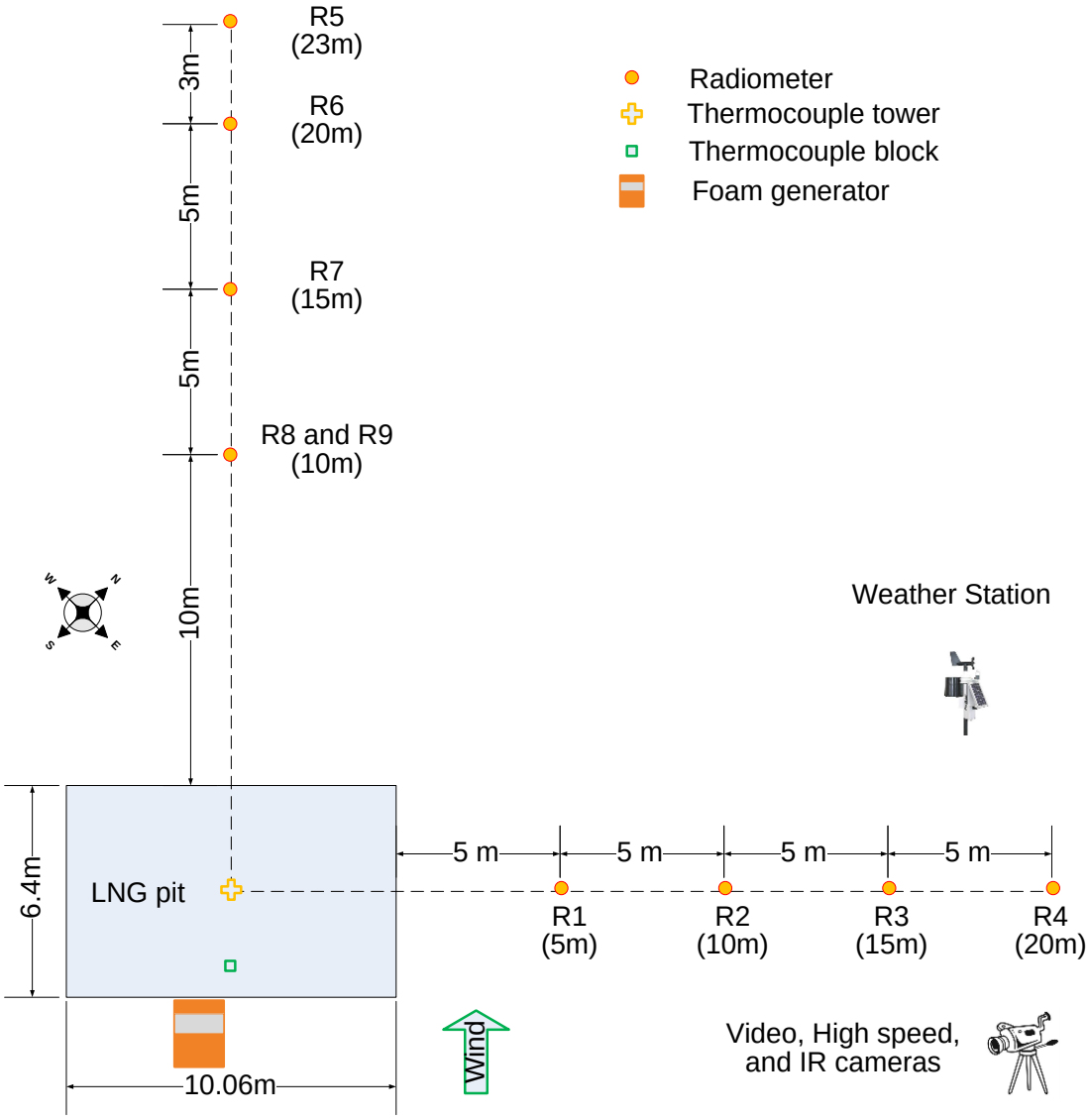

Figure 49 Schematic diagram of the experimental set-up

5.2.2 Foam generator

A new model of foam generator, JET-X-15A (LNG), was used in this work. This foam generator has a larger foam generation capacity. The maximum foam generation rate is 555 m^3/min with 100 psi water supply compared with 322 m^3/min in previous work [12, 17]. Also, this foam generator has a new feature to contain the undesirable water discharge. This foam generator, as shown in Figure 50 left, has a foam solution tray in front of the foam discharge point, which helps to temporarily contain the water and direct it to the drainage system through a hose. Previous work used another type of foam generator without the foam solution tray, as shown in Figure 50 right, which allows any water from the foam generator to discharge into the pit and cause an initial negative effect [17]. By using the foam generator with a foam solution tray, this effect is expected to be minimized and even eliminated.

Figure 50 Comparison of foam generators. (left: current one, right: previous one [17]**)**

The test was started by releasing LNG into the pit. The release was stopped when the LNG level was about 12.6 cm high, which took about 70 minutes to accumulate approximate 8.2 m^3 of LNG in the pit. Before the ignition of the fire, water curtains at the downwind direction were turned on to prevent the vapor from traveling too far with wind, which ensured the safe operation during the LNG release. Once there was enough LNG in the pit, the pool fire was ignited by the fire fighter on site using a torch. After 75 seconds of uncontrolled burning, high expansion foam was applied to mitigate the fire. Foam was stopped once and reapplied during the end of the test. The test was finished by exhausting the LNG in the pit.

5.2.3 Image processing

The CCD camera images were processed by using the Matlab Image Processing toolbox [50] to extract the time evolution of the pool fire flame length. The images are first converted to grayscale, cut to remove most of the environmental background surrounding the flame, and finally converted to black and white (BW) using a threshold determined with the Otsu method [51] . The flame boundary is then detected by the Moore-neighbor tracing algorithm modified by Jacob's stopping criteria [50][10]. The flame length is calculated from the flame boundary as the distance between the pool fire bottom and the highest pixel position of the boundary.

The high-speed images were processed using the Large Scale Particle Image Velocimetry (LS-PIV) technique [52], which calculates the flow velocity from an image pair using PIVLab, cross-correlation algorithms for Particle Image Velocimetry (PIV) developed by Thielicke and Stamhuis [53, 54]. The images were processed with an

initial window size of 32x32 pixels, two iterations, 50% overlapping, and an adaptive interrogation window shift was applied. For each set of 4000 images, the frame rate was decimated by two to allow a larger displacement between each image couple, allowing the computation of around 1000 flow fields per set (one flow field requiring an image pair). Before being averaged, improperly matched vectors were eliminated by removing all spurious high calculated displacement from a scatter plot and by using a standard deviation filter with a threshold of 7 times the standard deviation. [53, 54]. In addition, a filtering based on the light intensity of the original images was performed to remove velocity vectors that would correspond to areas where no structures are visible [55]. Finally, the resulting averaged velocity fields in pixels/s are converted to m/s by using a magnification factor calculated by comparing the distance between two poles surrounding the pit measured from an image with its real dimension.

5.2.4 Summary of test parameters

The test parameters like the pit dimensions, LNG composition and release conditions, foam concentrate, generator and generation conditions, and weather conditions, are summarized in Table 10.

Table 10 Test summary

Pit	Area of the pit (m^2)	64.38
	Equivalent pit diameter (m)	9.05
	Pit depth (m)	1.22
LNG	LNG composition	99.5% methane, 0.5% nitrogen
	Average heating value (kJ/m^3)	35579
	LNG pool height (cm)	12.6
Foam	Foam generator	JET-X-15A (LNG)
	Foam concentrate	JET-X type C high expansion foam concentrate (2¾%)
	Water pressure for foam generation (psi)	100
	Foam expansion ratio	560
	Foam generation rate (m^3/min)	555
	Foam generation rate per area (m/min)	8.62
Weather	Average wind speed for fire(m/s)	3.1 ± 0.5
	Wind speed for free burning fire (m/s)	4.0
	Air temperature (˚C)	24.81 ± 0.26
	Dominant Wind direction	SE
	Humidity (%)	55.56 ± 2.67

5.3 Results and discussion

5.3.1 Mass burning rate

Mass burning rate is an important parameter for pool fire study, since many correlations of flame length require this parameter, more importantly, it determines the total combustion heat of the fire. LNG mass burning rate has been reported for tests with various conditions as shown in Figure 51. The details of the tests conditions are

summarized in Table 11. The mass burning rates of fires on water are usually higher than those of fires on land due to the larger heat transfer rate provided by water. For the fires on land, the substrate has an effect on the mass burning rate. The fires in concrete pits, including Suardin and this work, tend to have a higher burning rate than those in the ground pits and insulated concrete pits.

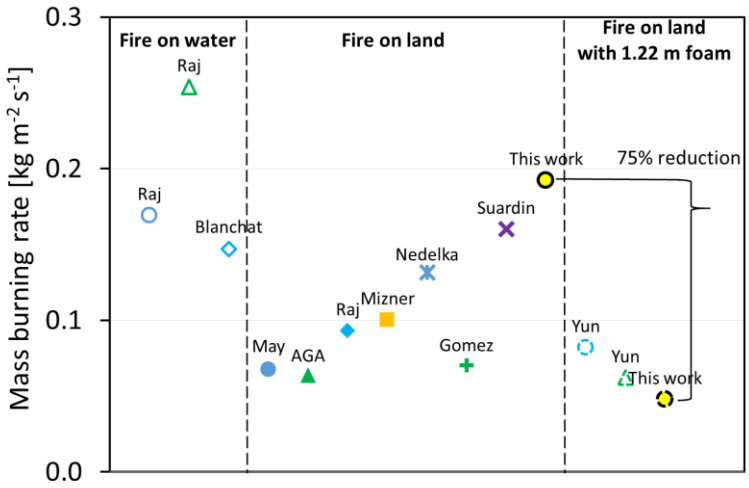

Figure 51 Summary of LNG mass burning rates at various conditions

The mass burning rate in this work was determined using the LNG level measurement through thermocouples on the block. The distance of two adjacent thermocouples on the block was 1 cm. The time for the LNG pool surface to move from one to the next one below was obtained using the LNG boiling temperature. Therefore, the mass burning rate can be calculated. The mass burning rate in this work was 0.192 kg/ (s m^2) in a 1.22 m deep concrete pit. With foam application, the mass burning rate was 0.048 kg/ (s m^2), which was 75% reduction compared with that of uncontrolled fire.

This work achieved a lower mass burning rate than previous tests in the same pit in 2009 with foam application, probably because this test had a higher foam generation rate.

Table 11 LNG pool fire mass burning rates

	Ref	Condition	Diameter [m]	Burning rate [kg m^{-2} s^{-1}]
Release on water	Raj et al. [56]	usnconfined pool with continuous release	13 [a]	0.169 [c]
	Raj et al. [56]	unconfined pool with continuous release	13 [a]	0.254 [c]
	Blanchat et al. [57]	unconfined pool	21	0.147
Release on land	May and McQueen [28]	land trench with continuous release	18 [b]	0.068 [c]
	AGA [58]	ground pit	1.8	0.063 [c]
	Raj and Atallah [29]	ground pit	6.1	0.093 [c]
	Mizner and Eyre [59]	insulated concrete pit	20	0.100 [c]
	Nedelka et al. [30]	insulated concrete pit	35	0.132 [c]
	Gomez [25]	insulated concrete pit	1.1 [b]	0.07
	Suardin [38]	concrete pit	9.1 [b]	0.16 [d]
	This work	concrete pit	9.1 [b]	0.192
Release on land with foam	Yun [17]	concrete pit with 1.2m foam	9.1 [b]	0.082
	Yun [17]	concrete pit with 1.2m foam	9.1 [b]	0.062
	This work	concrete pit with 1.2m foam	9.1 [b]	0.048

Note
a, the maximum diameter
b, the equivalent diameter
c, calculated from the liquid regression rate in [32] using LNG density of 423 kg/m^3
d, the minimum estimated value, the actual burning rate is larger

5.3.2 Flame geometry

Flame geometry is an important characteristic of a pool fire, since it helps to determine the fire model for radiation prediction. The point source model is widely used due to its simplicity; however, a sophisticated model, *e.g.*, the solid flame model, is more suitable for a large scale pool fire, since it has a better prediction of radiation for both near and far field by considering the flame shape and length [60, 61]. The flame is commonly treated as a cylinder as observed in Figure 52 left. The wind has an effect to tilt the flame; therefore, the flame is represented by a tilted cylinder, which was characterized by three parameters, flame length, diameter and tilted angle. With foam application, the flame diameter remained as same as the pit diameter, while the flame length was significantly reduced as shown in Figure 52 right.

Figure 52 LNG pool fire flame without (left) and with (right) foam application

The time evolution of the flame length determined from the CCD image processing is illustrated in Figure 53. The maximum measured flame length was 18.03 m before high expansion foam application; however, the flame occasionally went beyond

the images slightly due to oscillation as shown in Figure 52 left. Since the foam generator could not produce good foam right after it is started, the water discharge from foam generator escalated the fire and increased the flame size in previous work [17]. In this work, the foam solution tray could catch the water discharge before good foam was produced, the foam application could reduce the flame length immediately. A maximum of 79% reduction was achieved for the flame length during the steady state control. Once the foam was stopped, the flame begun to grow gradually until the second foam application.

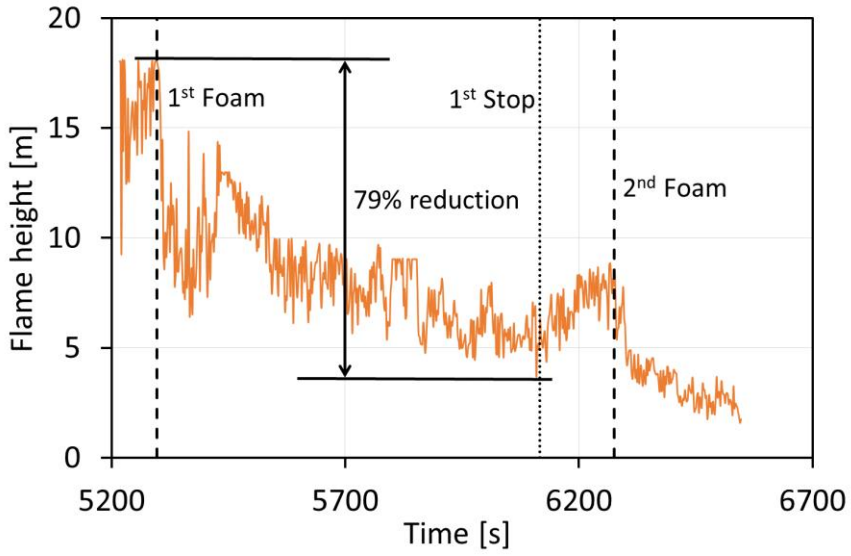

Figure 53 LNG fire flame length from CCD camera

Even at steady state conditions, diffusive flames oscillate with time, this is called flickering effect being related to the air entrainment [62]. The idea of intermittency *I(L)* was used to determine average flame length by Zukoski and Ferrero [63, 64], which is

defined as the time fraction that the flame length is larger than L. The average flame length is the flame length with intermittency of 0.5, which was 16.34 m at an average wind speed of 4 m/s before high expansion foam application in this work. The correlations in the literature mainly deal with the average flame length. For buoyancy dominated fires, the average flame length depends on the pool diameter (D), mass burning rate ($\dot{m}$) and wind velocity (u) as shown in Eq.(12), (13), and (14). This correlation was first proposed by Thomas [65]. Similar correlations were developed based on experimental data for various fuels. The correlation parameters a, b, and c were summarized by Laboureur [66], as shown in Table 12. Compared with the experimental result in this work, the majority of correlations tend to overestimate the average flame length, especially those that do not consider wind effect, such as Mangialavori and Thomas 1, Moorhouse correlation can provide a good prediction, since they were developed from LNG on land fires in a rectangular pit from 6.1m to 13.7 long. It was very similar with test conditions in this work. Moorhouse 1 used cylindrical flame, while Moorhouse 2 used conical flame. Surprisingly, Ferrero correlation is also fitting well even though it was designed for diesel. Given the fact that the flame length is considered as the distance from the ground to the top of flame, and the burning surface is 1.1 m below the ground in this work, therefore, the correlations giving sensibly higher flame length values are also fitting well this test.

$$\frac{L_{flame}}{D} = a(m^*)^b(u^*)^c \tag{12}$$

$$m^* = \frac{\dot{m}}{\sqrt{gD}\rho_a} \tag{13}$$

$$u^* = \frac{u}{\left(\frac{g\dot{m}D}{\rho_a}\right)^{\frac{1}{3}}} \tag{14}$$

Table 12 Pool fire flame length using different correlations

Author	a	b	c	L/D	L [m]	error [%]
Ferrero [64]	4.201	0.181	-0.082	1.92	17.37	6%
Mangialavori [67]	31.6	0.58		2.94	26.59	63%
Moorhouse 1 [68]	6.2	0.254	-0.044	2.14	19.39	19%
Moorhouse 2 [68]	4.7	0.21	-0.114	1.88	16.98	4%
Pritchard [69]	10.615	0.305	-0.03	3.00	27.13	66%
Thomas 1 [70]	42	0.61		3.45	31.25	91%
Thomas 2 [70]	55	0.67	-0.21	3.18	28.76	76%

5.3.3 Flame velocity field

The averaged velocity magnitude computed from the high-speed images using the LS-PIV technique can be observed in Figure 54. Before the foam application, as already observed from the CCD camera images, the fire is very large and titled due to the wind conditions. The velocity is larger at the center of the pool fire, and decreases as

the side extremities. The velocity is also smaller at the base of the fire, and accelerates along the flow centerline.

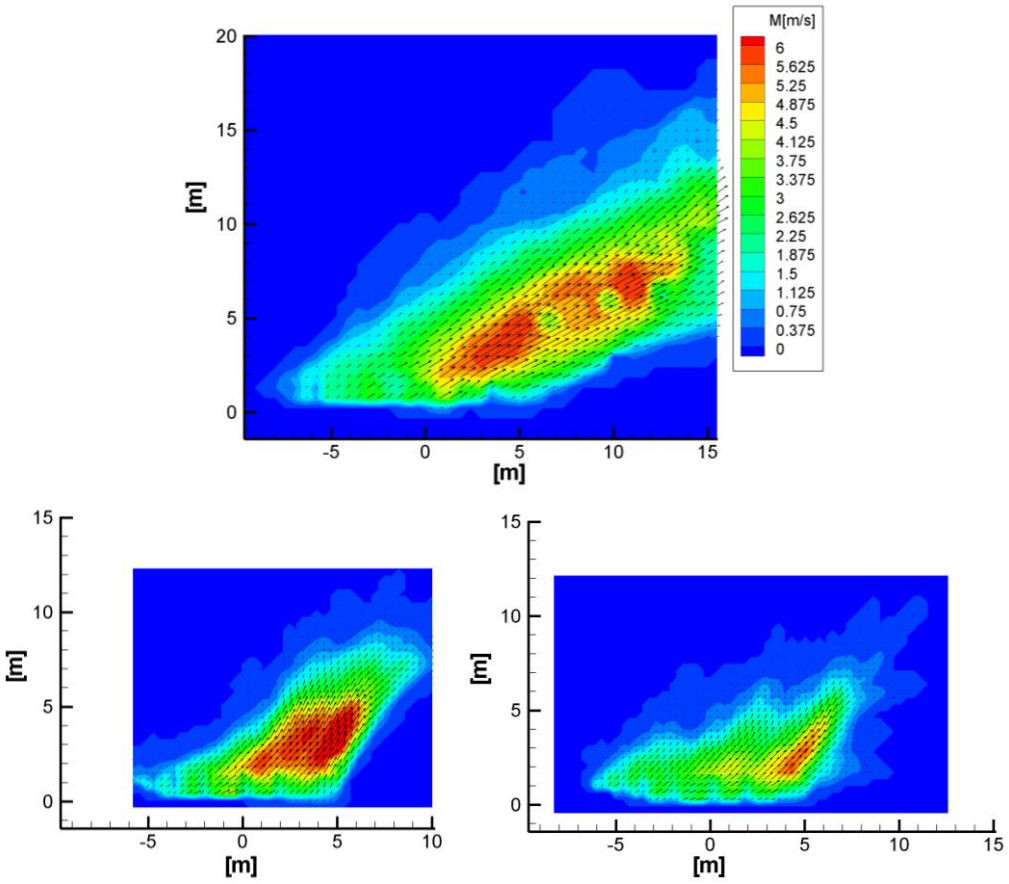

Figure 54 Averaged fire velocity magnitude. Top: Before foam application, Bottom: after foam application (left, immediately after, right, minutes after)

Not many studies have been found in literature about experimental study of pool fire velocity fields for LNG. A close study has been performed by Tieszen et al. [71], who performed PIV analysis of 1m methane pool fires and presented the averaged velocity field of 1331 images pairs, close in number to the 1018 image pairs average of

this study. The comparison between Tieszen experiments and these results for the vertical averaged velocity magnitude $(U^2+V^2)^{1/2}$ is showed in Figure 55. Although the fire is this study is tilted and larger than that in Tieszen study, the values of the velocity magnitude and the distribution of velocity are similar in both studies.

Looking at the averaged velocity magnitude for the fire after the application of foam, it can be observed that, right after the foam application, the flame has already decreased significantly in size, but the velocity is still high, especially at the center (Figure 54 bottom left). With time, the flame decreases in size as well as in velocity magnitude (Figure 54 bottom right). The flame tilted angle modification with time is due to a slight diminution of the wind speed. The decrease of the flame size between Figure 54 top and bottom is due to the application of the foam as the foam blanket reduces the fire burning rate due to its heat absorption and oxygen dilution effect [72]. The foam application does not a priori change the velocity field at the base of the flame, but a more extensive study zoomed at the base of the flame would be needed to confirm this conclusion. The velocity field at the center of the flame is not reduced by the foam application immediately as shown in Figure 54 bottom left, but it is reduced with continuous mitigation effect of foam as shown in Figure 54 bottom right.

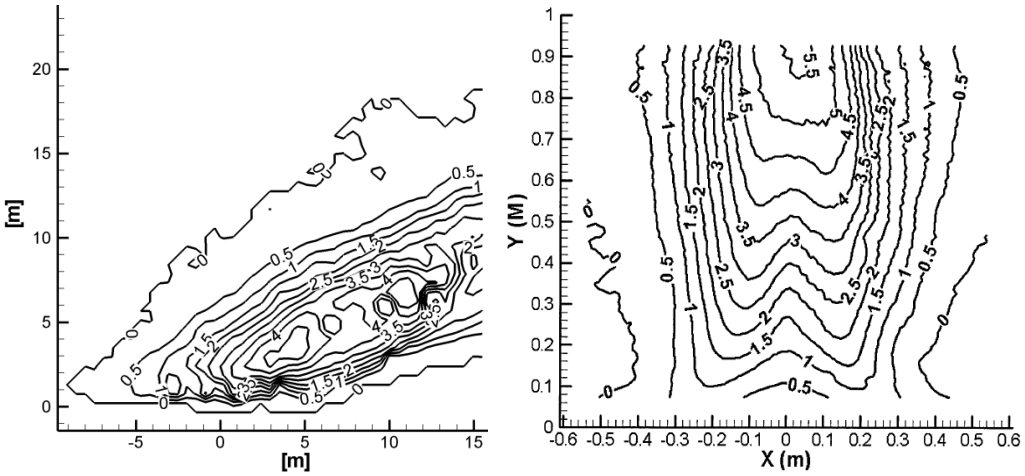

Figure 55 Vertical velocity contour plot. Left: LNG fire of this study (before foam application), Right: 1m methane fire [71]

5.3.4 Thermal radiation

The radiation was monitored for both crosswind and downwind direction, and results at the crosswind direction are shown in Figure 56. Before the first foam application, the radiation for all locations was high. Even at a location of 20 m away from the fire (R4), the radiation could be more than 10 kW/m^2, which is double of the radiation level for the exclusion zone defined by NFPA 59A. With respect to R1 (5 m from the fire), the radiation intensity was above the measurement limit of the radiometer before the first foam application; therefore, only a plateau of 30 kW/m^2 was shown for the measurement. With the foam application, the radiation intensities at all locations were reduced immediately due to reduced flame size and cooling effect of foam [72]. Not surprisingly, there was no sign of the initial negative effect, since water discharge into the LNG pool was eliminated by the foam solution tray. With the continuous foam application, the radiation intensities kept decreasing, except the turbulence caused by the

change of wind speed and shift of wind direction, such as the peak at approximate 5400s. Foam application was stopped after about 810 seconds. The existing foam blanket had a remaining effect of fire mitigation. The radiation intensities were decreasing before the foam blanket was broken by the fire. Then, the radiation intensities began to grow without an intact foam blanket, and decrease again after the second foam application.

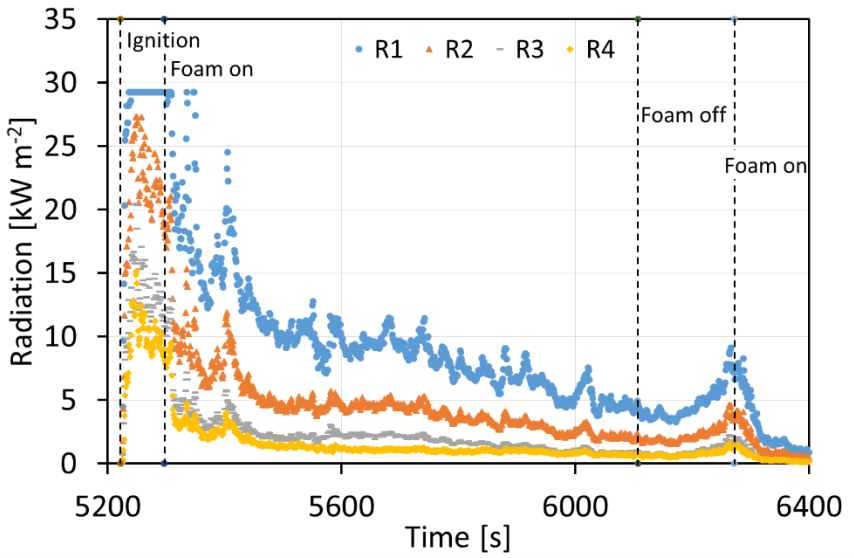

Figure 56 Radiation at the crosswind direction

The radiation intensities at the downwind direction had a similar trend in terms of the mitigation effect provided by the foam, but with much higher values. R9, which was 10 m away from the fire, had a maximum radiation intensity of 107 kW/m^2. R5, which was 23 m away from the fire, had a maximum radiation of 25.1 kW/m^2, which is five times the radiation level for the exclusion zone defined by NFPA 59A. The radiation was so large at the downwind direction that R7 and R8 were showing a plateau of 30 kW/m^2

until foam had been applied for a while, and the cables of R5, R6 and R9 were damaged shortly after they received the maximum radiation and resulted in loss of communication with the Data Acquisition System.

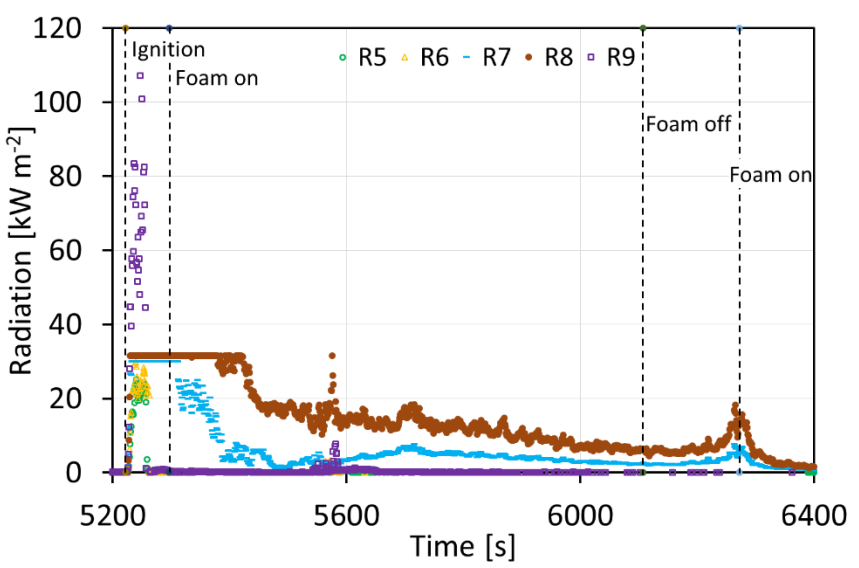

Figure 57 Radiation at the downwind direction

Suardin conducted a number of similar tests in the same pit, and the radiation at a distance of 30 meters was reported with and without foam application [12]. The radiation intensity at the crosswind direction in this work together with reported values by Suardin are shown in Figure 58. Several data points from Suardin's work are too similar so that they overlap in the figure. The data points in this work were extrapolated to 30 m exponentially, since this correlation could fit the data best. Compared with Suardin's results, the correlation slightly overestimates the radiation before foam application and underestimates the radiation with foam application. In both work, the

radiation was reduced significantly by high expansion foam application. The radiation could be higher than 5 kW/m^2 at 30 meters away from the fire with no foam application, while radiation was lower than 5 kW/m^2 at 5 meters away from the fire with foam application, which is at least six time reduction in terms of the thermal exclusion zone.

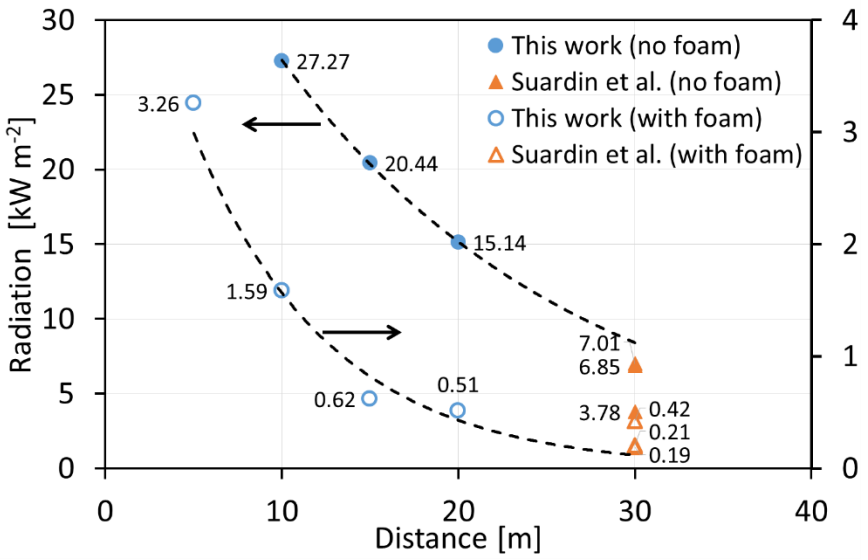

Figure 58 Comparison of radiation at the crosswind direction with reported radiation

5.3.5 Fire mitigation effect

Two parameters are used to characterize the fire mitigation effect in this work, fire control time and maximum radiant reduction. Fire control time is defined as the time that is required to reduce 90% of the maximum thermal radiation from the point of foam application. The maximum radiation reduction is the maximum percentage of radiation reduction provided by high expansion foam application.

The fire control time has been discussed in Suardin's work [12], which studied its effect of the foam application rate on fire control time. Clearly, higher foam application rate requires less time to control fire in term of the radiation reduction as shown in Figure 59. In the Suardin's work, the maximum foam application rate was 5 m/min, which is short for $m^3/ (m^2 min)$ and means the foam volume rate per area of the pit. The foam generator used in this work could provide a larger foam application rate, 8.62 m/min. The results in this work confirm previous conclusion about the effect of foam application rate on fire control time. If extrapolating the results in this work exponentially, the fire control time at 30 m will be 37 seconds, which is smaller than that using 5 m/min foam application rate, as shown in Figure 59. This work also reveals that the distance from the fire is a factor to affect the fire control time, since when the flame length is reduced, it affects more on the far target in terms of view factor calculation in the solid flame model [73] The fire control time increased significantly at locations within 15 meters away from the fire. The fire control time was about 10 times at 10 meters of that at 30 meters.

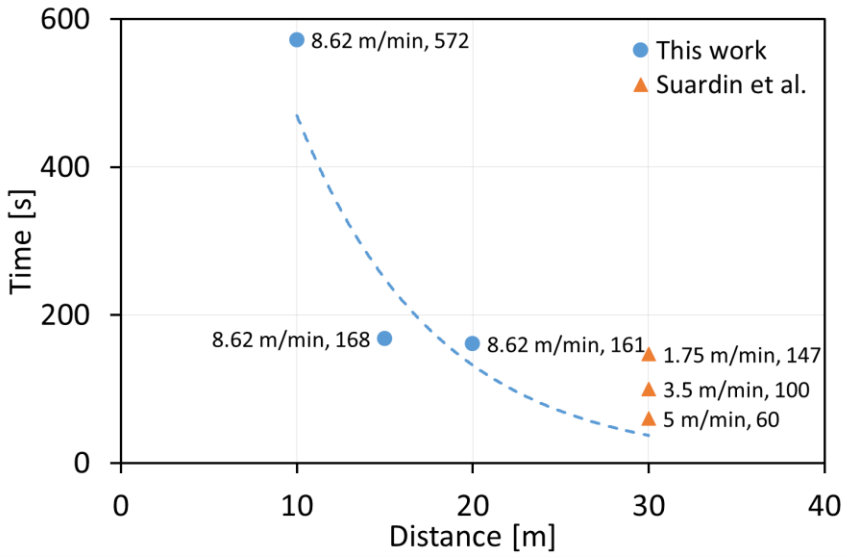

Figure 59 Fire control time at various distances and various foam application rates

Similarly, Suardin' work indicates that high foam application rate enhances maximum radiation reduction slightly [12]. The maximum reduction achieved by 5 m/min of foam application was 97%. University Engineers Inc. reported that good quality foam could reduce up to more than 95% of radiation [15] The distance from the fire also had some impact on the maximum radiation reduction base on this work as shown in Figure 60. The reduction was improved slightly from 94% to 97% at a location from 10 meters to 20 meters at the crosswind direction. The reduction of 97% is the highest value reported in these work above.

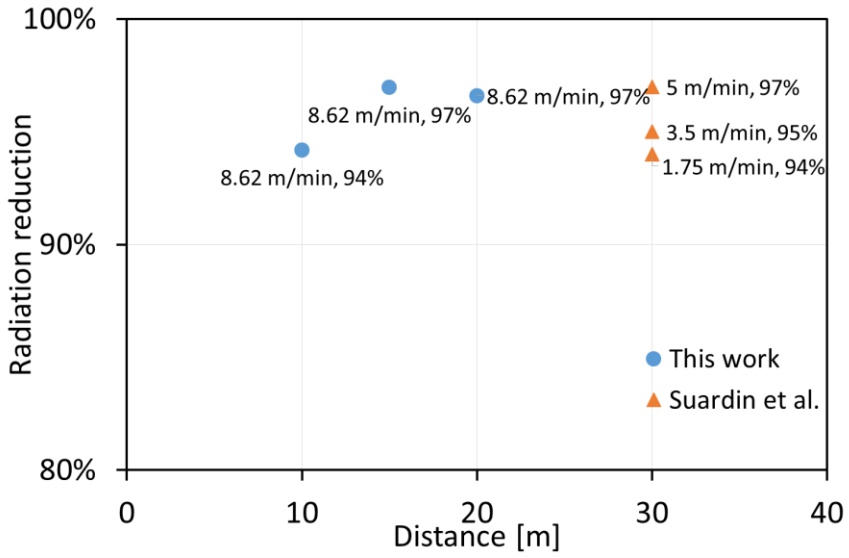

Figure 60 Maximum radiation reduction at various distance and foam application rates

5.3.6 Temperature profile

The thermocouples on the tower measured the temperature profile above the LNG pool as shown in Figure 61. The foam could reach as high as the pit height, *i.e.*, 1.22 m. Therefore, thermocouples above 1.22 m were always in the flame after ignition. Thermocouples below 1.22 m were covered by the foam after the foam application.

For the two thermocouples that were always in the flame, the one at 2 m generally had a higher temperature than that at 2.5 m. The temperature of these two thermocouples began to rise after the ignition of the fire. The temperature did not stop rising right after the first foam application. It began to decrease after the pit was well covered by the foam blanket as indicated by the temperature decrease at 1.1 m. The temperature at 2 m achieved a peak value of 868 ˚C before it began to decrease. The temperature at 2.5 m was more vulnerable to the weather conditions, since the position

was higher. The temperature evolution shows a same turbulence trend as radiation in Figure 56. For the two thermocouples that might be covered during the tests, the temperature began to rise after the ignition. The temperature began to decrease until the thermocouples were covered by the foam. The thermocouple at 0.8 m was first covered followed by the one at 1.1 m eventually. There were two stages to reduce the temperature in the foam. At the first stage, the temperature decreased slowly right after the thermocouples were covered by the foam, since the fire still had a significant effect when the foam layer above the thermocouple was thin. At the second stage, the temperature decreased rapidly after the foam layer above the thermocouple was thick enough to block the radiant heat from the flame. The temperature reduction rates at two stages were 3 ˚C /s and 16 ˚C /s at 0.8m, and 2 ˚C /s and 16 ˚C /s at 1.1 m. At the steady state control, the temperature dropped to around 30 ˚C, which was about 6 ˚C above the ambient temperature, and remained stable until the thermocouples exposed to the flame again after stopping the first foam application,. The temperature begun to rise as the foam layer became thinner without foam application. It began to drop after the second foam application. Since the temperature was so low in the foam blanket, the combustion could only exist above the foam. Also, the fire had little effect on LNG vaporization rate, because the temperature in the foam was very similar with the air temperature. The foam could block almost all the radiant heat from the flame. The conduction from the dike provided the dominant heat for LNG vaporization.

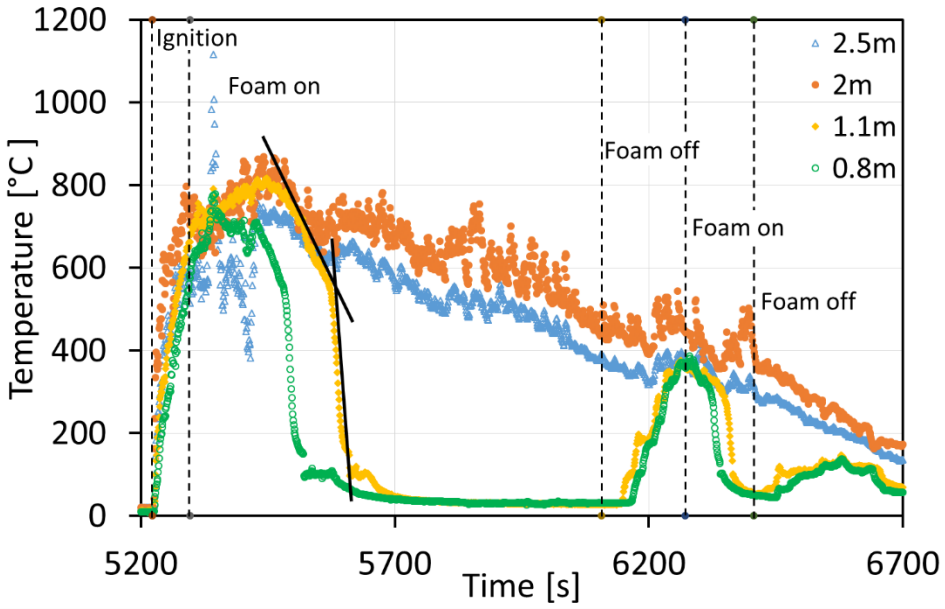

Figure 61 Temperature profiles in the flame and foam zone

5.4 Conclusion

The mass burning rate was obtained using thermocouples for the LNG fire. The high expansion foam application can reduce 75% of the mass burning rate. The work experimentally determined the flame length for LNG free burning fire and mitigated fire with high expansion foam. The measured flame length for LNG free burning fire was compared with correlations in the literature, which shown that the correlation developed for LNG fire had a good prediction for this test. The foam application can reduce the flame length by 79%. The flame velocity filed from the high speed camera had a similar behavior compared with a small scale methane fire. The burning velocity at the center of flame was reduced with continuous foam application. The mitigation effect of foam was characterized by fire control time and radiation reduction. The maximum mitigation

effect was 97% in terms of radiation. The temperature profile above the LNG liquid pool was studied, which indicated that the majority of the radiant heat from the fire was blocked by the foam blanket and the conduction from the pit provided the dominant heat for LNG vaporization.

6. CONCLUSION AND RECOMMENDATION

6.1 Summary and conclusions

This work experimentally studied the mitigation effect of high expansion foam on LNG vapor hazard and pool fire hazard for a spill on land. The study on vapor hazard mitigation included the blanketing effect on source term (vaporization rate), warming effect on vapor buoyancy and other physical interactions between LNG and high expansion foam. The study on LNG pool fire control focused the effect of high expansion foam on several key parameters of pool fire, *i.e.* mass burning rate, flame geometry, flame velocity field, thermal radiation, and flame temperature. The findings in this work will be used to provide recommendations on the application of high expansion foam to LNG on land spills during emergency response.

6.1.1 Blanketing effect on vapor hazard

The study on blanketing effect of high expansion foam was conducted in a wind tunnel using liquid nitrogen, in which the convection and radiation were provided manually. This work quantitatively studied the boil-off effect on increasing the LN_2 vaporization rate. Also, the study found the blocking effect on eliminating convection and radiation for LN_2 vaporization. The blanketing effect was quantified by combining boil-off effect and blocking effect together, which reduced 70 % of the heat flux from convection and radiation for LN_2 vaporization. The blanketing effect had no effect on conduction; therefore LN_2 kept vaporizing at a lower rate with high expansion foam application. The water from the foam caused the boil-off effect. Before the formation of

ice plate, the initial boil-off effect was larger than that after the formation of ice plate, but still small and negligible compared with the blanketing effect on reducing convection and radiation.

The water draining rate is important to determine the boil-off effect, therefore the blanketing effect. The physical properties can determine the water drainage rate. The external factors, *e.g.* wind speed and radiation, can also affect the water drainage rate.

6.1.2 Warming effect and other physical interactions

One new lab scale foam generator was built based on the schematic design of NFPA 11. Several improvements were made to enhance the safe operation, meet the experimental demands and simplify the system. The performance of the foam generator was studied in terms of foam expansion ratio and generation rate. With the current setup, the range of foam expansion ratio was from 300 to 850, and the foam generation rate ranged from 1.26 to 2.17 m^3/min.

The warming effect on LNG vapor was studied in lab scale tests using liquid nitrogen, which employed a self-designed foam test apparatus. A special thermocouple installation was designed and used, which aims to measure the temperature profile of foam and vapor. The results shown a temperature increase right after the foam application. Also, there was a temperature difference for two thermocouples at the same elevation, which is an evidence for the heat transfer between foam and vapor.

The vapor evolving from the bottom rose in the foam blanket. The vapor channel was formed along the vapor pathway. The location and size of vapor channel was discussed based on experimental observation. The foam breaking rate was obtained

through video analysis for tests conducted using two different methods. High vaporization rate tended to increase initial foam breaking rate, but had no obvious effect on foam breaking rate during steady state. The boil-off effect was studied with more details, which confirmed that the boil-off effect is small and does not last long. The oxygen concentration above the foam fence was studied, which depends on the scenarios of liquid nitrogen release and the location of the nitrogen vapor exit.

6.1.3 LNG pool fire mitigation

The LNG free burning pool fire was studied in terms of mass burning rate, flame geometry, flame velocity field, radiation and flame temperature. The mass burning rate was 0.192 kg m^{-2} s^{-1}, which was slightly larger than those tests conducted in the ground pit and insulated concrete pit. The measured average flame length was 16.34 m, which was well predicted by a correlation developed for LNG pool fire. The flame velocity field had a similar behavior with that of a small scale methane fire. The radiation were measured at both downwind and crosswind directions. The maximum flame temperature was 868 ˚C in this test.

The mitigation effect of foam was characterized by the effects on reducing mass burning rate, flame size and radiation. High expansion foam reduced 75% of the mass burning rate, 79% of flame length, and 97% of radiation. The flame velocity at the center of the flame was also reduced with continuous foam application. The temperature profiles above the LNG pool indicated that the LNG vapor could only burn above the foam blanket. The majority of radiant heat from the fire was blocked by foam blanket. The conduction from the pit provided the main heat source for LNG vaporization.

6.2 Recommendations for future research

The foam stability is very important for the ability to mitigate LNG spill hazards, because more stable foam has a smaller water drainage rate and boil-off effect. It will be very useful to conduct a research on increasing the foam stability. The work should identify a new formula of the foam concentrate with a reasonable cost. Also, a study on the relationship between the water drainage rate of foam and the external factors should be interesting. Various wind speeds and radiation levels should be applied to examine the effect on foam breaking rate experimentally.

High expansion foam is applied in a much larger pit for industrial application. It will take some time for foam to spread and cover the LNG pool surface. The study on foam spreading can help to understand the foam behavior in the pit and predict the time to cover the liquid pool.

The physical mechanisms of boil-off effect remains unclear. The water in the foam is considered as the heat source of boil-off effect, but how foam and LNG physically interact with each other has not been study. An apparatus should be designed to allow the observation of the process.

Regarding to LNG fire control, high expansion foam aims to control to the fire rather than extinguish the fire. In order to improve the performance, fire retardants can be added into the foam concentrate for foam application. The fire retardant foam should be tested through LNG field tests.

REFERENCES

1. International Energy Agency, “World Energy Outlook 2014, Executive Summary,” 2014. [Online]. Available: http://www.iea.org/.

2. “Cleveland East Ohio Gas explosion,” 2015. [Online]. Available: http://en.wikipedia.org/wiki/Cleveland_East_Ohio_Gas_explosion. [Accessed: 01-Jan-2015].

3. “NaturalGas.org,” 2015. [Online]. Available: http://naturalgas.org/. [Accessed: 01-Jan-2015].

4. Central Intelligence Agency, “The World Factbook.” [Online]. Available: https://www.cia.gov/index.html. [Accessed: 01-Jan-2015].

5. U.S. Energy Information Administration, “Annual Energy Outlook 2014,” 2014. [Online]. Available: http://www.eia.gov/.

6. Federal Energy Regulatory Commission, “Natural gas,” 2015. [Online]. Available: http://www.ferc.gov/industries/gas/indus-act/lng.asp. [Accessed: 01-Jan-2015].

7. J. C. Bronfenbrenner, M. Pillarella, and J. Solomon, “Selecting a suitable process,” 2009. [Online]. Available: LNGINDUSTRY.COM. [Accessed: 20-Aug-2015].

8. M. Pillarella, Y. Liu, J. Petrowski, and R. Bower, “The C3MR liquefaction cycle: versatility for a fast growing, ever changing LNG industry,” in *Proceedings of the 15th International Conference and Exhibition on Liquefied Natural Gas*.

9. The international group of liquefied natural gas Importers, “LNG information paper No. 5, Managing LNG Risks –Containment.” [Online]. Available: http://www.giignl.org/. [Accessed: 20-Aug-2015].

10. M. A. Rana, Y. Guo, and M. S. Mannan, “Use of water spray curtain to disperse LNG vapor clouds,” *J. Loss Prev. Process Ind.*, **23**, 1, 77–88 (2010).

11. M. A. Rana and M. S. Mannan, “Forced dispersion of LNG vapor with water curtain,” *J. Loss Prev. Process Ind.*, **23**, 6, 768–772 (2010).

12. J. A. Suardin, Y. J. Wang, M. Willson, and M. S. Mannan, “Field experiments on high expansion (HEX) foam application for controlling LNG pool fire,” *J. Hazard. Mater.*, **165**, 1–3, 612–622 (2009).

13. J. A. Suardin, R. Qi, B. R. Cormier, M. Rana, Y. Zhang, and M. S. Mannan, "Application of fire suppression materials on suppression of LNG pool fires," *J. Loss Prev. Process Ind.*, **24**, 1, 63–75 (2011).

14. K. Takeno, T. Ichinose, K. Tokuda, R. Ohba, K. Yoshida, and K. Ogura, "Effects of high expansion foam dispersed onto leaked LNG on the atmospheric diffusion of vaporized gas," *J. Loss Prev. Process Ind.*, **9**, 2, 125–133 (1996).

15. University Engineers Inc., "An Experimental Study on the Mitigation of Flammable Vapor Dispersion and Fire Hazards Immediately Following LNG Spills on Land," American Gas Association, Arlington, Va., (1974).

16. G. Yun, D. Ng, and M. S. Mannan, "Key Observations of Liquefied Natural Gas Vapor Dispersion Field Test with Expansion Foam Application," *Ind. Eng. Chem. Res.*, **50**, 3, 1504–1514 (2011).

17. G. Yun, D. Ng, and M. S. Mannan, "Key Findings of Liquefied Natural Gas Pool Fire Outdoor Tests with Expansion Foam Application," *Ind. Eng. Chem. Res.*, **50**, 4, 2359–2372 (2011).

18. Pittsburgh Corning, "FOAMGLAS® Insulation Systems for Industry," 2015. [Online]. Available: http://www.industry.foamglas.com/. [Accessed: 01-Jan-2015].

19. "Fire fighting foam," 2014. [Online]. Available: http://en.wikipedia.org/wiki/Fire_fighting_foam#cite_note-loran-0. [Accessed: 01-Jan-2015].

20. National Fire Protection Association, "NFPA 11: Standard for Low-, Medium, and High-Expansion Foam." 2010.

21. Tyco Fire Protection Products, "JET-X HIGH-EXPANSION FOAM GENERATORS Data / Specifications." 2012.

22. H. C. Goldwire, H. C. Rodean, R. Cederwall, E. J. Kansa, R. P. Koopman, J. W. Mcclure, T. G. Mcrae, L. K. Morris, K. L, K. RD, U. PA, and L. (UWC) CD, "Coyote Series Data Report LNL/NWC 1981 LNG spill Tests Dispersion,Vapor burn and rapid phase transition," DE84 005138, (1983).

23. R. Qi, D. Ng, B. R. Cormier, and M. S. Mannan, "Numerical simulations of LNG vapor dispersion in Brayton Fire Training Field tests with ANSYS CFX.," *J. Hazard. Mater.*, **183**, 1–3, 51–61 (2010).

24. P. Cleaver, M. Johnson, and B. Ho, "A summary of some experimental data on LNG safety," *J. Hazard. Mater.*, **140**, 3, 429–438 (2007).

25. C. Gomez, "Experiments for the Measurement of LNG Mass Burning Rates," Texas A&M University, College Station, TX, 2011.

26. U.S. Department of Energy (DOE), "Liquefied Natural Gas (LNG) Safety Research. Report to Congress.," Washington, DC 20585, (2012).

27. G. A. Mizner and J. A. Eyre, "Radiation From Liquefied Gas Fires On Water," *Combust. Sci. Technol.*, **35**, 33–57 (1983).

28. W. G. May and W. McQUEEN, "Radiation from Large Liquefied Natural Gas Fires," *Combust. Sci. Technol.*, **7**, 51–56 (1973).

29. P. Raj and S. Atallah, "Thermal radiation from LNG spill fires," in *Adv. Cryog. Eng.; (United States)*, **20**, 1975.

30. D. Nedelka, J. Moorhouse, and R. F. Tucker, "The Montoir 35m Diameter LNG Pool Fire Experiments," in *9th Intl. Conf. & Expo on LNG*, 1989.

31. S. Coldrick, C. J. Lea, and M. J. Ivings, "Validation Database for Evaluating Vapor Dispersion Models for Safety Analysis of LNG Facilities," Quincy, MA, USA, (2010).

32. P. K. Raj, "LNG fires: a review of experimental results, models and hazard prediction challenges.," *J. Hazard. Mater.*, **140**, 3, 444–64 (2007).

33. R. Hiltz, "Foam blanketing: the use of foam to mitigate the vapor hazard of spilled volatile chemicals," in *Prevention and control of accidental releases of hazardous gases*, 216–231, John Wiley & Sons, 1993.

34. Energy Information Administration, "Natural Gas 1998 Issues and Trends," Washington, DC, (1999).

35. U.S. Energy Information Administration, "International Energy Outlook 2013," Washington, DC, (2013).

36. National Fire Protection Association, "NFPA 59A: Standard for the Production, Storage, and Handling Of Liquefied Natural Gas (LNG)." 2013.

37. National Fire Protection Association, "NFPA 471: Recommended Practice for Responding to Hazardous Materials Incidents." 2002.

38. J. A. Suardin, "The application of expansion foam on liquefied natural gas (LNG) to suppress LNG vapor and LNG pool fire thermal radiation," Texas A&M University, College Station, TX, 2008.

39. "Measurement of Solar Radiation," 2014. [Online]. Available: http://www.pveducation.org/pvcdrom/properties-of-sunlight/measurement-of-solar-radiation. [Accessed: 01-May-2014].

40. R. C. Reid, "Boiling of LNG on Typical Dike Floor Materials," Massachusetts Institute of Technology, LNG Research Centre, Cambridge, MA, (1980).

41. F. Briscoe and P. Shaw, "Spread and evaporation of liquid," *Prog. Energy Combust. Sci.*, **6**, 2, 127–140 (1980).

42. E. Haynes, William M., *CRC Handbook of Chemistry and Physics*, 92nd ed. CRC Press, 2011.

43. L. Véchot, T. Olewski, C. Osorio, O. Basha, Y. Liu, and S. Mannan, "Laboratory scale analysis of the influence of different heat transfer mechanisms on liquid nitrogen vaporization rate," *J. Loss Prev. Process Ind.*, **26**, 3, 398–409 (2013).

44. F. P. Incropera and D. P. DeWitt, *Fundamentals of heat and mass transfer*. New York: John Wiley, 2001.

45. J. L. Woodward and R. M. Pitblado, *LNG Risk Based Safety: Modeling and Consequence Analysis*. Wiley-AIChE, 2010.

46. Federal Energy Regulatory Commission, "LNG," 2015. [Online]. Available: http://www.ferc.gov/industries/gas/indus-act/lng.asp. [Accessed: 01-Jan-2015].

47. B. Zhang, Y. Liu, T. Olewski, L. Vechot, and M. S. Mannan, "Blanketing Effect of Expansion Foam on Liquefied Natural Gas (LNG) Spillage Pool," *J. Hazard. Mater.*, **280**, 380–388 (2014).

48. United States Government Accountability Office, "Public Safety Consequences of a Liquefied Natural Gas Spill Need Clarification," Washington, DC, (2007).

49. P. K. Raj, "A review of the criteria for people exposure to radiant heat flux from fires," *J. Hazard. Mater.*, **159**, 1, 61–71 (2008).

50. R. C. Gonzalez, R. E. Woods, and S. L. Eddins, "Digital Image Processing Using Matlab," *Education*, **624**, 2. 609, 2004.

51. N. Otsu, "A Threshold Selection Method from Gray-Level Histograms," *IEEE Trans. Syst. Man Cyber*, **1**, 62–69 (1979).

52. D. Laboureur, L. Aprin, A. Osmont, J. M. Buchlin, and P. Rambaud, "Small scale thin-layer boilover experiments: Physical understanding and modeling of the water

sub-layer boiling and the flame enlargement," *J. Loss Prev. Process Ind.*, **26**, 6, 1380–1389 (2013).

53. W. Thielicke and E. J. Stamhuis, "PIVlab – Towards User-friendly, Affordable and Accurate Digital Particle Image Velocimetry in MATLAB," *J. Open Res. Softw.*, 2(1):e30 (2014).

54. W. Thielicke, "The Flapping Flight of Birds – Analysis and Application," University of Groningen, Groningen, Netherlands, 2014.

55. I. A. Horvath, "Extreme PIV applications: Simultaneous and instantaneous velocity and concentration measurements on model and real scale car park fire scenarios," Universite Libre de Bruxelles, Brussel, Belgium, 2012.

56. P. P. K. ; Raj, A. N. ; Moussa, and K. Aravamudan, "Experiments Involving Pool and Vapor Fires from Spills of Liquefied Natural Gas on Water," Washington, DC, (1979).

57. T. Blanchat, P. Helmick, R. Jensen, A. Luketa, R. Deola, J. Suo-, J. Mercier, T. Miller, A. Ricks, R. Simpson, S. Tieszen, and M. Hightower, "Summary of the Phoenix Series Large Scale LNG Pool Fire Experiments," Albuquerque, NM; Livermore, CA, (2011).

58. American Gas Association, "LNG Safety Program: Interim Report on Phase II Work," American Gas Association, Columbus, Ohio, USA, Project IS-3-1, (1974).

59. G. A. Mizner and J. A. Eyre, "LARGE-SCALE LNG AND LPG POOL FIRES," in *I. CHEM.E.SYMPOSIUM SERIES No.71*, 147–163, 1982.

60. K. S. Mudan, "Thermal radiation hazards from hydrocarbon pool fire," *Prog. Energy Combust. Sci.*, **10**, 1, 59–80 (1984).

61. P. J. Rew, W. G. Hulbert, and D. M. Deaves, "Modelling of thermal radiation from external hydrocarbon pool fire," *Trans. Inst. Chem. Eng.*, **75**, Part B, 81–89 (1997).

62. E. J. Weckman and A. Sobiesiak, "The oscillatory behaviour of medium-scale pool fires," *22nd Symp. Combust.*, 1299–1310 (1988).

63. E. E. Zukoski, B. M. Cetegen, and T. Kubota, "Visible structure of buoyant diffusion flames," *Symp. Combust.*, **20**, 1, 361–366 (1985).

64. F. Ferrero, M. Muñoz, and J. Arnaldos, "Effects of thin-layer boilover on flame geometry and dynamics in large hydrocarbon pool fires," *Fuel Process. Technol.*, **88**, 3, 227–235 (2007).

65. P. H. Thomas, C. T. Webster, and M. M. Raftery, “Some experiments on buoyant diffusion flames,” *Combust. Flame*, **5**, 359–367 (1961).

66. D. Laboureur, “Experimental characterization and modeling of hazards : BLEVE and Boilover,” The von Karman Institute for Fluid Dynamics, Sint-Genesius-Rode, Belgium, 2012.

67. G. Mangialavori and F. Rubino, “Experimental tests on large hydrocarbon pool fires,” in *7th International Symposium on Loss Prevention and Safety Promotion in the Process Industries*, 1992.

68. J. Moorhouse, “Scaling criteria for pool fires derived from large scale experiments,” *IChemE Symp. Ser.*, **71**, 165–179 (1982).

69. M. Pritchard and T. Binding, “FIRE 2: a new approach for predicting thermal radiation levels from hydrocarbon pool fires,” *Symp. Major Hazards Onshore Offshore*, **130**, 491–505 (1993).

70. P. H. Thomas, “The size of flames from natural fires,” *Symp. Combust.*, **9**, 1, 844–859 (1963).

71. S. R. Tieszen, T. J. O’Hern, R. W. Schefer, E. J. Weckman, and T. K. Blanchat, “Experimental study of the flow field in and around a one meter diameter methane fire,” *Combust. Flame*, **129**, 4, 378–391 (2002).

72. J. W. Fleming and R. S. Sheinson, “Development of a Cup Burner Apparatus for Fire Suppression Evaluation of High-Expansion Foams,” *Fire Technol.*, **48**, 3, 615–623 (2010).

73. J. R. Howell and M. P. Menguc, “Chapter 7 Radiation,” in *Handbook of heat transfer*, New York, US: McGraw-Hill, 1998.